Biological Water: Properties and Roles in Muscle Development and Function

Sang Hyok Yoo

A dissertation

Submitted In partial fulfillment of the

requirements for the degree of

Doctor of Philosophy

University of Washington

2014

Reading Committee:

Gerald H. Pollack, Chair

Peter Simkin

R. Jeffrey Wilkes

Program Authorized to Offer Degree:

Bioengineering and Nanotechnology

University of Washington

Abstract

Biological Water: Properties and Role in Muscle Development and Function

Sang Hyok Yoo

Chair of the Supervisory Committee:

Professor Gerald H. Pollack, PhD

Bioengineering

Water is the most abundant substance on planet Earth and present in large part of our daily lives. Despite such abundance, liquid water still remains mysterious for we do not understand its structure. Similarly, biological systems are largely composed of water and life is believed to have originated from water. However, the properties and functional role of biological water still remains an enigma. Thus, more wholesome understanding of biological water is needed to gain further purchase on workings of biological systems.

The first part of this work was aimed at better understanding the properties of biological water. In biological systems, most of water is 'interfacial'. Therefore, interfacial water near hydrophilic surface was characterized to model biological water. The results show

that hydrophilic surfaces, including broad biological surfaces, can alter properties of nearby water extensively. These included increased viscosity, decreased kinetic energy, faster NMR spic-lattice (T1) relaxation and lower self-diffusion coefficient of water. The findings collectively indicate more ordered state of water near surfaces.

In the second part of this work, water inside living muscle cells and intact myofibril was studied using molecular spectroscopy techniques. Both studies show that intracellular water within muscle has significantly stronger hydrogen bonding and hindered dynamics. In addition, changes in water properties have been correlated with muscle contraction and differentiation. Hence, water takes an active role at broad range of biological processes of varying time-scales.

Table of Contents

List of Figures

List of Tables

Acknowledgements

In leading up to this dissertation, I have been very fortunate to have encountered countless people that have helped me to shape my views on nature. I would like to thank all the friends I have come across and their meaningful conversations. I would also like to thank my committee members. I especially thank my advisor Dr. Pollack for teaching me science as an inquiry and courage to seek the truth. I would also like to thank my mother and father for their devotion towards my education and all the support and endless love I have gratefully received throughout my life. I would like to thank my brother, Sam, for being the best friend I can turn to for intellectual discussions on broad topics. I would like to acknowledge my lovely wife, Katya, who has been immensely patient and understanding in my quest for this dissertation. She was not only there for emotional support and love, but for numerous scientific discussions. Lastly, I would like to acknowledge my sons, Aleks and Miky. You guys are by far the best bioengineering projects of mine, and your simple questions humble me of how much more we can learn from the nature.

Chapter 1. Introduction

1.01 Water: an overview

Water is the most familiar substance known to mankind as we are born out of it and live immersed in it throughout our lives. Whether it is through raindrops on a fall day or sipping on a glass of water, water makes our living experiences possible. The oceans cover 75 % of Earth's surface and make up most of water supply on Earth (figure 1), and much smaller fraction is fresh water in form of polar ice caps, groundwater, lakes and rivers, etc. More recently, a water reservoir three times the volume of ocean water has been found 700 kilometers beneath earth's surface, trapped inside ringwoodite in the mantle. [1] Hence, with little doubt, our beautiful planet Earth can be considered a sphere of water.

Perhaps due to such abundance and familiarity, it is presumed by most people water is a simple liquid and its properties are well understood. This sentiment cannot possibly be further away from the truth, when one considers simple observation of ice floating on water. Water has over hundred known anomalies; it behaves differently from any other simple liquids.

Figure 1.1 Photograph of earth taken by NASA's Moderate Resolution Imaging Spectroradiometer (MODIS) from 700 km above the Earth. Most of Earth's surface is covered with Water.

1.02 The Water Molecule

Individually, the water molecule is well known as H_2O. As shown in figure 1.2, it is composed of electronegative oxygen covalently bonded to two electropositive hydrogen atoms with bonding energy of 458.9 kJ/mol.

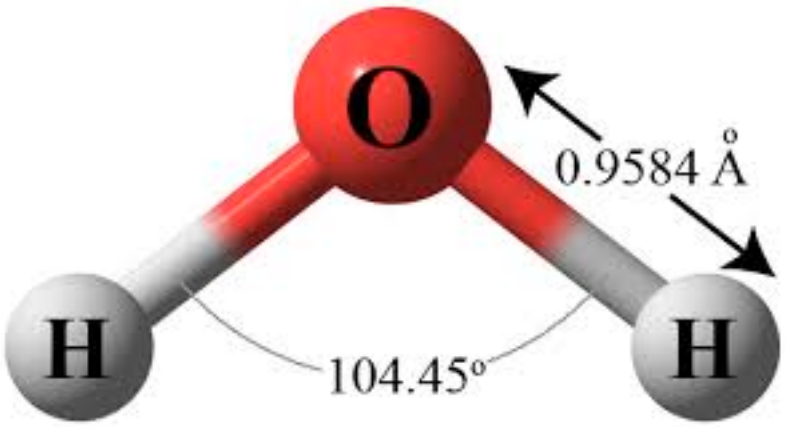

Figure 1.2 Water Molecule is made up of two hydrogen and one oxygen, H_2O. The two OH covalent Bonds have bond length of 0.9584 Å and make an angle of 104.45°.

1.03 Structure of Liquid Water

Of the known phases of water, liquid water presents most challenges due to extensive intramolecular bonding between the water molecules, otherwise known as hydrogen bonding. Such character of liquid water has resulted in many dozens of anomalies in water, whose explanations still remain amiss. Of these, well known anamolies include density maximum at 4 °C, unusually high specific heat and viscosity among many others.

On the classical theoretical front, there are broadly two models to describe liquid water: 'Mixture' and 'Continuum' models. Mixture model treats liquid water as an equilibrium mixture of water molecules having varying number of hydrogen bonds per molecule [2,3]. In the 'mixture' model each water molecule can have up to four hydrogen bonds making up a tetrahedral structure found in ice. Therefore, the fully coordinated water molecule is also known as 'ice-like' water. Water molecules with three or few hydrogen bonds are referred to as partially hydrogen-bonded water and those with zero hydrogen bonds are known as free OH. The continuum model treats water as a fully hydrogen bonded network with varying hydrogen bonding energies and geometries [4,5]. In this model, ice is said to have stronger average hydrogen bonding energy compared to that of liquid water. While these two theories have been around for almost half a century and do not quite explain the entirety of liquid water's anomalies, they remain the backbone of most modern theories on water structure.

Experimental efforts to understand the structure of liquid water have broadly included x-ray and neutron diffraction studies and infrared spectroscopy. Of these, the diffraction data provides radial distribution functions, but they do not provide information on geometries [6,7]. More recent studies on the structure of first coordination shell in liquid water was carried out using x-ray absorption spectroscopy, where most of water molecules at room temperature was observed to have two hydrogen bonds per molecule [8] However, the finding in this study showed significant discrepancies with

structures determined by molecular dynamics (MD) studies, further complicating the complete understanding of water.

Infrared spectrum is a sensitive marker of hydrogen bonding strength as the frequency OH stretch vibration is observed to decrease linearly with stronger hydrogen bonding [9]. For water, the OH stretch frequency increases as water goes from solid to liquid to gas, and this is confirmed in the infrared spectra shown in figure 3. Despite such straightforward correlation between the hydrogen bonding strength and vibrational frequency of OH stretch, a significantly broad OH stretch peak of liquid water has puzzled many theoreticians to interpret the infrared spectrum of liquid water over the years. Today, the most widely used interpretation involves decomposing several components of the OH stretch peak via peak-fitting, second-derivative or Fourier de-convolution. All three methods give similar results-there are three components with their centroid centered around 3200, 3400 and 3600 cm-1 [10]. These are interpreted as 'ice-like' water, partially hydrogen bonded water and free OH respectively.

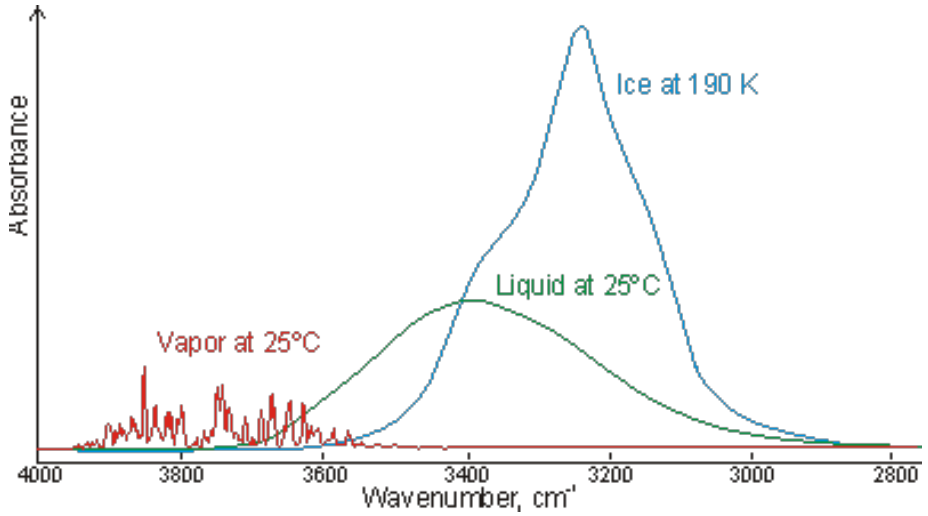

Figure 1.3 Infrared spectra of water vapor (red), liquid water [11] and ice (blue). [12]

More recent studies on the structure of liquid water have concentrated more on the dynamics of hydrogen-bonded water network. In these studies, ultrafast time-resolved infrared spectroscopy was used, and the results showed fluctuations in liquid water on the time scales ranging from picoseconds to femtoseconds [13,14]. It is largely due to these studies that resulted in currently accepted structure of liquid water, that is described as hydrogen bonded network of water molecules with ultra-fast flickering hydrogen bonds. Consequentially, theories involving long lasting water structures have been abolished.

1.04 Interfacial Water and Exclusion Zone (EZ)

It is commonly accepted that in the vicinity of hydrophilic interfaces water organizes into ice-like water, which project from the surface by a few layers [15,16]. The surface water, also known as 'interfacial water', has distinct physco-chemical properties

compared to bulk liquid water. These properties include viscosity as much as six order of magnitude higher than 'bulk' water [17]; higher specific heat, diffusion constant and dielectric constant [18]. Partly due to the rapid development of surface-characterization techniques, most recent work has focused almost exclusively on near-surface dynamics confined to the first few molecular layers. Consequently, possible macroscopic surface effects on nearby water have not been widely studied.

On the other hand, decades of early work has demonstrated that water can exhibit physical properties quite different than those of bulk water, out to distances on the order of micrometers [19]. Further, such an extensive surface water zone near many biological surfaces, known as the unstirred layer, has been broadly observed to significantly impact the rate of colloidal diffusion across cell membranes [11].

Recent studies of water near hydrophilic surfaces indicates that the interfacial water zone may extend unexpectedly far from hydrophilic surfaces [20]. Those surfaces include a wide range of materials such as ion-exchange resins, polymers, hydrogels, functionalized monolayers, muscle tissues and metal oxides. The near-surface aqueous zones exhibit a number of unique properties, the most notable being that suspended particles (e.g., monodisperse colloids) are excluded from the surface to distances of several hundred micrometers; thus, these particle-free zones have been termed exclusion zones (EZs). A typical micrograph of EZ is shown in the figure 1.4. EZs exhibit a number of physical

properties differing from those of bulk water. They bear negative electrical potential, as much as 150−200 mV near the nucleating surface, they exhibit anomalous UV absorption at 270 nm, and they show diminished infrared emissivity, and retarded T2 relaxation times [21-23]. These properties collectively imply that the water within EZs may be more ordered than bulk water.

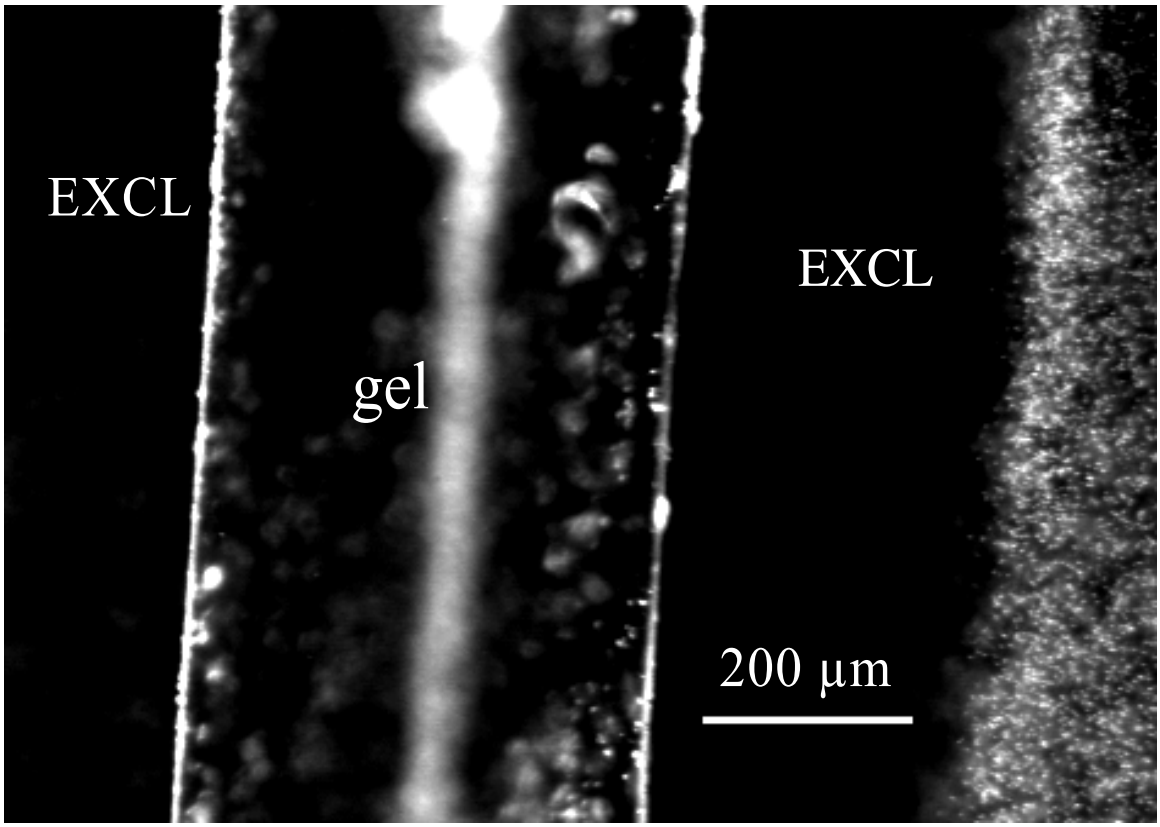

Figure 1.4 Solute exclusion in the vicinity of polyacrylic acid (PAA) gel. Gel runs vertically. The blurred vertical white element to the right of "gel" is an optical artifact. The gel was placed on a coverslip, superfused with a suspension of 1-μm carboxylate-coated

polystyrene microspheres, and observed in an inverted microscope equipped with a 20x objective. Image obtained 20 min. after superfusion.

1.05 Water in Biological Systems

Water plays a crucial role in biological systems. While the role of water for sustaining life is well recognized, the exact role of water in biological processes and energetics remains unclear. On the other hand, an increasing number of recent studies show that biological processes such as protein-ligand binding, protein folding and DNA sequence recognition are heavily influenced by interfacial water dynamics [24].

Of these, the protein folding problem is significant as it sits the base of biological function [25-27]. X-ray crystallography studies had revealed that there are a couple of hydration layers, which persisted on the protein surface even under very high vacuum [28,29]. Due to such small extent of hydration water, the following studies on water protein interaction had largely focused on the interaction of water with protein backbone and highly charged side chains [30]. However, recent development of THz and florescence spectroscopy techniques have reveled that dynamic hydration shell around proteins can extend out to much longer distances [31,32], demonstrating long-range effects of protein on nearby water. Further, recent dielectric spectroscopy studies show that protein folding is largely 'slaved' by dynamics of water beyond the first couple hydration layers

[33]. Combined together, these results indicate that water plays a central role in determining protein structure and dynamics, as important as the protein itself.

1.06 Infrared Spectroscopy

Infrared light is part of the electromagnetic spectrum that lies between visible light and microwave. Infrared spectroscopy along with Raman spectroscopy is a type vibrational spectroscopy, and probes molecular vibrations. For its ease of use, infrared spectroscopy has become one of the most widely used techniques for determining of chemical structure of molecules. When radiant energy is the same as the energy of molecular vibration, absorption occurs. A molecule is said to be infrared active, when absorption of infrared light results in change of dipole moment, also known as selection rule. Because most biological molecules vibrational frequency fall within the mid-IR region, infrared spectroscopy has been especially useful in determining the structure of biomolecules such as protein and enzymes.

1.07 Synchrotron radiation FTIR (SR-FTIR) spectromicroscopy

In the modern era, the most common form of infrared spectroscopy is Fourier transform IR (FTIR) spectroscopy. FTIR utilizes a miniature Michelson-Morley type interferometer and results in quick generation of spectrum with relatively simple sample preparation. Briefly, a source infrared light goes through a beam splitter, with one beam reflecting off of stationary mirror while the other is reflecting off of moving mirror. The split beams are then re-combined to reach the detector and this give an interferogram. Taking the Fourier transform of the interferogram results in a spectrum. The performance of FTIR spectrometer is generally dependent on the source brightness. Typical infrared source used in FTIR spectrometers has thermal globar source that has a large beam waist. For this region, in most practical use of spectrometers, an aperture is placed in the beam path to limit the size of the beam reaching the sample. Such constraint in the optical set-up results in poor spatial resolution in globar source based FTIR spectrometers, typically bigger than 30 micrometers.

To deal with the limitations faced by Globar sources, synchrotron radiation based infrared spectroscopy has been developed in the last couple of decades. Synchrotron stores electrons moving at relativistic speed along the curved path through magnetic field, and therefore produces extremely bright IR light that are two to three orders of magnitude brighter than conventional thermal source. In addition, the small opening angle of synchrotron radiation produces a beam profile that is close to an ideal point source. A typical set-up for a SR-FTIR spectro-microscope is shown in figure 1.5.

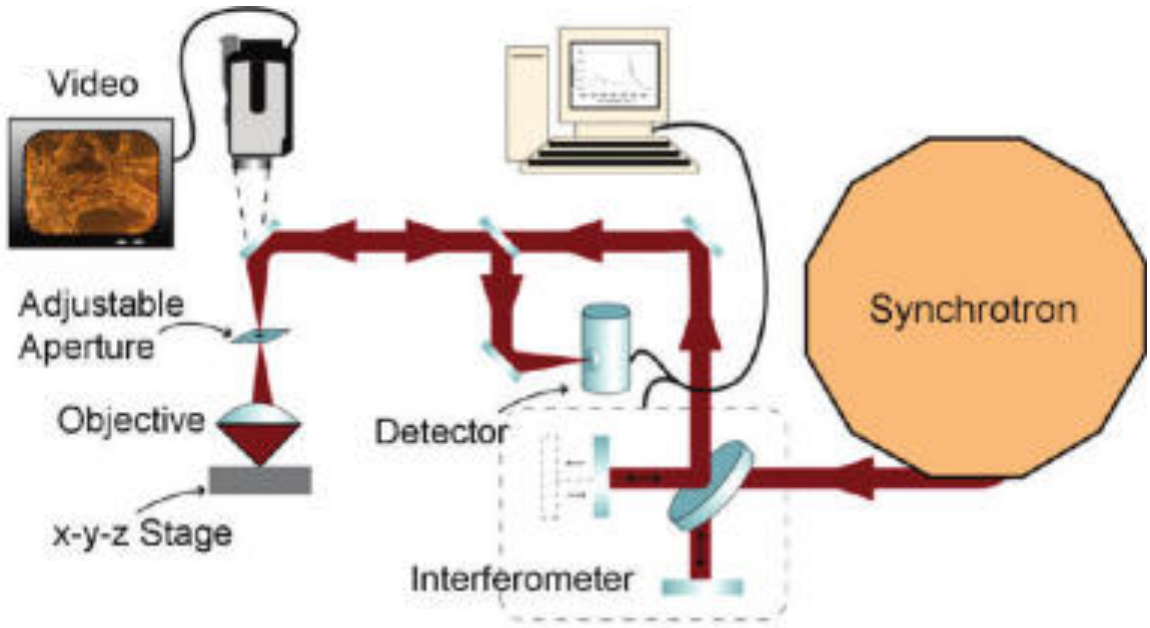

Figure 1.5 Set-up of SR-FTIR spectro-microscope [34]

Owing to its high brightness and small beam size, recent development of synchrotron radiation (SR) FTIR spectro-microscopy has enabled non-invasive probing of biological tissues and living cells with unprecedented spectral sensitivity and diffraction-limited spatial resolution in determination of chemical species and structures within biological samples [34-36]. A comparison of spectra collected with conventional thermal source and synchrotron radiation is shown in figure 1.6. Evidently, synchrotron radiation gives superior signal with high spectral sensitivity in a much shorter time.

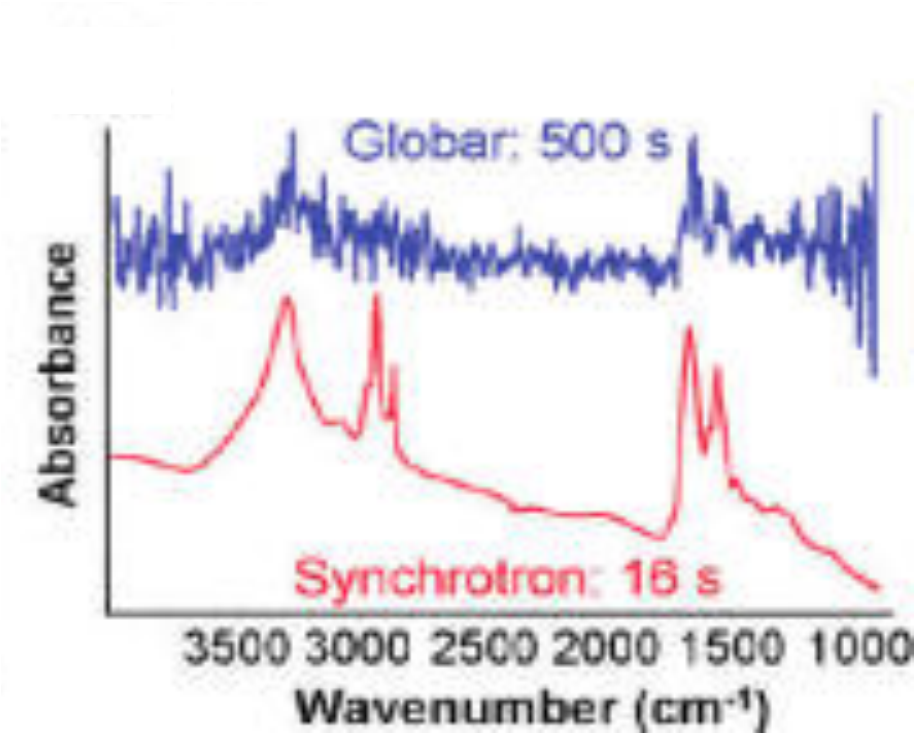

Figure 1.6 Comparison of FTIR spectra of a single cell collected with conventional thermal globar source (blue) and synchrotron source (red). The collection time for the synchrotron source was ~16 s compared to ~200 s for the thermal source [34]

1.08 Muscle Architecture

Muscle is one of the major organ systems in our body, consisting of cardiac, skeletal and smooth muscle. It regulates wide range of important physiological activities such as movements, blood circulation and maintaining posture. Muscle is an intricately organized hierarchal system with unique assembly geometry ranging over broad length scales from nanometers to centimeters as shown in figure 1.7. Skeletal muscle is

composed of cylindrical muscle fibers, which are tightly held together along the length by collagen. Muscle fiber or multi-nucleated muscle cell contains tightly packed cylindrical myofibrils of same length. The myofibrils are the smallest intact contractile unit and composed of muscle protein filaments packed in a hexagonal array. The major contractile proteins in muscle are actin and myosin, and their assemblies are also called thin and thick filaments respectively.

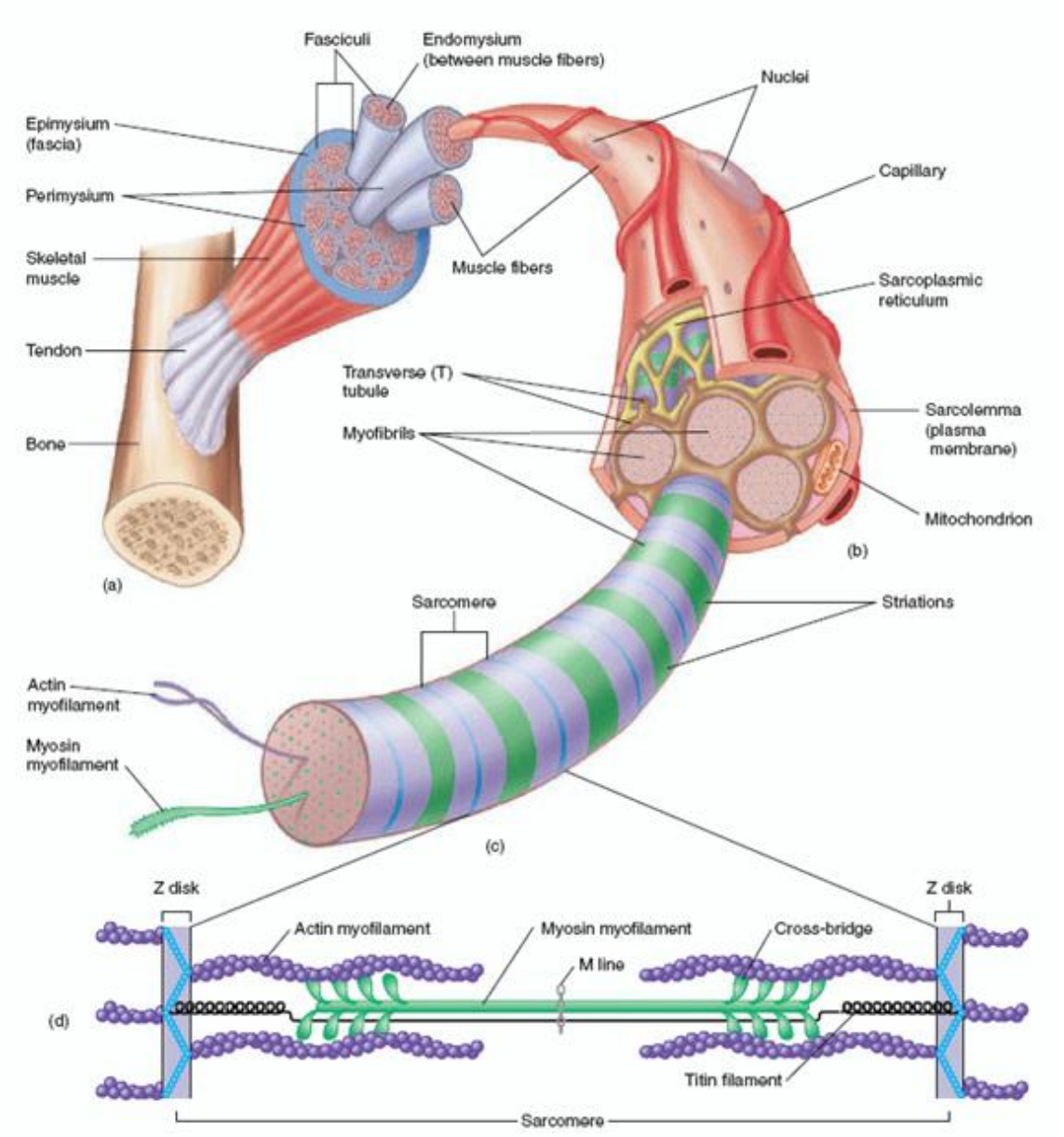

Figure 1.7 Architectures of skeletal muscle system at several organizational levels (a) muscle (b) muscle fiber (c) myofibril (d) Sarcomere. [37]

1.09 'Cross-bridge' Theory of Muscle Contraction and Alternative Views

Modern understanding on the molecular mechanism of muscle contraction is largely dominated by the 'cross-bridge' theory originally proposed by Sir Andrew Huxley and H.E. Huxley [38,39]. A pictorial diagram of molecular muscle contraction is shown in figure 1.8. In this theory, an ATP first binds to the myosin head, bringing the myosin to lower energy state and allowing the myosin head to detach from the actin filament. Next, ATP goes through hydrolysis and splits into ADP and phosphate to bring myosin to higher energetic state. Release of phosphate by the myosin head results in 'swinging' of myosin head, causing the actin filament to slide past myosin filament. ADP is then released to lock the head into the 'rigor' configuration. As the next ATP binds to the myosin head, another cycle begins. Despite wide acceptance of this model. many experimental results remain at odds with that theory. The most notable are shortening of thick filaments during contraction [40], and generation of force even with no apparent overlap of thick and thin filaments [41], where no attachment of myosin heads to actin filaments can occur. Both findings indicate the need for an alternative mechanism [42,43].

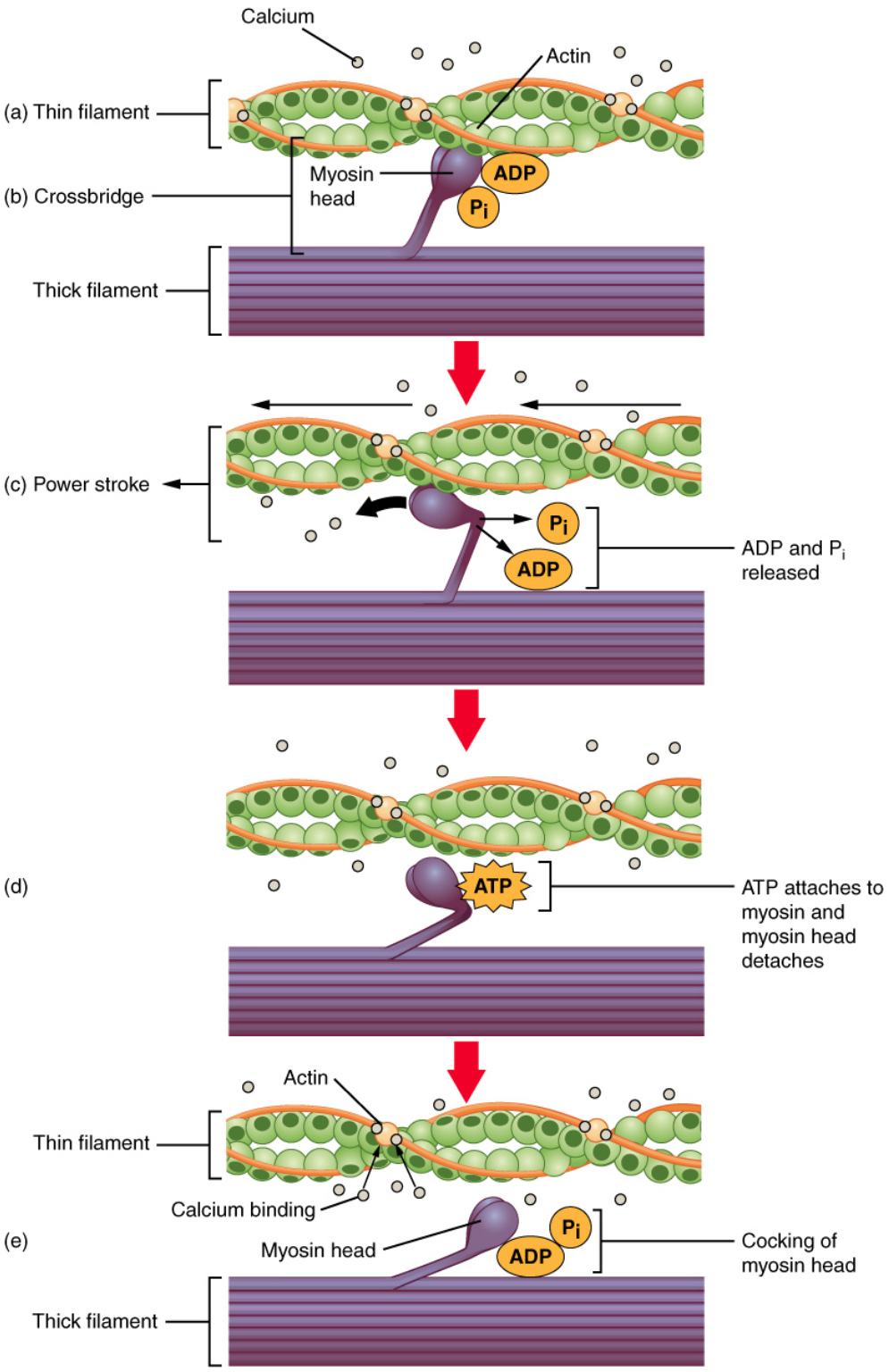

Figure 1.8 Pictorial diagram of molecular muscle contraction proposed by the 'cross-bridge' theory. [44]

Moreover, numerous experimental observations indicate that water may play an important role in muscle activation (for summary, see [42,45]). Several recent findings indicate that interfacial water near surfaces is at least an order of magnitude more viscous than bulk water, with several groups reporting as high as 6-fold viscosity increase near hydrophilic surfaces [46]. This high viscosity implies that the theory's required molecular swinging may encounter difficulty, and that ATP splitting alone might not account for the energy needed to contract the muscle.

1.10 References

1 Schmandt, B., Jacobsen, S. D., Becker, T. W., Liu, Z. & Dueker, K. G. Dehydration melting at the top of the lower mantle. *Science* **344**, 1265-1268 (2014).

2 Nemethy, G. & Scheraga, H. A. Structure of Water and Hydrophobic Bonding in Proteins. I. A Model for the Thermodynamic Properties of Liquid Water. *The Journal of Chemical Physics* **36**, 3382-3400 (1962).

3 Marchi, R. P. & Eyring, H. Application of Significant Structure Theory to Water1. *The Journal of Physical Chemistry* **68**, 221-228, doi:10.1021/j100784a001 (1964).

4 Glew, D. N. AQUEOUS SOLUBILITY AND THE GAS-HYDRATES. THE METHANE-WATER SYSTEM1. *The Journal of Physical Chemistry* **66**, 605-609, doi:10.1021/j100810a008 (1962).

5 Pople, J. A. Molecular Association in Liquids. II. A Theory of the Structure of Water. *Proceedings of the Royal Society of London. Series A. Mathematical and Physical Sciences* **205**, 163-178 (1951).

6 Narten, A. H. & Levy, H. A. Observed Diffraction Pattern and Proposed Models of Liquid Water. *Science* **165**, 447-454 (1969).

7 Head-Gordon, T. & Hura, G. Water Structure from Scattering Experiments and Simulation. *Chemical Reviews* **102**, 2651-2670, doi:10.1021/cr0006831 (2002).

8 Wernet, P. *et al.* The Structure of the First Coordination Shell in Liquid Water. *Science* **304**, 995-999 (2004).

9 G. C. Pimentel, A. L. M. *The hydrogen bond*. (Freeman, 1960).

10 Falk, M. & Ford, T. A. INFRARED SPECTRUM AND STRUCTURE OF LIQUID WATER. *Canadian Journal of Chemistry* **44**, 1699-1707, doi:10.1139/v66-255 (1966).

11 Green, K. & Otori, T. Direct measurements of membrane unstirred layers. *The Journal of Physiology* **207**, 93-102 (1970).

12 Chaplin, M. *Water Absorption Spectrum*.

13 Fecko, C. J., Eaves, J. D., Loparo, J. J., Tokmakoff, A. & Geissler, P. L. Ultrafast Hydrogen-Bond Dynamics in the Infrared Spectroscopy of Water. *Science* **301**, 1698-1702 (2003).

14 Lawrence, C. P. & Skinner, J. L. Ultrafast infrared spectroscopy probes hydrogen-bonding dynamics in liquid water. *Chemical Physics Letters* **369**, 472-477, doi:http://dx.doi.org/10.1016/S0009-2614(02)02039-0 (2003).

15 Ostroverkhov, V., Waychunas, G. A. & Shen, Y. R. New Information on Water Interfacial Structure Revealed by Phase-Sensitive Surface Spectroscopy. *Physical Review Letters* **94**, 046102 (2005).

16 Ruan, C.-Y., Lobastov, V. A., Vigliotti, F., Chen, S. & Zewail, A. H. Ultrafast Electron Crystallography of Interfacial Water. *Science* **304**, 80-84 (2004).

17 Zhu, Y. & Granick, S. Viscosity of Interfacial Water. *Physical Review Letters* **87**, 096104 (2001).

18 Sun, C. Q. *et al.* Density, Elasticity, and Stability Anomalies of Water Molecules with Fewer than Four Neighbors. *The Journal of Physical Chemistry Letters* **4**, 2565-2570, doi:10.1021/jz401029z (2013).

19 Henniker, J. C. The Depth of the Surface Zone of a Liquid. *Reviews of Modern Physics* **21**, 322-341 (1949).

20 Zheng, J.-m. & Pollack, G. H. Long-range forces extending from polymer-gel surfaces. *Physical Review E* **68**, 031408 (2003).

21 Yoo, H., Paranji, R. & Pollack, G. H. Impact of Hydrophilic Surfaces on Interfacial Water Dynamics Probed with NMR Spectroscopy. *The Journal of Physical Chemistry Letters* **2**, 532-536, doi:10.1021/jz200057g (2011).

22 Zheng, J.-m., Chin, W.-C., Khijniak, E., Khijniak Jr, E. & Pollack, G. H. Surfaces and interfacial water: Evidence that hydrophilic surfaces have long-range impact. *Advances in Colloid and Interface Science* **127**, 19-27, doi:http://dx.doi.org/10.1016/j.cis.2006.07.002 (2006).

23 Hyok Yoo, D. R. B., Christopher M. Pirie, Basil Hovakeemian, and Gerald H. Pollack. in *Water: The fogotten biological molecule* (ed Hidenao Fukuyama Denis Le Bihan) Ch. 7, (Pan Stanford Publishing, 2011).

24 Chaplin, M. Do we underestimate the importance of water in cell biology? *Nat Rev Mol Cell Biol* **7**, 861-866 (2006).

25 Frauenfelder, H. *et al.* A unified model of protein dynamics. *Proceedings of the National Academy of Sciences* **106**, 5129-5134 (2009).

26 Cheung, M. S., Garcia, A. E. & Onuchic, J. N. Protein folding mediated by solvation: water expulsion and formation of the hydrophobic core occur after the structural collapse. *Proceedings of the National Academy of Sciences of the United States of America* **99**, 685-690, doi:10.1073/pnas.022387699 (2002).

27 Makarov, V., Pettitt, B. M. & Feig, M. Solvation and hydration of proteins and nucleic acids: a theoretical view of simulation and experiment. *Accounts of chemical research* **35**, 376-384 (2002).

28 Svergun, D. I. *et al.* Protein hydration in solution: Experimental observation by x-ray and neutron scattering. *Proceedings of the National Academy of Sciences* **95**, 2267-2272 (1998).

29 Burling, F. T., Weis, W. I., Flaherty, K. M. & Brünger, A. T. Direct Observation of Protein Solvation and Discrete Disorder with Experimental Crystallographic Phases. *Science* **271**, 72-77 (1996).

30 Ernst, J. A., Clubb, R. T., Zhou, H. X., Gronenborn, A. M. & Clore, G. M. Demonstration of positionally disordered water within a protein hydrophobic cavity by NMR. *Science* **267**, 1813-1817 (1995).

31 Born, B., Kim, S. J., Ebbinghaus, S., Gruebele, M. & Havenith, M. The terahertz dance of water with the proteins: the effect of protein flexibility on the dynamical hydration shell of ubiquitin. *Faraday Discussions* **141**, 161-173, doi:10.1039/b804734k (2009).

32 Ebbinghaus, S. *et al.* An extended dynamical hydration shell around proteins. *Proceedings of the National Academy of Sciences* **104**, 20749-20752 (2007).

33 Fenimore, P. W., Frauenfelder, H., McMahon, B. H. & Young, R. D. Bulk-solvent and hydration-shell fluctuations, similar to α- and β-fluctuations in glasses, control protein motions and functions. *Proceedings of the National Academy of Sciences of the United States of America* **101**, 14408-14413 (2004).

34 Holman, H.-Y. N., Bechtel, H. A., Hao, Z. & Martin, M. C. Synchrotron IR Spectromicroscopy: Chemistry of Living Cells. *Analytical Chemistry* **82**, 8757-8765, doi:10.1021/ac100991d (2010).

35 Holman, H.-Y. N., Hao, Z., Martin, M. C. & Bechtel, H. A. Infrared Spectromicroscopy: Probing Live Cellular Responses to Environmental Changes. *Synchrotron Radiation News* **23**, 12-19, doi:10.1080/08940886.2010.516737 (2010).

36 Holman, H.-Y. N. *et al.* Real-Time Chemical Imaging of Bacterial Activity in Biofilms Using Open-Channel Microfluidics and Synchrotron FTIR Spectromicroscopy. *Analytical Chemistry* **81**, 8564-8570, doi:10.1021/ac9015424 (2009).

37 Jayna. *Animal systems VII-Musculoskeletal system (Part 2)*, 2013).

38 Huxley, H. & Hanson, J. Changes in the Cross-Striations of Muscle during Contraction and Stretch and their Structural Interpretation. *Nature* **173**, 973-976 (1954).

39 Huxley, A. F. Muscle structure and theories of contraction. *Progress in biophysics and biophysical chemistry* **7**, 255-318 (1957).

40 Nagornyak, E. M., Blyakhman, F. A. & Pollack, G. H. Stepwise Length Changes in Single Invertebrate Thick Filaments. *Biophysical journal* **89**, 3269-3276 (2005).

41 Carlsen, F., Knappeis, G. G. & Buchthal, F. Ultrastructure of the Resting and Contracted Striated Muscle Fiber at Different Degrees of Stretch. *The Journal of Biophysical and Biochemical Cytology* **11**, 95-117, doi:10.2307/1603813 (1961).

42 Pollack, G. H. *Muscles & molecules : uncovering the principles of biological motion*. (Ebner & Sons Publishers, 1990).

43 Pollack, G. H. *Cells, gels and the engines of life : a new, unifying approach to cell function*. (Ebner & Sons, 2001).

44 *Talk: Muscle Contraction*, 2014).

45 Oplatka, A. Critical review of the swinging crossbridge theory and of the cardinal active role of water in muscle contraction. *Critical reviews in biochemistry and molecular biology* **32**, 307-360, doi:10.3109/10409239709082575 (1997).

46 Goertz, M. P., Houston, J. E. & Zhu, X. Y. Hydrophilicity and the Viscosity of Interfacial Water. *Langmuir* **23**, 5491-5497, doi:10.1021/la062299q (2007).

Section I

Interfacial Water as a Model System for Biological Water

Chapter 2. Physicochemical Properties of Interfacial Water Near Hydrophilic Surfaces

2.1 Abstract

Near hydrophilic surfaces, water molecules are believed to form distinct phase from bulk water out to a few molecular layers. However, recent studies have demonstrated that water can have markedly different physco-chemical properties and this interfacial zone can extend out to several tens and hundreds of micrometers. In this study, these findings are extended to investigate the generality of exclusion zone (EZ) nucleating surfaces in biological realm. In addition, the origin of negative potential within the EZ

water is studied by observing the pH distribution within and just outside of EZ using molecular pH dyes. Finally, the presumed ordered nature of EZ is tested by measuring the viscosity of water inside EZ. Our results show that three vastly different biopolymers, brown algae, cow tendon and gel of Ampullae of Lorenzini from sharks, all show EZ near their surfaces extending up to about 200 μm. Hence, EZ nucleation is a general feature of biological surfaces. The following pH measurements showed that EZ can exclude solutes of molecular dimensions, and EZ's negative potential has it roots in ejection of acidic water moieties out of the interfacial zone. This results in negatively charged interfacial zone juxtaposed to a bulk portion with access positive charge. Finally, viscosity measurements showed significantly higher viscosity of water within the EZ. The viscosity largely resembled spatial feature of negative electrical potential; the higher the negative potential, the more viscous water is. The findings reported here help to assemble a wholesome picture of EZ and confirm the generality of EZ in biological realm.

2.2 Introduction

Water is the most abundant substance on earth and influences our lives daily. Despite such abundance and importance, water is yet to be completely understood due to its anomalous properties.[1,2] Of these, particularly challenging to understand is water near surfaces. Water is rarely in its deionized form in natural settings, but rather contains some impurities, which provide interfaces to interact with water molecules. Therefore, understanding properties of Interfacial water is critically important for numerous chemical, biological, and atmospheric processes.

Water molecules lying next to hydrophilic interfaces are organized into ordered arrays. Such ordering is thought to project out by several molecular layers from the interface. The water molecules lying beyond them are undergoing thermal motion intense enough to preclude much additional ordering. Hence, beyond those few layers, water molecules are widely considered to lie within the bulk phase (Israelachvili, 1992).

On the contrary to widely accepted views, recent findings suggest that physico-chemical properties of water can differ much further from the surface. [3,4] The central observation is rather unexpected. In he vicinity of hydrophilic surfaces, colloids and solutes are extensively excluded from the nucleating surface out to hundreds of micrometers and hence, this zone is termed exclusion zone (EZ). Another notable property of EZ, which

differ markedly from bulk water, is negative electrical potential, up to 200 mV at the surface and diminish down to 0 mV over 200 μm from the surface. In addition, the EZ has anomalous 270 nm UV absorption and lowered NMR spin-spin (T2) relaxation time. Collectively, these findings indicate that water within EZ is of more ordered phase of water compared to bulk.

While these findings are counterintuitive, a similar result had been broadly published four decades ago: in addressing the origin of the so-called “unstirred layer” adjacent to biological tissues. Unstirred layer was observed near broad range of biological tissues including cornea, intestinal lining, skin and cell membranes, as well as synthetic surfaces such as polyHEMA. Inside unstirred layer, particle diffusion was observed to be significantly slower than what is expected in liquid water, hence indicating higher viscosity of water within this region. Additionally, a number of studies have shown that unstirred layer largely regulate solute transport within biological systems. Though seemingly important aspect of biology, the nature of unstirred layer still remains a mystery and to date, there has not been a suitable physical model to explain unexpected observations from unstirred layers. In light of recent observation of EZ, it looks that EZ and unstirred layer share a number of similar properties and better understanding the properties of EZ can shed fresh insights into the nature of unstirred layer and its biological implications.

Hence, there is little doubt that interfacial water near hydrophilic surfaces differs in its properties from those of bulk water. Additionally, earlier results indicate that EZ water may well be more statically and dynamically ordered than bulk water. This difference in physicochemical properties is what appears to lead to the observed exclusion of solutes.

In this study, we extend these findings in three ways. In order to further our understanding in biological implications of EZ and establish broader generality of EZ nucleating surfaces, a new set of biopolymers will be used to observe EZ. Second, we will investigate the nature of negative electric potential within EZ. If EZ is negatively charged, the positive charges ought to be directed nearby as water is expected to be electrically neutral in bulk form. Next, we will employ fall-ball viscometry to measure viscosity of water within EZ. Viscosity is a fundamental property of liquids, and more stable phase of liquid is expected to have higher viscosity compared to bulk.

2.3 Methods and Materials

2.3.1 General

For all experiments, deionized water (type I HPLC grade (18.2 MΩ-cm)) was collected from a Barnstead D3750 Nanopure Diamond purification system. All experimental chambers were washed with deionized water extensively prior to experiments in order to prevent contamination of experimental materials.

2.3.2 Biological Sample preparation

In order to test the generality of EZ nucleating surfaces, we will use three biopolymers. First one is *Saccharina*, a type of brown algae broadly used as a delicacy in eastern Asian countries. The algae was purchased from a local Asian market in dried form. Prior to experiments, the algae was soaked in deionized water for three hours followed by triple wash with deionized water.

The second biopolymer used was tendon from Ox-tail of cows. The tendon is rich with type I collagen, which is largely present in collective tissues of animals. Ox-tail was purchased at a local grocery shop. After removing the meat with knife blade, the tendon was chopped into 0.5 m x 0. 5 cm x 1 mm pieces for experiments. Prior to experiments, tendon pieces were rinsed in deionized water for 24 hours to remove all other contaminants such as blood.

The third biopolymer sample used was a gel contained within Ampullae of Lorenzini (AOL) found in cartilaginous fish (sharks, rays and chimaeras). AOL is a special electromagnetic sensor, which helps the fish to navigate by sensing electromagnetic

field. These sensors are mostly located near the mouth of fish and are also thought to be used in temperature sensing by fish.

For experiments, frozen cat fish were acquired from Professor Adam Summer's group at Friday Harbor Laboratories, University of Washington. After slow thawing of fish at 0 °C over 48 hours, the AoL pores containing the gel were softly pressed until clear gel dribble out of the pores. The gel was then collected using knife blade and store in Eppendorf tubes at -20 °C for future experiments. Each catfish yielded roughly 0.5 mL of the gel for future experiments.

2.3.3 Microscopy of EZ near biopolymers

For visual observation of EZ near biopolymers, inverted bright-field microscope (Zeiss Axiover 150) was used for all experiments with a 10 X objective. For both polymers, 2 µm diameter microspheres were used as a marker for EZ. The microsphere suspension was prepared by adding two drops of carboxylated polystyrene bead stock suspension (Polysciences, inc. # 18327-10) into 10 mL of deionized water.

The samples were first hydrated in deionized water for two hours prior to experiment. For experiments, the polymer sample was first placed in custom made glass chamber of dimensions 2 cm x 2 cm x 1mm and the chamber was then filled with microsphere

suspension. After EZ has stabilized in about 10 minutes, EZ was observed. The collected images were processed with imageJ to determine the size of EZ.

2.3.4 pH Dye Experiments

For the pH dye experiments, a chamber with transparent glass walls was constructed using ordinary 1-mm-thick, 50 x 73 mm glass microscope slides held apart by 1-mm glass spacers, which formed the sides of the chamber. Epoxy glue (cat. #: 14250, Devcon, MA) was applied to around the resulting box-like chamber to prevent water leakage. At the bottom of the chamber, we glued either a sheet of Nafion (Sigma-Aldrich #: 274674). To make a pH dye solution, universal pH-indicator dye (Sigma #36803) was added to the water per manufacture's recommended concentration. The pH dye solution was then poured slowly into the chamber and corresponding changes in color was recoreded. For recordings of changes in dye color (pH), a macro lens was attached to a Scion CCD camera with resolution of 1600 x 1200 pixels to yield viewing area of 75 mm x 56.25 mm. pH color scale and corresponding RGB values were calibrated by carefully titrating water with HCL and NaOH from pH of 3 to 10.

2.3.5 Measurement of interfacial water viscosity

For the viscosity experiments, falling-ball viscometry was used. To track the descent of spheres, a chamber with transparent glass walls was constructed using ordinary 1-mm-thick, 50 x 73 mm glass microscope slides held apart by 1-mm glass spacers, which formed the sides of the chamber. Epoxy glue (cat. #: 14250, Devcon, MA) was applied to around the resulting box-like chamber to prevent water leakage. At the bottom of the chamber, we glued either a sheet of Nafion (Sigma-Aldrich #: 274674) or, as a control, a strip of aluminum or steel, which generated little or no exclusion zone. Polystyrene microspheres, 5, 10, and 15-µm diameter (Bangs Laboratory, Cat #: 5623, 6955, 6716, respectively) were used as falling balls. These spheres are nearly neutral, thereby minimizing any electrostatic interaction among the spheres.

To carry out experiments, the chamber was first filled with deionized water (see above). To make sure that the Nafion was fully hydrated, the microspheres were added several minutes after the chamber had been filled.

A small loop, diameter ~600 µm, was constructed out of 100-µm diameter copper wire for suspending microspheres into the chamber. By dipping the loop into the prepared microsphere suspension, it was possible to obtain a thin film of microsphere suspension (< 0.5 µl) containing only a few microspheres. This loop was then dipped into the top of the chamber. Typically 10-20 microspheres were seen to descend.

As microspheres descended, downward displacement was tracked using a Nikon bright field microscope with a 5x objective (Model 76023) and Scion CCD digital camera (Model CFW-1310C). A green LED (Phillips Luxeon R5JG) with a narrow localized peak at 530 nm was used as a light source. Minimizing intensity tended to minimize thermal convection. To compute the vertical component of descent (some sideways motion was often present), screens showing 1200 µm high zones were examined using ImageJ at one frame every five seconds, and velocity was computed. This was done at a series of heights — 4,800, 3,300 and 1800, 1000, 500, 200, 100 and 50 µm. Five runs were made at each height for microspheres of each size.

2.4 Results

Exclusion zone has been observed near variety of surfaces including both natural and synthetic polymers. In biological realm, one EZ nucleating surface was skinned muscle fiber, where EZ was shown to extend out to about 100 µm from the surface. However, more biopolymers need to be examined for EZ nucleation in order to reach a generality that EZ is necessarily induced by all biopolymers. In order to further test the generality of EZ near biological surfaces, three more samples were used as EZ nucleating surfaces.

The samples were all chosen to represent larger class of biological surfaces with an aim of reaching generality. The first sample is brown algae, which is omnipresent throughout oceans. Hence, brown algae offer a good model of marine plants. The second sample

was chosen to be tendon from cow ox-tail for its high content of collagen I proteins. Collagen I is the most prominent proteins in animal connective tissues, and hence can model broad range of animal tissue. The last same of a gel from Ampullae of Lorenzini (AoL). AoL is one of a very few organs that is sensitive to electromagnetic waves. Given the charged nature of EZ, it is hypothesized that EZ water properties paly an important role in electromagnetic sensing.

Figure 2.1 shows a representative micrograph of EZ next to brown algae. The size of EZ is comparable to EZ's previously found next to other surfaces, about 200 μm. EZ is present around the whole piece of brown algae and persisted for at least six hours. Therefore, there is a stable EZ next to surface of brown algae. Figure 2.2 Shows a representative micrograph of EZ next to ox-tail tendon. Similar to brown algae and other EZ nucleating surfaces, the tendon shows a sizable EZ of about 200 μm. The EZ next to ox-tail tendon also showed robustness and stability as it persisted for a minimum of eight hours. Ox-tail tendon is mostly composed of collagen I, which is omnipresent throughout connective tissues in animals. Hence, EZ is largely expected to be present within our connective tissues.

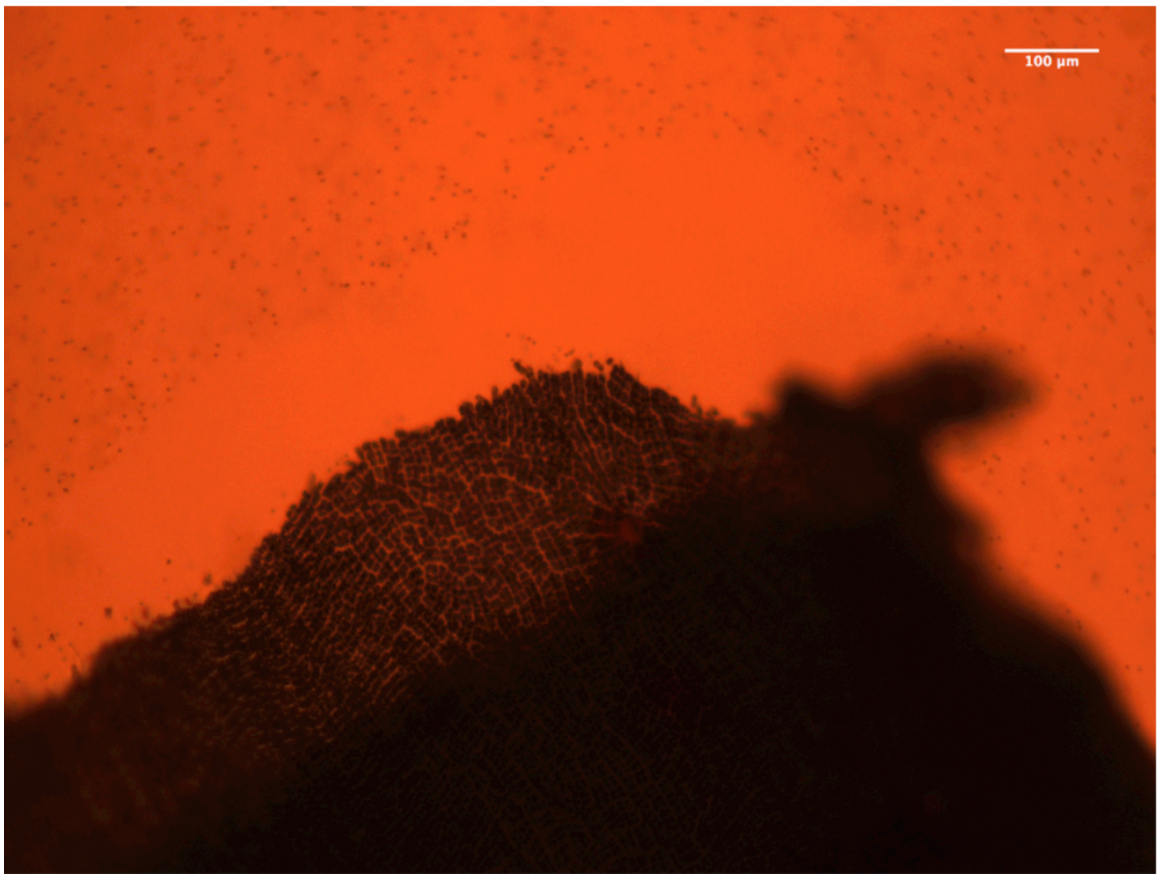

Figure 2.1 Exclusion zone (EZ) near *Saccharina*, a type of brown algae. Brown algae is at the bottom of the image. The scale bar denotes 100 µm.

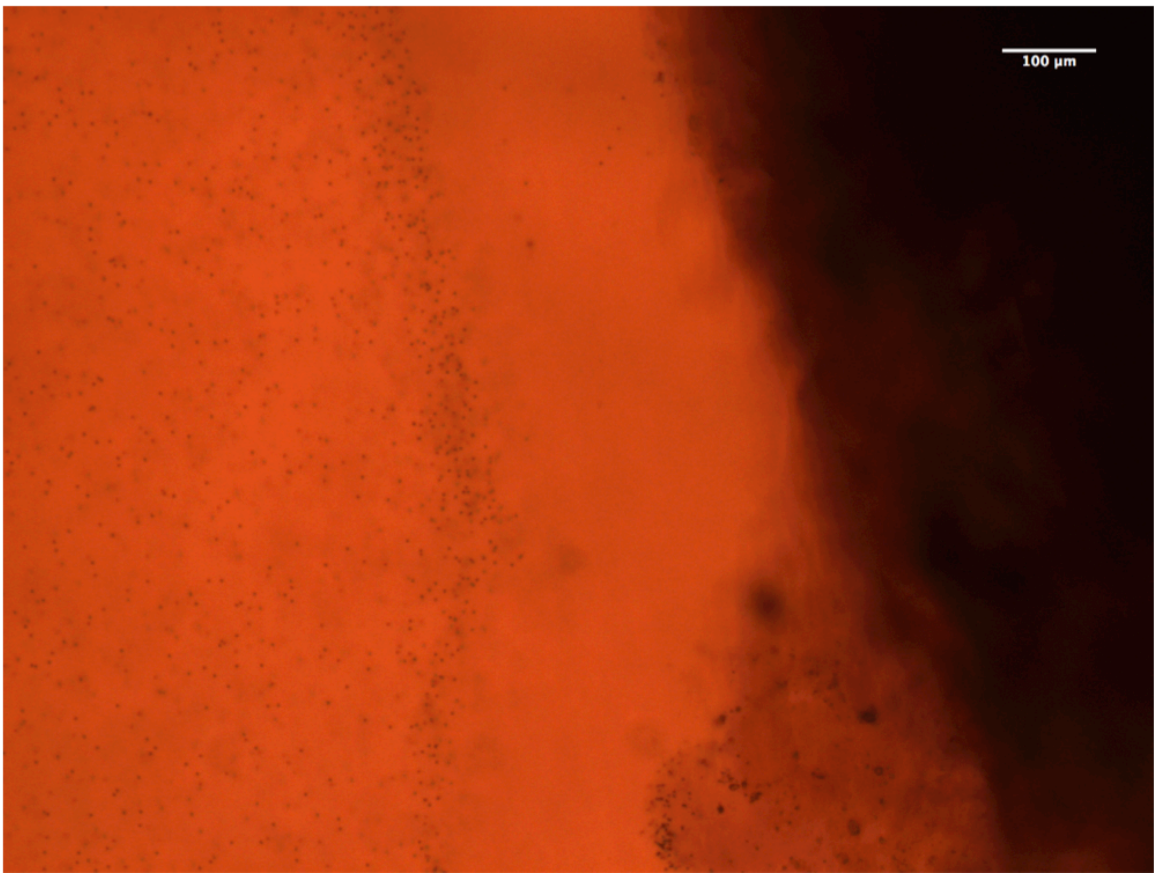

Figure 2.2 Exclusion zone (EZ) next to ox-tail tendon. The dark region to the right of the figure is tendon. The scale bar denotes 100 µm.

The gel from Ampullae of Lorenzini (AoL) was next used to check for EZ and representative micrograph is shown in figure 2.3 Unlike the tendon and brown algae, AoL gel showed rather 'patchy' exclusion zone at its surface. There were regions of EZ, but other parts did not show notable EZ. Another notable feature is that the size of EZ is notably smaller than those found near tendon and brown algae, about 80 µm.

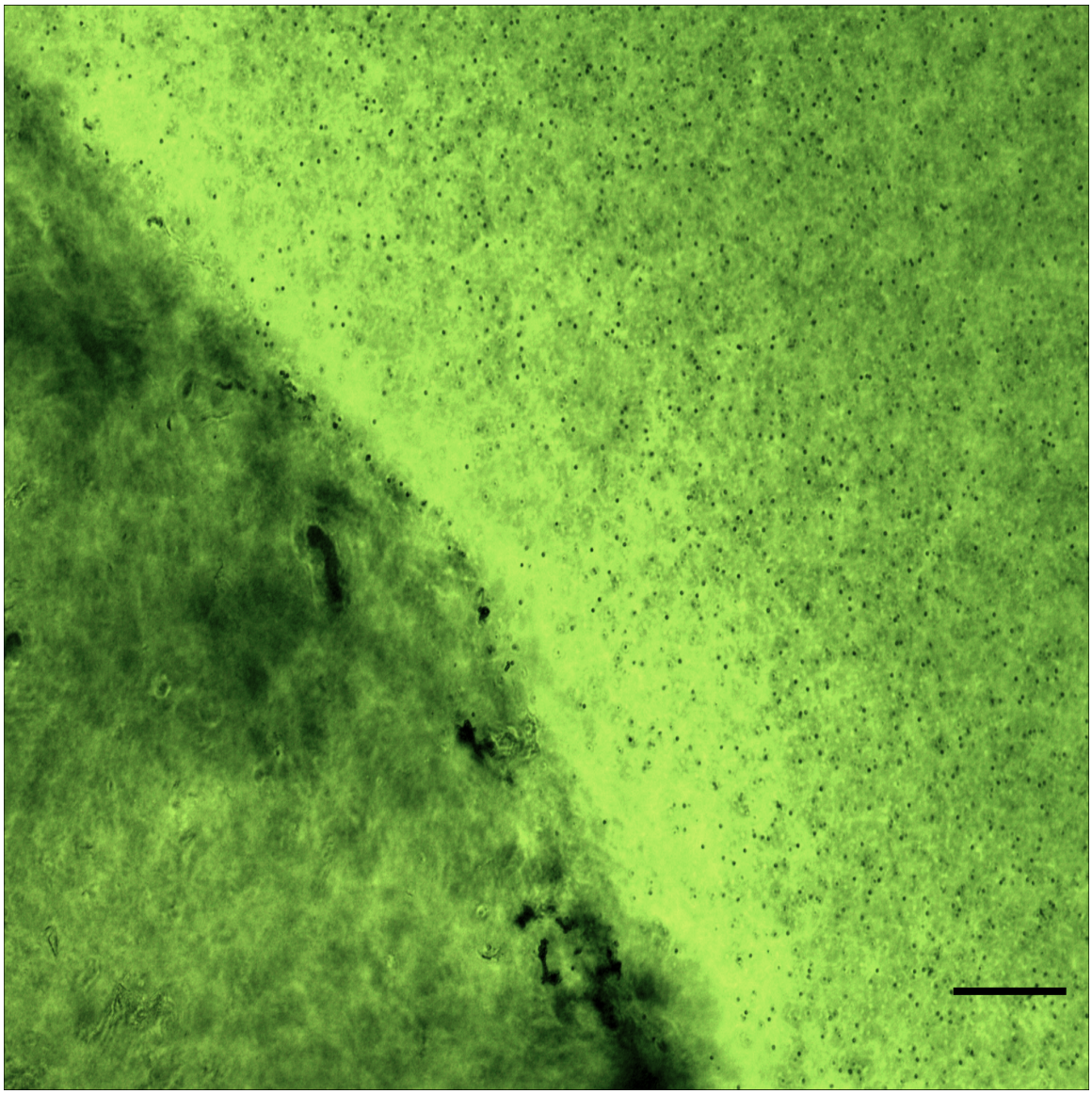

Figure 2.3 Exclusion zone (EZ) next to gel from Ampullae of Lorenzini. The darker part to the left of image is the gel. The scale bar denotes 100 μm.

A significant aspect of the exclusion zone (EZ) is its negative electrical potential. The potential is most negative next to the nucleating surface and diminishes toward zero at the EZ-bulk water boundary. The implication of the negative potential is that the EZ

may contain negative charge. But, if the EZ were negatively charged, then a positively charged counterpart ought to exist somewhere, and we considered whether the bulk water might have excess unbound protons ejected from EZ.

Figure 2.4 shows an image of a narrow water-containing chamber with a Nafion sheet placed at the bottom. A universal pH-indicator dye was added to the water in concentration as per the manufacturer's recommendation. The Nafion sheet appears dark red because of the local acidity. Just above and below the Nafion are clear zones, from which the dye is excluded in much the same way as microspheres are excluded. Above this exclusion zone is a rainbow of colors, indicating a steep pH gradient. The red color indicates pH <3; the colors above indicate progressively higher pH levels, with near neutrality (pH=7) at the top.

The dye-free regions above and below show roughly the same dimension as EZ marked with microspheres. Hence, it seems that EZ effectively exclude solutes of molecular dimensions. Further, EZ size does not depend much on the size of the solutes. The result gathered here represent a more complete story of charge separation associated with EZ formation. It seems that water becomes negatively charges as it ejects protons or hydronium ions out to the bulk, creating charge separation across the boundary of EZ.

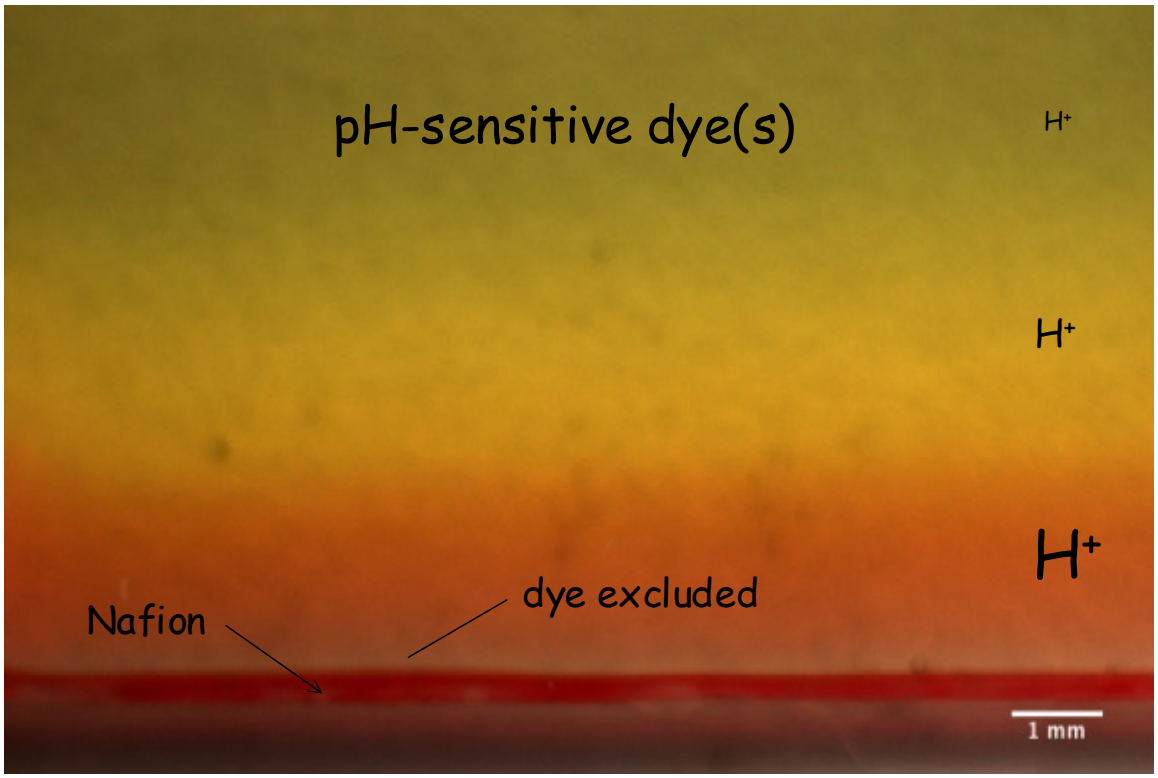

Figure 2.4 pH distribution next to exclusion zone. The nafion strip is colored red due to local acidity. The clear zone above and below nafion shows exclusion of molecular dyes out to ~200 µm. The region above nafion shows diminishing acidity further away from nafion.

The EZ's liquid-crystalline-like nature implies a cohesiveness among constituent elements, which in turn implies that the ensemble should have higher viscosity than bulk water. To test this expectation, we used falling ball viscometry. A strip of Nafion

was glued to the bottom of an experimental chamber, which was filled with water. The velocity of descent of spheres was tracked in order to determine whether spheres might slow down as they descended into the EZ.

The results are shown in Figure 2.5 A reduction of velocity near the Nafion surface was found for both the 10 and 15µm spheres. For the 5 µm spheres the decline in velocity was most pronounced, reaching a value less than 0.01 µm/sec at heights less than 1,000 µm.

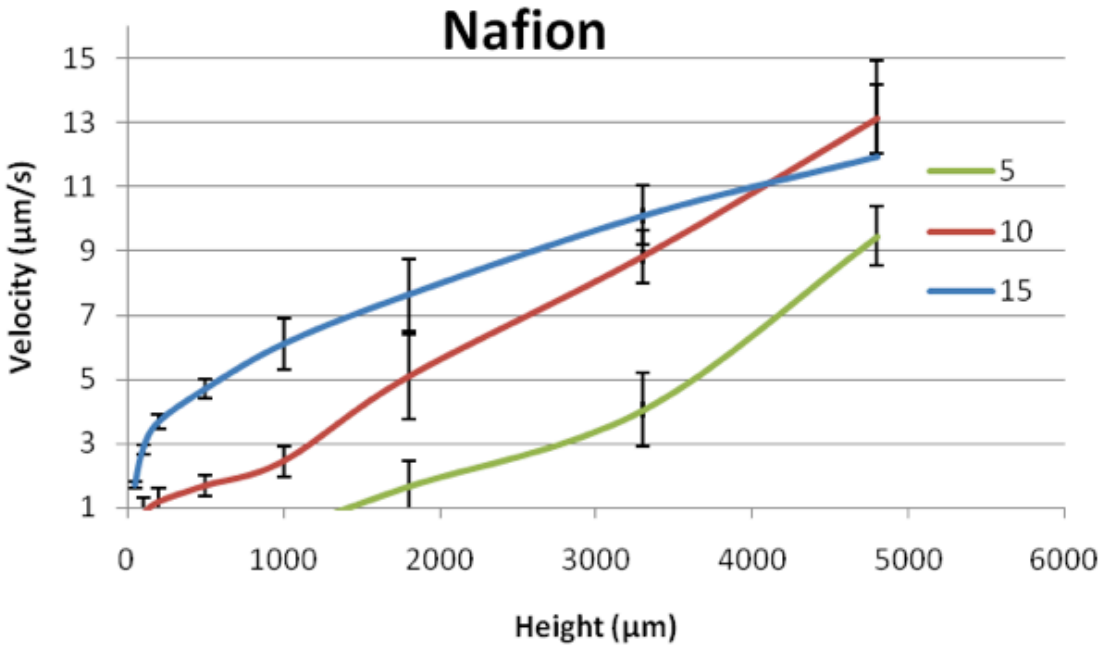

Figure 2.5 Velocity as a function of height above the Nafion surface, for 5, 10 and 15-µm diameter polystyrene microspheres.

From the values of velocity, it was possible to compute the viscosity from the simplified version of the Navier-Stokes equation. Thus,

$$V_s(y) = \frac{2}{9}\frac{r^2 g(\rho_p - \rho_f)}{\eta}\vec{y}$$

where V_S is the particle's settling velocity (m/s), *r* is the Stokes radius of the particle , *g* is the gravitational acceleration, ρ_p is the density of the particles, ρ_f is the density of the fluid, and η is the fluid viscosity. For simplicity, nonlinear convective forces were not considered and fluid density was assumed constant. It was also assumed that the microspheres were falling at their terminal velocity.

The computed results for viscosity are shown in Figure 2.6 Note that computed viscosity increases markedly near the Nafion surface. By contrast, results of Figs 2.7 show that the near-surface viscosity increase is absent for substances that have little or no exclusion zone. Hence, the EZ is considerably more viscous with viscosity of up to six times higher, compared with water next to non-EZ-generating surfaces.

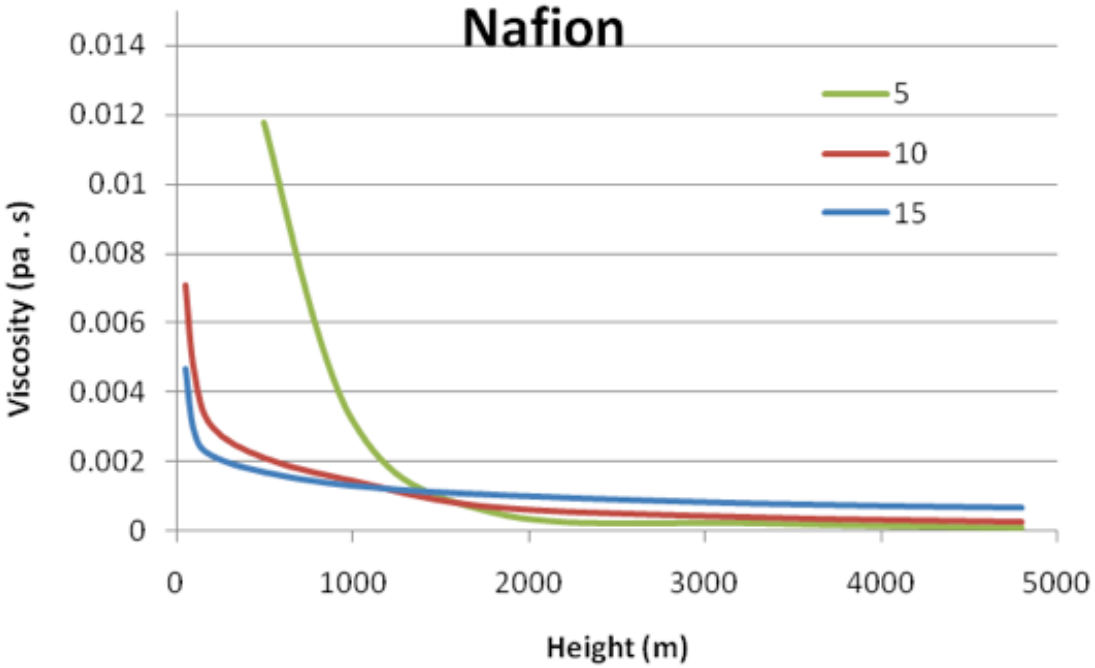

Figure 2.6 Computed viscosity as a function of distance from Nafion surface for 5, 10 and 15 μm diameter polystyrene microspheres.

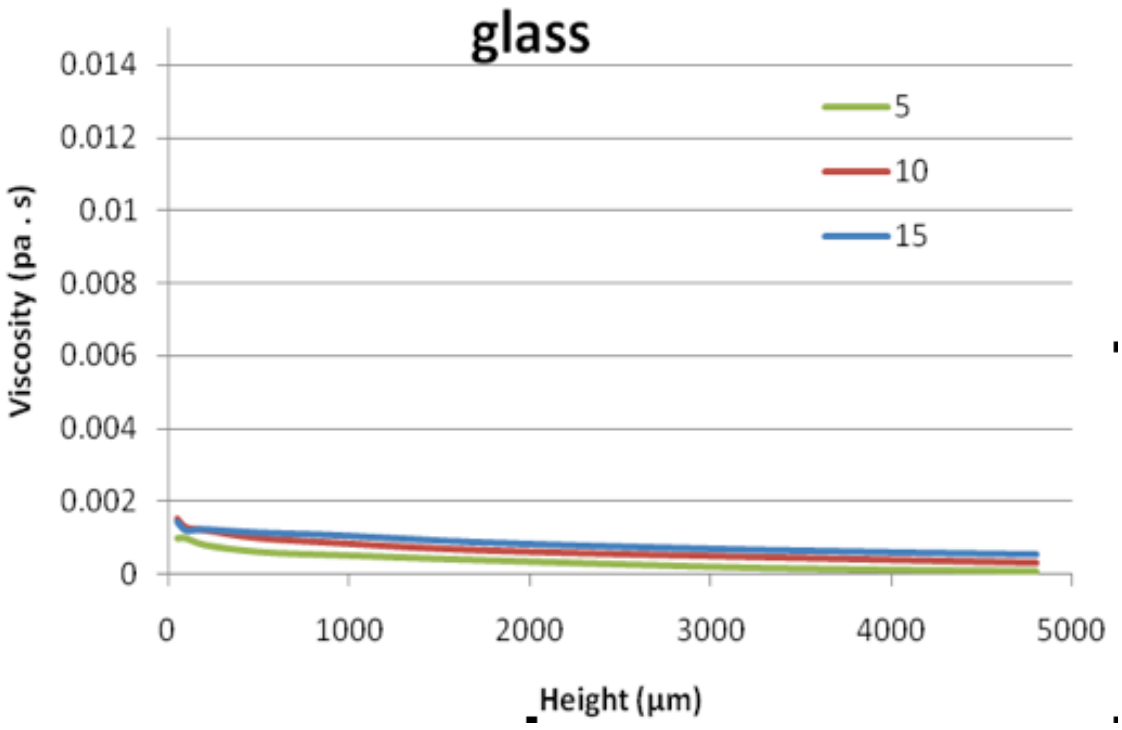

Figure 2.7 Computed viscosity as a function of distance from control glass surface for 5, 10 and 15 µm diameter polystyrene microspheres.

2.5 Discussion

This study was carried with a goal of further examining the generality of EZ nucleating surfaces in biological realm and EZ's physico-chemical properties. Three different biopolymers were used as model systems: brown algae, cow tendon and gel of Ampullae of Lorenzini (AoL). Though the origin of the three biological samples are vastly different, all of them showed similar results. All three samples showed distinct EZ with its dimension reaching hundreds of micrometers. Of these the brown algae and cow tendon showed more robust EZ with dimensions comparable to the EZ shown next to

nafion. The EZ next to gel of AoL, however, were more patchy. This difference is presumed to arise from the highly salty environment of gel of AoL. Previous results have shown that salt can decrease or almost eliminate EZ at sufficiently higher concentrations, and the much higher concentration of salt within the gel of AoL might be responsible for diminished EZ size and patchy EZs.

To better understand the process of EZ formation and the source of its negative electrical potential, conventional molecular pH dye was used to measure the pH of the zone beyond EZ. As in the case of microsphere markers, the molecular dyes were excluded from the EZ, demonstrating invariability of EZ formation on the size of the solutes. Further, highly acidic environment was observed at the EZ-bulk water boundary, indicating that the EZ acquired its negative charge by ejecting the acidic moieties of water in form of protons and hydronium ions. Hence, It is presumed that the rejection of acidic moieties of water is a necessary condition for EZ to from into its stable structure. Further, the resulting EZ induced charge separation opens new doors to clean source of energy, solely based on water.

The viscosity of EZ was next determined by using falling-ball viscometry, and the results indeed show that the viscosity of EZ is significantly higher compared to that of bulk water. Further, the viscosity of water is highest near the nucleating surface, and diminish over the distance away from surface. Once striking feature of the viscosity

measurement is its resemblance to electric potential measurement. When spatial distribution of electrical potential is measured, the near surface zone has the biggest negative electrical potential and the potential diminish with distance away from the surface. Hence, one can draw the conclusion that the higher viscosity if correlated with negative potential. In other words, the most negatively charged zone has the biggest degree of structuring.

From these results, we can come up with a physical model of EZ. Next to EZ generating surface, water is the most structured and are organized in liquid crystalline-like array. With distance away from the nucleating surface, there are more and more defects, presumably consisted of proton rich water, hence diminishing the negative potential.

2.6 References

1 Mishima, O. & Stanley, H. E. The relationship between liquid, supercooled and glassy water. *Nature* **396**, 329-335 (1998).

2 Wernet, P. *et al.* The Structure of the First Coordination Shell in Liquid Water. *Science* **304**, 995-999 (2004).

3 Zheng, J.-m. & Pollack, G. H. Long-range forces extending from polymer-gel surfaces. *Physical Review E* **68**, 031408 (2003).

4 Zheng, J.-m., Chin, W.-C., Khijniak, E., Khijniak Jr, E. & Pollack, G. H. Surfaces and interfacial water: Evidence that hydrophilic surfaces have long-range impact. *Advances in Colloid and Interface Science* **127**, 19-27, doi:http://dx.doi.org/10.1016/j.cis.2006.07.002 (2006).

Chapter 3. Dynamics of Interfacial Water Studied with NMR Spectroscopy

3.1 Abstract

In suspensions of Nafion beads and of cationic gel beads, NMR spectroscopy showed two water–proton resonances, one representing intimate water layers next to the polymer surface, the other corresponding to water lying beyond. Both resonances show notably shorter spin–lattice relaxation times (T1) and smaller self-diffusion coefficients (*D*) indicating slower dynamics than bulk water. These findings confirm the existence of highly restricted water layers adsorbed onto hydrophilic surfaces and dynamically stable water beyond the first hydration layers. Thus, aqueous regions on the order of micrometers are dynamically different from bulk water.

3.2 Introduction

Water is arguably the most important liquid on earth. Despite its significance and abundance, water remains mysterious in many ways, and many anomalous features remain incompletely understood [1]. Among the lingering mysteries are the dynamics at interfaces. Dynamics of interfacial water is of critical importance to biology, chemistry, and geo-climatic and atmospheric processes, as many catalytic reactions occur at interfaces [2, 3]. Yet the properties of interfacial water are poorly understood.

It is commonly accepted that in the vicinity of hydrophilic interfaces water organizes into ice-like water, which project from the surface by a few nanometers [4-6]. Partly due to the rapid development of surface-characterization techniques, most recent work has focused almost exclusively on near-surface dynamics, i.e., dynamics of the first few molecular layers. Consequently, possible macroscopic effects have not been widely studied.

On the other hand, decades of early work has demonstrated that water can exhibit physical properties quite different than those of bulk water, out to distances on the order of micrometers [7].

Work begun several years ago in our group indicates that the interfacial water zone may extend unexpected far from hydrophilic surfaces [8]. Those surfaces include a wide range of materials such as ion-exchange resins, polymers, hydrogels, functionalized monolayers, biological tissues and metal oxides. The near-surface aqueous zones exhibit a number of unique properties, the most notable being that suspended particles (e.g. mono-disperse colloids) are excluded from the surface to distances of several hundred micrometers; thus, these particle-free zones have been termed exclusion zones (EZs). EZs exhibit a variety of physical properties differing from those of 'bulk' water. They bear negative charge, as much as 150 - 200 mV near the nucleating surface; they exhibit increased dynamic viscosity; and they show diminished infrared emissivity and retarded T2 relaxation times [9]. These properties imply that the water within exclusion zones may be more ordered than 'bulk' water.

Nuclear magnetic resonance (NMR) spectroscopy is a well-established technique for determining the chemical structure and environment in aqueous systems [10]. NMR chemical shift, relaxation, and self-diffusion measurements have proved especially successful for probing interfacial water structure and dynamics near various biological and polymeric surfaces [11-13]. In the present study, high-resolution NMR spectroscopy was employed to measure chemical shift, spin-lattice (T1) relaxation and self-diffusion coefficient of interfacial water in order to obtain a more detailed physical picture of molecular environment within the exclusion zone.

3.3 Methods and Materials

3.3.1 General

For all experiments, deionized water (type I HPLC grade (18.2 MΩ-cm)) was collected from a Barnstead D3750 Nanopure Diamond purification system. A 5% D2O/H2O (v/v) solution was used in all experiments, and was prepared by diluting 99.9% deuterium oxide (Cambridge Isotopes DLM-4-100) with deionized water.

Two types of polymer beads were used as EZ-nucleating surfaces. One was analytical-grade cationic ion-exchange resin, 180-425 µm diameter, in H-form (AG 50W-X8, Bio-Rad, CA) with cross-linking of 8% divinylbenzene (DVB). The other was Nafion, a sulfonated tetrafluoroethylene based fluoropolymer, with dimensions on the order of 300-500 µm in H-form (495786, Sigma-Aldrich, MO). Both types of polymer have abundant sulfonic acid sites, providing highly hydrophilic environments.

Beads were first hydrated in experimental solvent for one hour to ensure sufficient level of hydration. Once hydrated, the beads were placed in a standard 5 mm OD NMR tube (WG-1241-7, Wilmad Glass, NJ) and left to settle in 100 mL of 5% D2O/H2O (v/v). For both types of bead systems, the final height of tightly packed beads was 3 cm as measured from the bottom of the tube.

3.3.2 NMR spectroscopy

The 1H NMR spectra were recorded on a 750 MHz Bruker AVANCE II NMR spectrometer equipped with a 1H {C,N} high-resolution triple resonance probe with Z-gradient. A spectroscopic standard sample of 1% sucrose in 10% H2O/D2O (v/v) solvent mixture was used to shim the magnet to optimal B0 field homogeneity prior to recording the spectra from the resin beads and Nafion beads. Raw data were collected with 8K time-domain points with a spectral width of 10 ppm centered at 5.0 ppm, recycle delay of 1 s, and acquisition time of 0.55 s. These were then Fourier transformed without zero filling.

Proper referencing of spectra was ensured by adding a trace quantity of DSS (4,4-dimethyl-4-silapentane-1-sulfonic acid) as external reference for one sample and the ensuing spectrum reference frequency was used for calibrating the 0 ppm in subsequent sample preparations. Five identical NMR sample tubes were prepared for repeating the measurements and establishing consistency of the results. The sample temperature was set to 298 K +/- 0.1 K and the accuracy of this value at the sample was confirmed by measuring the chemical shift difference of the doublet of neat methanol and cross checking against published values.

3.3.3 Spin-echo (T1) Relaxation Measurements

Spin-lattice (T1) relaxation of water in the polymer/water system was measured using inversion-recovery (π - τ_1 - π/2) pulse sequence. Longitudinal magnetization was collected with 10 time delays varying from 1 ms to 25 s. A standard inversion recovery curve with three unknowns was fitted to the integrated volume of each resonance as a function of the delay. When a single T1-component fit exhibited a substantial number of outliers leading to poor chi-square statistics, a two-component fit was employed, leading to excellent fits with no outliers from the recorded set of data points.

3.3.4 Self-diffusion Coefficient Measurements

Self-diffusion measurements of the two chemical shifts of water in polymer/water system were carried out using the stimulated spin-echo pulse sequence $\left(\frac{\pi}{2} - \ g(\delta) - \frac{\pi}{2} - \ \Delta - \frac{\pi}{2} - g(\delta)\right)$. The attenuation in spin-echo amplitude was recorded as a function of increasing gradient strength, g. In an isotropic system, where diffusion is unrestricted, the echo attenuation is given by the Stejskal-Tanner equation:

$$\psi(\delta, g, \Delta) = exp\left(-\gamma^2\delta^2 g^2 D\left(\Delta - \frac{\delta}{3}\right)\right)$$

Here γ is the gyromagnetic ratio, δ and g are duration and amplitude of the magnetic-field gradient, respectively, Δ is the duration for phase encoding the diffusing magnetization, and D is the bulk self-diffusion coefficient of the solvent. D was

computed from the slope obtained by fitting eq. (1) as a function g2 to the echo amplitude decay. Prior to making measurements with the bead systems, the bulk self-diffusion coefficient of deionized water was measured at 298 K and confirmed to agree with literature values.

3.4 Results

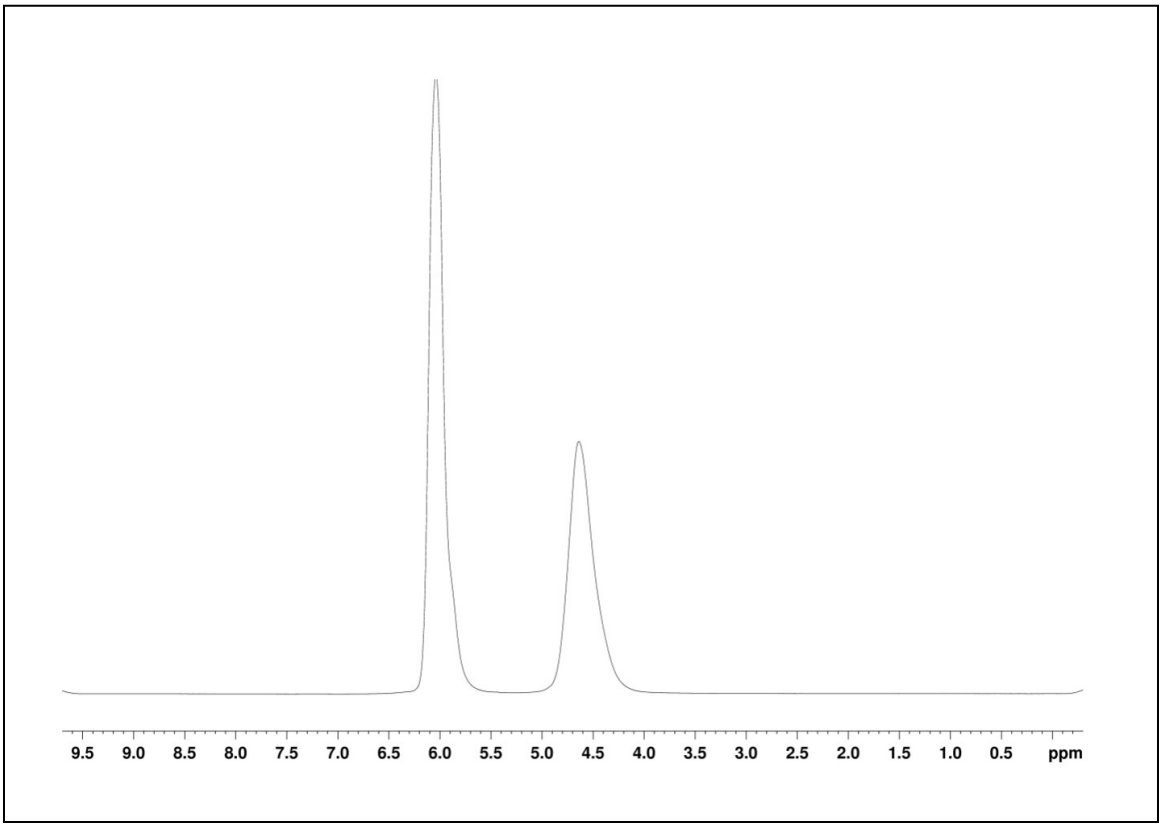

Figure 3.1 A fully relaxed 1D-1H NMR spectra of cationic resin/water system. Two water proton resonances are observed at 6.0 ppm and 4.63 ppm each corresponding to 'internal' and 'interstitial' water respectively.

Figure 3.1 is a representative 1H NMR spectrum of cationic resin/water system at 298° K in thermal equilibrium. Two water-proton resonances are evident, at 4.63 ppm and 6.00 ppm, indicating two distinct and magnetically unique water species as observed within the NMR timescale. The standard chemical shift value of 1H resonance at 298 K for the HOD peak in an H2O: D2O mixture is 4.8 ppm [14]. Since the frequency axis was referenced to an external standard, i.e. DSS, it is reasonable to identify the up-field resonance at 4.6 ppm as that of less restricted water in the interstitial region between the beads. The down-field shift to the resonance at 6.00 ppm is indicative of a more 'deshielded' environment of the water, and therefore corresponds to highly restricted water layers adsorbed onto polymer surface inside and around the resin. Integrating a fully relaxed 1H spectrum shown in Fig. 1 yielded 1: 1 ratio of area under the peaks corresponding to internal water and the interstitial water respectively. FWHM line widths of the downfield-shifted peak are approximately 80% of the peak for interstitial water at 4.63 ppm.

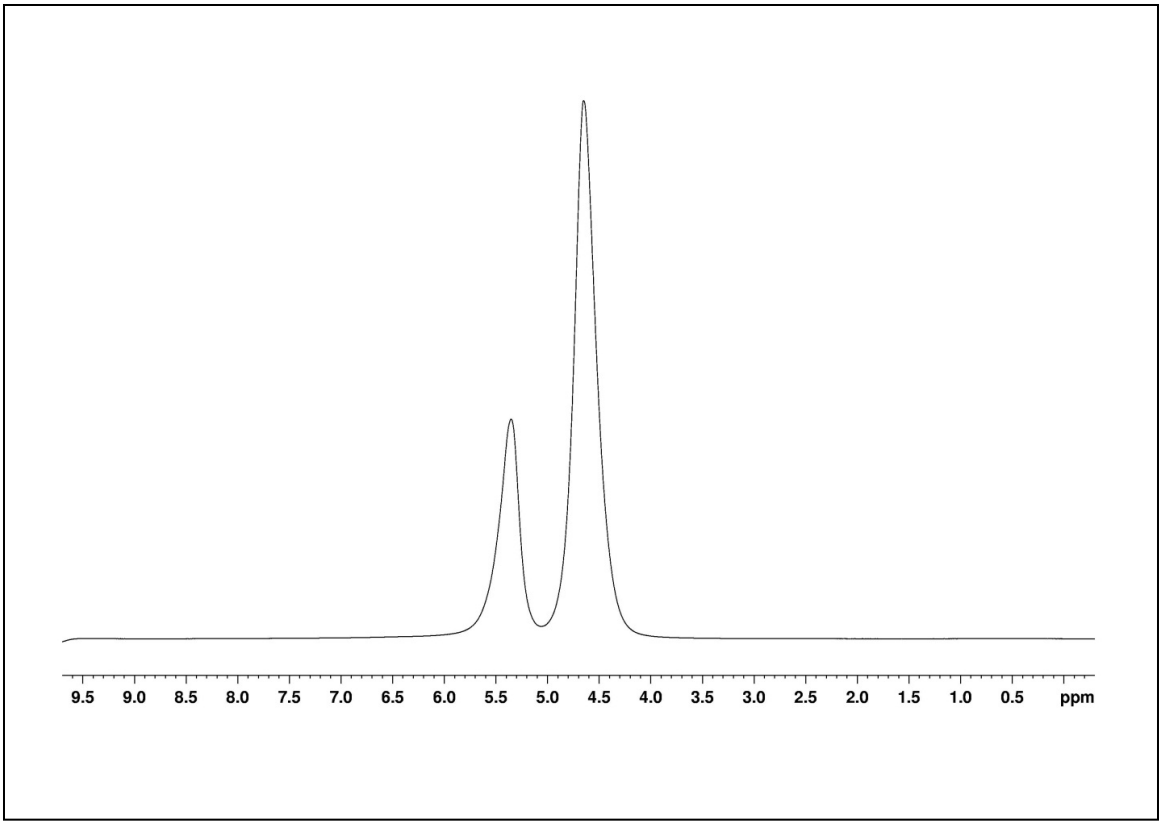

Figure 3.2 A fully relaxed 1D-1H NMR spectra of Nafion bead/water system. Two water proton resonances are observed at 5.35 ppm and 4.61 ppm each corresponding to 'internal' and 'interstitial' water respectively.

Figure 3.2 shows a representative 1 H NMR spectrum of Nafion bead/water system at 298° K in thermal equilibrium. As in the cationic resin/water system, two chemical shifts of water protons are observed. The up-field resonance at 4.61 ppm is assigned as interstitial water lying between the Nafion beads, while the down-field resonance at 5.35 is assigned to adsorbed water inside and around Nafion beads. The integrated area

under each resonance peak shows an intensity ratio of 7 to 3, interstitial to internal water respectively. FWHM line widths of the two resonances are roughly the same.

To further characterize the observed water species in each system, longitudinal relaxation (T1) and self-diffusion coefficients were measured for the respective chemical shifts. Five samples were used for T1 relaxation and self-diffusion measurements to verify the robustness and consistency of the results.

T1 relaxation and diffusion coefficients of the two water proton resonances in cationic resin/water system are shown Table 3.1. T1 relaxation for interstitial water identified by the peak at 4.63 ppm was measured to be 1.82 s, which is significantly shorter than T1 relaxation time of 'bulk' water at 298K [15]. The corresponding self-diffusion coefficient of interstitial water, 14.91E-10 m2/s, was measured to be about 60% of the known diffusion coefficient of 'bulk' water at 298K, namely, 23.00E-10 m2/s [16].

Table 3.1 Longitudinal relaxation (T1) times and self-diffusion coefficients of water species in cationic exchange bead/water system.

δ_{HOD} (ppm)	6.00		4.63
T1 (s)	Component 1	Component 2	1.82
	0.532	1.511	

D_{HOD} (1E-10 m2/s)	6.47	14.91

Corresponding results for the Nafion resin/water system are shown in Table 3.2. T1 relaxation of up-field peak at 4.61 ppm corresponding to 'interstitial' water was 1.34 s at 298K, indicating faster longitudinal relaxation than bulk water as in the case of cationic resin/water system. The diffusion coefficient of 'interstitial' water in Nafion resin/water system was determined to be 16.91E-10 m2/s, about 25 % smaller than that of 'bulk' water. In order to rule out radiation damping as the cause of the observed shorter T1 values, the same measurements were made with 300, and 500 MHz spectrometers and relaxation times on the same order of magnitude was confirmed.

Table 3.2 Longitudinal relaxation (T1) times and self-diffusion coefficients of water species in Nafion bead/water system.

$\boldsymbol{\delta_{HOD}}$ (ppm)	5.35		4.61
T1 (s)	Component 1	Component 2	1.34
	0.190	2.053	
D_{HOD} (1E-10 m2/s)	5.39		16.91

In both systems, the T1 curve-fitting procedure for the down-field water peak yielded rather poor results if only a single exponential recovery curve was employed, indicating that a single T1 component cannot explain the data accurately. In contrast, when a two-component fit was used, the same set of experimental data gave excellent fit statistics without the necessity to remove even a single data point. This indicates that there are two distinct relaxation times. Thus, both tables show a faster and a slower T1 component for the down-field peaks, which correspond to highly-restricted water adsorbed on the hydrophilic sulfonate-group sites within the polymer matrix.

The self-diffusion coefficient of water inside the cationic resin matrix at 298K was 6.47E-10 m2/s. The self-diffusion coefficient of water inside Nafion resin matrix at 298K was slightly smaller, albeit on the same order of magnitude, 5.39 E-10 m2/s. The fact that both D values of 'internal' water were significantly lower than that of bulk water is self-consistent with the observed shorter T1 values compared to that of bulk. At room temperature, T1 relaxation is mainly mediated by translational and rotational diffusion in a solution, and the relaxation efficiency is inversely proportional to the rate of diffusion. The shorter diffusion constants of both 'internal'' and 'interstitial' waters are indicative of restricted environments that the water molecules experience. Fundamental NMR relaxation theory of liquids indeed stipulates that the T1 relaxation times are correspondingly shorter than that of water in 'bulk' in slow-diffusing environments.

3.5 Discussion

The most notable finding in this study is that there is no 'bulk' water present in both bead suspensions, as indicated by T1 relaxation and self-diffusion measurements. The adsorbed water in and around both Nafion and ion-exchange beads is shown to be anisotropic due to confined geometry within polymer matrix [17-19], and therefore it is expected that 'internal' water has much slower self-diffusion and shorter T1 relaxation than 'bulk', indicating highly restricted molecular environment.

Interestingly, our experimental data show that the 'interstitial' water as well has notably shorter T1 relaxation and smaller self-diffusion coefficient than 'bulk' water. This was true in both experimental systems. In the case of the cationic resin system, maximal packing of 180 μm diameter spherical beads in face center cubic lattice-like arrangement would leave the interstitial region to be on the order of tens of micrometers in size. Assuming that the packing was not ideal and taking into account the variability in ion-exchange resin size, one can expect even larger dimensions of interstitial water region. For the Nafion system, this interstitial region is expected to be even larger due to the beads' irregular shape and larger dimensions, and this is demonstrated by larger 'interstitial' to 'internal' water peak area ratio shown in Figure 3.2 vs. Figure 3.3.

While such extensive effects of the surface on nearby water dynamics may seem counter-intuitive, previously observed characteristics of the EZ near hydrophilic surfaces indicates that nearby water can take on a more stable form out to distances of tens of micrometers [9]. Further, convergence of EZs extending from two neighboring nucleating surfaces within 100 μm, as in this case, have been observed [20]. It is then reasonable to assume the 'interstitial' water in both systems to be composed of mostly EZ water, and thus, the restricted water dynamics within the 'interstitial' region observed here complements other known EZ characteristics.

T1 relaxation time and the self-diffusion coefficient of solutions can be profoundly affected by the solute that is dispersed in the medium, and the presence of trace impurities could in theory account for observed changes in T1 relaxation and diffusion coefficient of water. However, the 1H chemical shift spectrum of a given compound is a robust fingerprint of what is present in a solution. One may then state with reasonable certainty that there are no impurities of unknown origin in our experimental system, evidenced by the absence of any anomalous peaks present other than water proton peaks.

Invoking impurities as cause of change in water dynamics also lacks theoretical rationale. No well-established theory of chemical shifts in solution NMR can account for the observed 'multiple resonance' spectra of water found in two distinct sample

preparations studied here, as due to the effect of 'trace impurities' of unknown origin. Indeed, to our knowledge, there are no aqueous NMR spectra that exhibit anything other than a single 'bulk' water NMR peak in and around 4.8 ppm at 298 K. This is true, independent of the kind of solute that is dissolved in water, ranging from small organic molecules to large biomolecules such as proteins or nucleic acids.

The only reports found in literature that had recorded such multiple resonances of water are associated with biological tissues or polymer systems that are quite similar to the ion exchange resins or Nafion that were used in this study [21-23]. These studies, however, did not address the dynamics of water lying outside the polymers or tissues.

Thus, the unique dynamic properties of water presented in this study are evidently not due to the presence of impurities, but rather caused by presence of hydrophilic surfaces. While chemical shift provides unique structural identification of a molecule, it does not report the possible existence of intermolecular interactions and the resulting long-range ordering of a solution system. In contrast, T1 relaxation and self-diffusion measurements do provide this crucial information, as shown here. In fact, although the chemical shift of EZ water is quite similar to that of bulk-water, albeit the small difference of 0.2 ppm, the T1 and D values turn out to be clear identifiers of the more restricted and long-range coupled nature of EZ water.

Hence, the most interesting implications of this study may be that in the presence of Nafion, resin beads, or other hydrophilic surfaces, water is readily organizing and changing its otherwise 'bulk' dynamic properties extensively. The results of this study therefore underscore the organizational and dynamic complexity of water juxtaposed next to certain classes of surface.

3.6 References

1. Finney, J.L., Philosophical Transactions: Biological Sciences, 2004. 359(1448): p. 1145-1165.

2. Catalano, J.G., P. Fenter, and C. Park, Geochimica et Cosmochimica Acta, 2009. 73(8): p. 2242-2251.

3. Senadheera, L. and M.S. Conradi, Journal of Physical Chemistry B, 2007. 111(42): p. 12097-12102.

4. Noguchi, H., et al., Physical Chemistry Chemical Physics, 2008. 10(32): p. 4987-4993.

5. Tian, C., et al., J Am Chem Soc, 2008. 130(39): p. 13033-9.

6. Smith, J.D., et al., Science, 2004. 306(5697): p. 851-3.

7. Henniker, J.C., Reviews of Modern Physics, 1949. 21(2): p. 322-341.

8. Zheng, J.M. and G.H. Pollack, Phys Rev E Stat Nonlin Soft Matter Phys, 2003. 68(3 Pt 1): p. 031408.

9. Zheng, J.M., et al., Adv Colloid Interface Sci, 2006. 127(1): p. 19-27.

10. Levitt, M.H., Spin Dynamics: Basics of Nuclear Magnetic Resonance. 2002, New York: Wiley.

11. Siemer, A.B. and A.E. McDermott, J of the Am Chem Soc, 2008. 130(51): p. 17394-17399.

12. Mao, Y.G. and Y. Ba, Biophysical Journal, 2008. 95(1): p. 493-493.

13. Nunes, T.G., E.W. Randall, and G. Guillot, Solid State NMR, 2007. 32(2): p. 59-65.

14. Gottlieb, H.E., V. Kotlyar, and A. Nudelman, J of Organic Chemistry, 1997. 62(21): p. 7512-7515.

15. Simpson, J.H. and H.Y. Carr, Physical Review, 1958. 111(5): p. 1201.

16. Holz, M., S.R. Heil, and A. Sacco, Physical Chemistry Chemical Physics, 2000. 2(20): p. 4740-4742.

17. Webber, J.B.W., et al., Journal of Physics-Condensed Matter, 2007. 19(41): p. -.

18. Webber, J.B.W., et al., Magnetic Resonance Imaging, 2007. 25(4): p. 533-536.

19. Liu, E., et al., Journal of Physics-Condensed Matter, 2006. 18(44): p. 10009-10028.

20. Mao, Y.G. and Y. Ba, Biophysical Journal, 2006. 91(3): p. 1059-1068.

21. Gough, T.E., H.D. Sharma, and Subraman.N, Canadian Journal of Chemistry, 1970. 48(6): p. 917-&.

22. Lenk, R., M. Bonzon, and H. Greppin, Chemical Physics Letters, 1980. 76(1): p. 175-177.

23. OConnor, P.J., et al., Macromolecules, 1996. 29(24): p. 7872-7884.

Chapter 4. Thermodynamic Studies of Interfacial Water and the Role of Hydrophilicity

4.1 Abstract

Understanding interfacial dynamics is crucial in broad natural and industrial processes. In order to study energetics of interfacial water, forward-looking infrared (FLIR) camera was used to image freezing induced latent heat release from interfacial water. Image analysis revealed that water next to Nafion showed significantly lowered magnitude of latent heat release in distance dependent manner. The magnitude of latent heat release was the smallest right next to the surface and increased out to about 300 μm from the surface, from which point on the magnitude stayed the same. Unlike the water near Nafion, water next to its hydrophobic counterpart, Teflon, did not show any distance dependence on latent heat release. Hence, the presence of hydrophilic surface lowers the magnitude of latent heat of nearby water. The results in turn indicate that the kinetic energy of water is lowered in the vicinity of hydrophilic surfaces.

4.2 Introduction

Water is omnipresent throughout our planet and influences us all throughout our daily lives. Hence, understanding the properties of water in different environments is crucial for ascertaining a fundamental understanding of nature. Despite such widely accepted central role of water within our natural systems, liquid water still remains a scientific challenge, as its properties differ vastly from those of other simple liquids [1]. Specifically, water near surfaces portrays unusual behaviors, and acts as though it is an entirely different phase of water from liquid [2,3].

It is generally believed that water near surfaces has distinct properties. On the theoretical front, such behavior derives largely on the DLVO theory, which combines van der Waals attraction force and electrostatic repulsion force due to electrical double layer [4]. As a consequence of the theory, the electrical double layer zone of water next to charged surfaces is believed to extend out to a few molecular layers of water, and no significant changes to that idea have been made for the past half a century.

On the contrary, more recent studies have shown that water near hydrophilic surfaces has markedly different properties from bulk water, and such surface effects can extend out extensively, to tens and hundreds of micrometers [5]. This surface zone of water,

termed exclusion zone (EZ), has many unique properties. It excludes wide range of solutes and particles; it has decreased diffusion and relaxation times of water protons; it has increased viscosity and negative electrical potential, among others [6,7].

Of these features, one particularly interesting result is decreased emission of infrared light from water near hydrophilic surfaces. While lowered infrared emission is generally interpreted to mean lower temperature according to Plank's law of blackbody radiation, lowered emissivity of water provides an alternative possibility. One plausible explanation is that water molecules near hydrophilic surfaces have lower kinetic energy, and hence lower emissivity compared with bulk water. Such interpretation of the IR emission data also complements previously observed properties of surface water, which collectively point to more stable state of water.

Traditionally, thermodynamic studies of liquids and phase transitions are explored using differential scanning calorimeter (DSC) [8]. In such experiments, heat is either added or removed from the liquid to bring the system to phase transition, and the resulting heat up-take or release is compared with another liquid of well-defined specific heat, such as deionized water. While DSC has been tremendously successful in describing thermal properties of widely varying systems, it does not provide any spatially resolved information. On the other hand, with recent advancements in infrared detector

technology, infrared thermography has been offered as an alternative. Combining with suitable IR optics, IR thermography can give spatially relevant information [9].

In this study, a forward-looking infrared (FLIR) camera is used to study liquid-solid phase transition of water near surfaces in order to understand spatially resolved energetics of water. From observing the latent heat of crystallization, kinetic energy of water near surfaces can be approximated with high-spatial resolution. Further, we study the effects of surface hydrophilicity on kinetics of nearby water.

4.3 Materials and Methods

4.3.1 General

For all experiments, type I water with a resistivity of 18.2 MΩ cm^{-1} was collected from Barnstead Nanopure water purification system and used in experiments. Before each experiment, all experimental chambers were thoroughly washed in type I water to remove impurities.

4.3.2 Chamber and freezing system

The experimental chamber was made from transparent acrylic and had a 25-mm threaded cylindrical hole in the center as shown in Figure 4.1. The threaded hole housed, in sequence from the bottom up: an aluminum disk, a water sample, a 200 µm thick Teflon ring spacer and an IR-transparent CaF_2 window (both from Specac Ltd, Slough, Great Britain), and a threaded compression ring to bring the CaF_2 window tightly to the Teflon spacer. A second Teflon ring spacer was place on top of the CaF_2 window in order to protect the window from being damaged by the top metal compression screw.

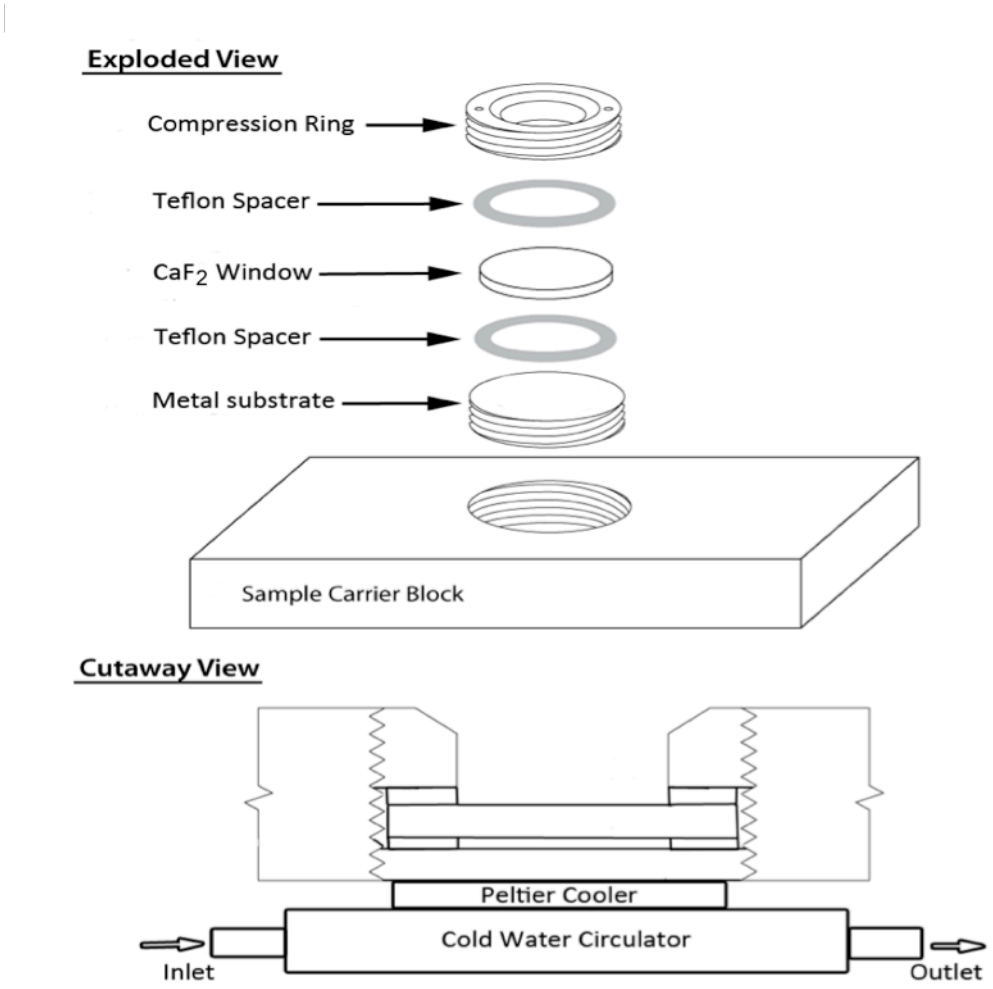

Figure 4.1 Schematic of experimental chamber and freezing set-up

The 5 mm-thick cylindrical disc of aluminum lying at the bottom of the chamber was in direct contact with the cold side of a Peltier device. The warm side of the Peltier device, beneath, contacted a metal jacket with cold (- 5 °C) ethylene glycol circulating through a refrigerating circulator (VWR International) for efficient removal of heat. A thermocouple was placed between the aluminum bottom and the Peltier device to feed back to the temperature controller (Omegaette PV) of the Peltier device.

In order to determine the effects of hydrophilicity, two types of surfaces were used. 200 µm thick Teflon was used as a model hydrophobic surface, while Nafion 117 (Sigma cat #: 31175-20-9) was used as a hydrophilic surface. Nafion was chosen as hydrophilic surface due to its chemical similarities to Teflon, so the two could be contrasted. As shown in figure 4.2. Nafion contains hydrophilic sulfonic acid groups attached to Teflon backbone. Hydrated thickness of the Nafion sheet was 200 µm. We set the target temperature to -20 °C.

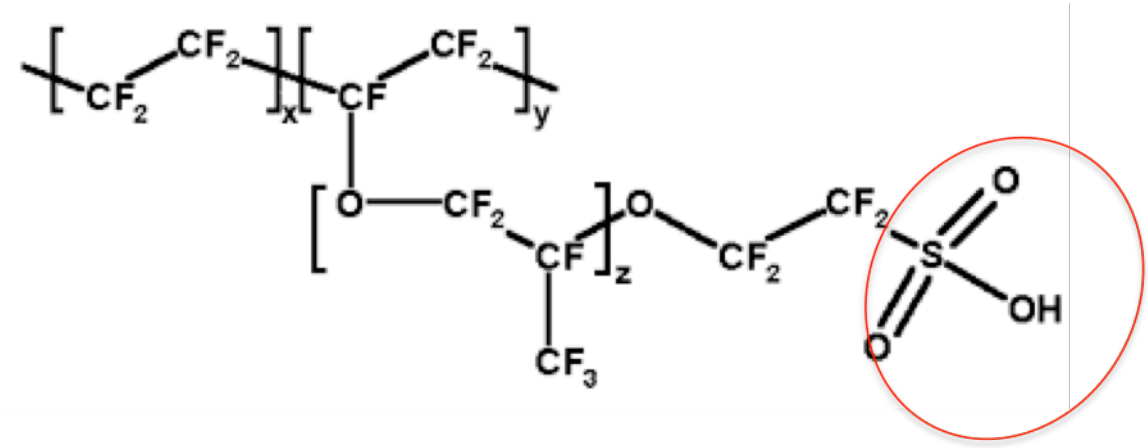

Figure 4.2 Chemical structure of Nafion. The red circle indicates hydrophilic sulfonate group; the rest of the structure is the same as Teflon

4.3.3 Forward-looking Infrared Imaging and Image Processing

The infrared radiation emitted from freezing of surface water was recorded using a forward-looking infrared (FLIR) camera located directly above the sample chamber. The camera used was a ThermoVision SC-6000 (FLIR Systems), equipped with InSb detector with spectral range of 3-µm to 5-µm, 640 X 512 pixel resolution, and 50 mK temperature sensitivity. To resolve the interfacial zone, a 4X infrared microscope lens (W.D. 3 cm) was attached to yield XX µm/pixel. The camera was placed above the interfacial zone of the freezing water, looking directly downward and focused on the top surface of the water as it cooled naturally.

The software used for visualization of the data was ExaminIR 1.2.0.1076 (FLIR Systems). ExaminIR generates a false-color image, with different colors or shades representing the intensities of the infrared radiation emitted by the subject and received by the InSb detector. In order to ascertain distance-dependent thermal characteristics of water from surface, a region of interest (ROI) was drawn as lines parallel to the surface at 100 μm intervals from the surface. The radiance value of each pixel was then averaged over the line-length to get average temperature values.

4.4 Results

In order to gain further insights into physical properties of interfacial water and the effects of hydrophilicity, water near Nafion and Teflon surfaces were cooled down to freezing and spatially resolved latent heat release in the interfacial zone was measured. Latent heat release is generally accepted to be a consequence of first-order water phase transition from liquid to solid. The energy corresponding to the difference in kinetic energies of the two states is released as heat.

When water was rapidly cooled from below, the freezing of water was signaled by emission of infrared light. Figure 4.3 shows sequential pictures of water freezing near the Nafion surface. As shown in the figure, the onset of IR radiation always starts at

Nafion-water interface. Another intriguing feature is that the propagation of infrared light is faster parallel to the surface than normal to the surface. This was especially the case within ~ 200 μm from the surface, the region corresponding to extent of exclusion zone. The infrared emission from water within Nafion was notably weaker than that observed next to the surface, indicating smaller kinetic energy of water inside the Nafion polymer.

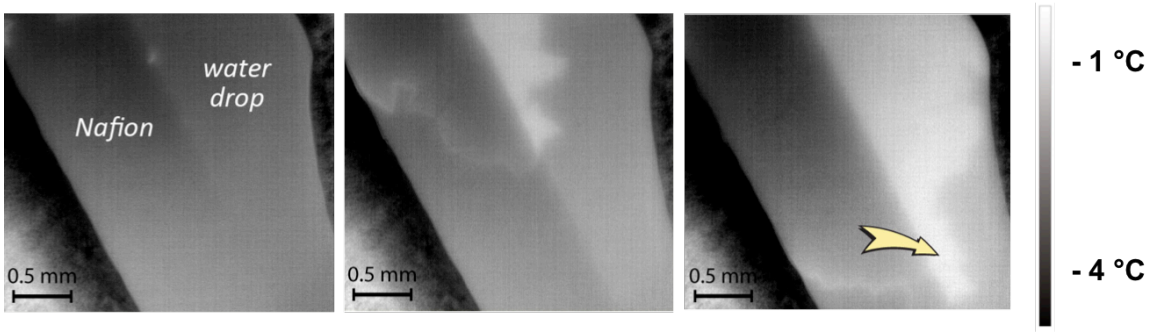

Figure 4.3 Sequential pictures showing the initial onset of infrared emission from freezing interfacial water next to Nafion with 100 ms delay between the frames. The gray strip in the middle is Nafion. Water is placed to the right of the Nafion strip. The gray color scale on the right of the figures denotes temperature, calibrated according to blackbody radiation from infrared photon count.

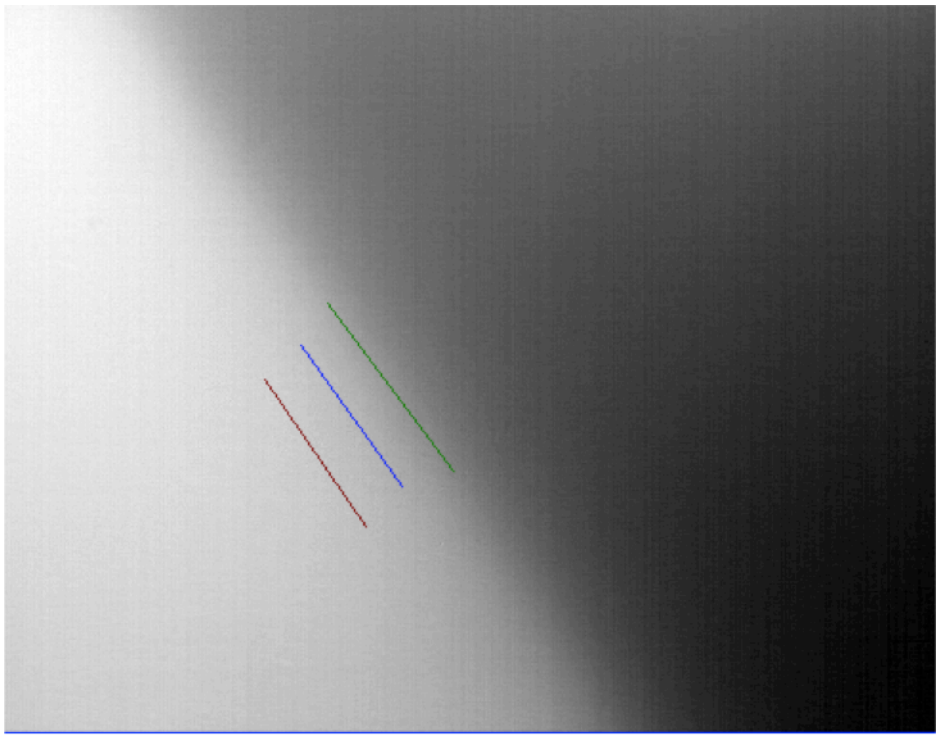

Figure 4.4 An image showing regions of interests (ROIs) near Nafion surface. The darker region to the right is Nafion, and the light region to the left is water at the moment of IR emission. The green line along the surface is taken as the Nafion-water interface and ROIs are drawn at 100 µm increments from the interface. The pixel values along the line are averaged to gain time-dependent mean temperature from freezing induced IR emission near the Nafion surface.

In order to study spatially resolved latent heat release and therefore kinetic energy of water, regions of interest (ROIs) were drawn as lines at 100 µm increments from the surface as shown in figure 4.4 and the average value across the line ROI was computed as a time series. A representative result is shown in figure 4.5. Several features are of

interest. First, if infrared emission is taken to be an initial event to signal liquid-water phase transition, water does not freeze until temperatures descend down to about –13.6 °C. This is contrary to widely accepted water freezing temperature of 0 °C. In fact, water froze at much lower temperatures than 0 °C in all experiments.

Looking more closely into figure 4.5 reveals more interesting features. Figure 4.6 is a zoomed-in version of figure 4.5, showing the time duration of infrared emission. There is a distance dependence of latent heat release. The amplitude of latent heat release is smallest at 100 μm away from the surface. Going from 100 μm to 200 μm, the amplitude increases and the trend continues up to 300-400 μm away from the surface, at which point the amplitude stops increasing. Assuming that the eventual ice formed at different distances away from surface has the same kinetic energy throughout, this indicates that the kinetic energy of water is the smallest closest to the surface and increases with increasing distance from the Nafion surface. Further, the dimension of decreased kinetic energy roughly matches the size of EZ. For example, the EZ has negative electrical potential energy and this is the biggest right near the surface. That negative potential decreases in amplitude over the dimension of EZ. Hence, there is a direct correlation linking the electrical potential gradient to gradient of kinetic energy within EZ; water with the most negative electrical potential has the lowest kinetic energy. This result complements previous studies demonstrating more ordered state of water next to the Nafion surface.

In addition to distance-dependent changes in amplitude of latent heat, the rate of heat release is significantly influenced by presence of the Nafion surface. where the rate of heat release is approximated by given slope in figure 4. At 100 µm away from the surface, the rate of temperature jump at the moment of freezing is much slower than farther away from the surface, and this indicates that the radiation starts and ceases at a much slower rate. At 200 µm away from the surface, the slope is still less than longer distances.

The last point of interest in figure 4 is the dip that precedes sudden increase in temperature. Prior to the infrared emission, water is largely believed to be still in liquid state with a given specific heat. Since heat is removed at the same rate throughout the freezing experiment, change in slope indicates a specific heat distinct from that of liquid water. Hence the dip prior to emission of infrared may indicate that water goes through a more subtle phase transition before freezing.

A significant feature of exclusion zone is that it is nucleated at hydrophilic surfaces. In order to confirm that the diminished latent heat release in the vicinity of Nafion is not an optical artifact due to presence of the interface, the same freezing experiment was carried out with a Teflon surface of the same thickness. Teflon has the same backbone

chemistry as Nafion, but does not have the hydrophilic sulfonate groups. Hence, Teflon was chosen as a control. No exclusion zone is observed next to hydrophobic Teflon. If the distance-dependent changes in latent heat release of water near Nafion is correlated with the exclusion zone, such effects are not expected near Teflon surfaces.

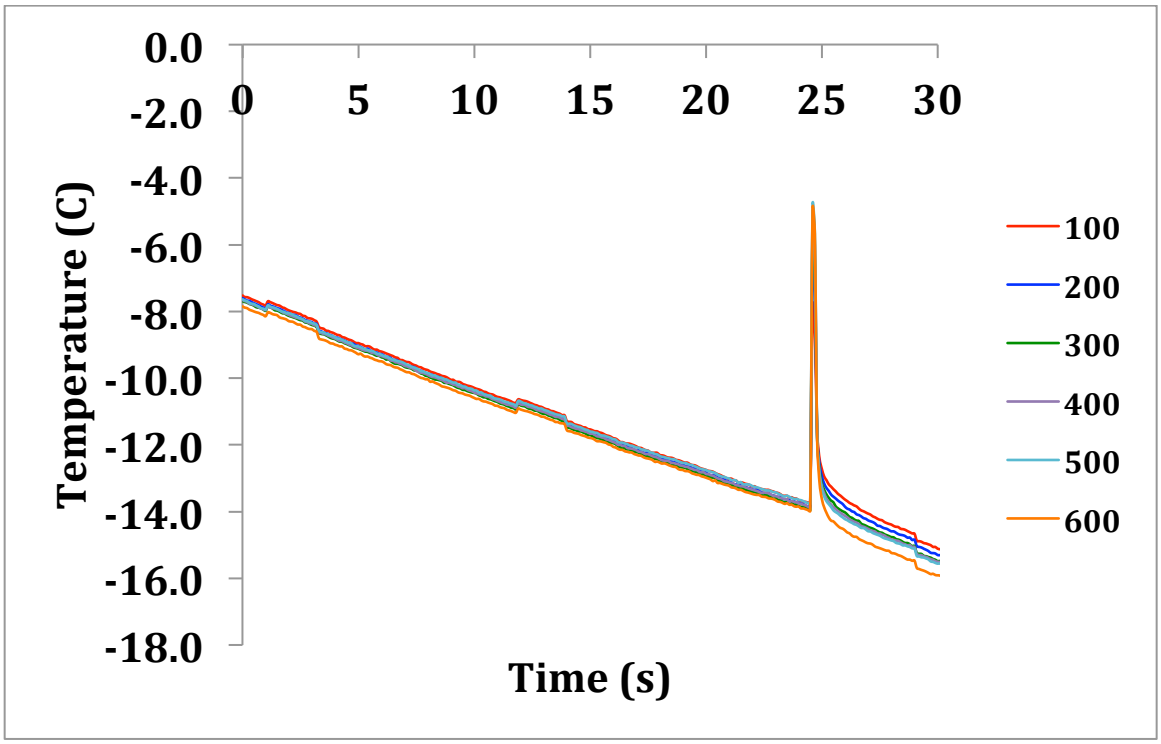

Figure 4.5 Representative time-course plot of averaged temperature at 100 incremental distances from Nafion surface.

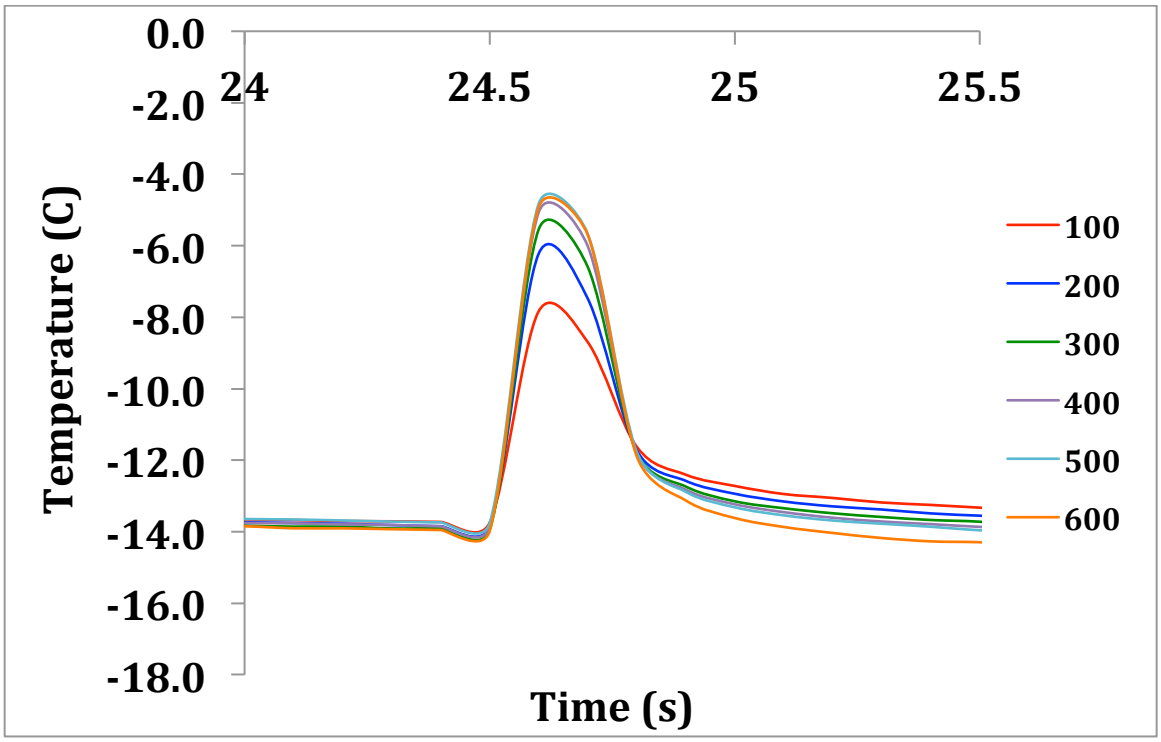

Figure 4.6 Zoomed-in plot of figure 3 showing the moment of latent heat release.

Figure 4.7 shows the time course of latent heat release next to the Teflon surface. As in the case of Nafion, line ROIs parallel to the surface were chosen at 100 µm increments from the surface, and the average values are computed. Compared to water next to Nafion, water next to Teflon freezes at notably higher temperature, ~ - 7.9 °C vs. -13.8 °C. A further look into the plot also reveals that there is no notable decline in amplitude of latent heat as we go from 100 µm to 300 µm. In other words, there is no detectable effect of the Teflon surface on nearby water. This is consistent with no observable EZ next to Teflon.

Another feature distinguishable from that of the Nafion-water interface is that both the amplitude and duration of latent heat release from Teflon-water interface is cut in half. As in the case of Nafion, water near Teflon showed a dip in temperature immediately before the onset of IR emission. However, the duration and amplitude of the dip were significantly less than that observed from water next to Nafion. Hence, the dip may indicate a genuine phase of water associated with freezing of EZ.

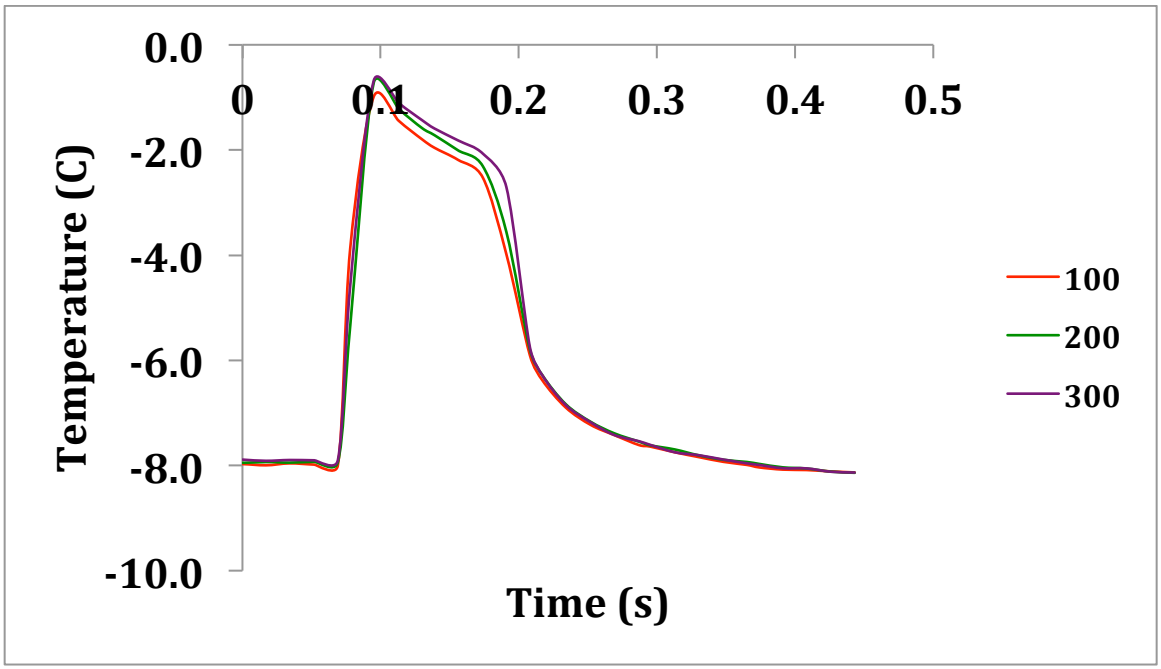

Figure 4.7 Representative time-course plot of averaged temperature at 100 incremental distances from Teflon surface

4.5 Discussion

This study was carried out to characterize the thermodynamic properties of water next to the Nafion surface, otherwise known as exclusion zone (EZ). The water next to Nafion was cooled down to freezing temperatures, and the resulting infrared emission associated with the phase transition was imaged using a FLIR camera. Spatial analysis of the IR emission data shows that the latent heat release is the lowest next to the surface and increases in amplitude out to about 300-400 μm from the surface. This indicates that kinetic energy of water next to the surface is relatively smaller than that farther away from the surface.

In order to test for artifacts and further understand the role of surface hydrophilicity on nearby water kinetics, Teflon surfaces were used as controls. Unlike next to Nafion, Teflon showed no distance dependent changes in latent heat release. Such findings confirm that the distance dependent changes observed within EZ was a not an optical artifact, but a genuine effect of hydrophilic surface on water. Seemingly, Teflon does not have extensive effects on nearby water as does Nafion.

Besides the dynamics of latent heat release, an interesting change in specific heat of water was observed immediately before the onset of infrared emission for both Nafion

and Teflon. It is widely believed that water goes through the first-order phase transition from liquid to solid. However, the observed changes in slope of the temperature time course may indicate that water goes through another phase before crystallization. It has been recently hypothesized that water goes through EZ phase prior to freezing and the region of dip prior to initiation of crystallization may signal existence of such a phase. This hypothesis is further supported by observing the 270 nm UV absorption peak of freshly thawed water. Since 270 nm UV absorption peak is a signature of EZ, the dip region may correspond to the EZ.

The most notable conclusion of present study is that there are extensive effects of hydrophilic surfaces on thermodynamic properties of nearby water. The freezing-induced latent heat release is the smallest closest to the surface, and increases in amplitude up to about 300 μm from the surface, at which point the increase stops. In other words there is a gradient of kinetic energy with the EZ, similar to negative potential gradient. The most negative region of EZ correlates with the lowest kinetic energy. The less negative potential farther away from the surface can also be correlated with increasing kinetic energy with distance from the surface. This conclusion is further supported by the absence of such gradient of kinetic energy next to Teflon. Next to Teflon surfaces, there is no visible EZ and no electrical potential.

4.6 References

1 Keutsch, F. N. & Saykally, R. J. Water clusters: Untangling the mysteries of the liquid, one molecule at a time. *Proceedings of the National Academy of Sciences* **98**, 10533-10540 (2001).

2 Ruan, C.-Y., Lobastov, V. A., Vigliotti, F., Chen, S. & Zewail, A. H. Ultrafast Electron Crystallography of Interfacial Water. *Science* **304**, 80-84 (2004).

3 Zhu, Y. & Granick, S. <title>Viscosity of Interfacial Water</title>. *Physical Review Letters* **87**, 096104 (2001).

4 Ninham, B. W. On progress in forces since the DLVO theory. *Advances in Colloid and Interface Science* **83**, 1-17, doi:http://dx.doi.org/10.1016/S0001-8686(99)00008-1 (1999).

5 Henniker, J. <title>The Depth of the Surface Zone of a Liquid</title>. *Reviews of Modern Physics* **21**, 322-341 (1949).

6 Zheng, J.-m., Chin, W.-C., Khijniak, E., Khijniak Jr, E. & Pollack, G. H. Surfaces and interfacial water: Evidence that hydrophilic surfaces have long-range impact. *Advances in Colloid and Interface Science* **127**, 19-27, doi:http://dx.doi.org/10.1016/j.cis.2006.07.002 (2006).

7 Zheng, J.-m. & Pollack, G. H. Long-range forces extending from polymer-gel surfaces. *Physical Review E* **68**, 031408 (2003).

8 Chen, S. C., Sturtevant, J. M. & Gaffney, B. J. Scanning calorimetric evidence for a third phase transition in phosphatidylcholine bilayers. *Proceedings of the National Academy of Sciences* **77**, 5060-5063 (1980).

9 Ienna, F., Yoo, H. & Pollack, G. H. Spatially resolved evaporative patterns from water. *Soft Matter* **8**, 11850-11856, doi:10.1039/C2SM26497H (2012).

Section II

Cellular Water Dynamics and Changes During

Skeletal Muscle Differentiation

Chapter 5. Dynamics of Cellular Water and changes associated with muscle development

5.1 Abstract

The nature of water inside biological systems has been a topic of broad debate, for water is thought to be critical for biological activity. Earlier studies on muscle water demonstrated there exists at least two different types of water inside muscle, indicated by multi-component T1 and diffusion coefficient present inside intact muscle tissue. However, no agreed interpretations of these results have been offered to date. The interpretation of multiple water components in muscle has been criticized, partly due to several other non-muscle components present inside intact muscle and difficulty in correlating the distinct water populations to corresponding biophysical models. In an effort to simplify the problem to water within just muscle cells instead of whole muscle tissue, well-studied in-vitro model of C2C12 mouse myoblast cells were used in this study in conjunction with NMR spectroscopy. Chemical environment and dynamics of water within skeletal muscle and their correlations with skeletal muscle differentiation are studied in order to understand the long-term role of water in muscle development. The muscle water showed mostly two distinct chemical shifts over the course of skeletal differentiation and over broad temperature range. Of these, the down-field peak was identified as cell water, while the up-field peak was identified as the water in-between

the cells. The changes in dynamics of water during myogenisis was signaled by increase in T1 relaxations times and lower activation energy of cellular water. Intriguingly, larger degree of changes were seen with formation of myofibril network during later part of development, from day 3 to 8 of differentiation, rather then the earlier membrane fusion process, from day 0 to 3.

5.2 Introduction

Water is ubiquitous in biological systems and makes up ~65% of one's body weight. Despite its abundance, the properties of water inside biological systems and their general functional roles in sustaining life remain incompletely understood [1]. One possible reason for the difficulty in understanding of biological water may be the cell's crowded molecular environment. Cells are crowded with biomolecules, thus providing high surface area-to-volume ratio. In such an environment, most of water is confined and interfacial, and thus may have distinct physico-chemical properties.

Notable earlier studies on biological water employed nuclear magnetic resonance (NMR) spectroscopy to investigate dynamics of water inside skeletal muscle systems. These studies demonstrated at least two different types of water inside intact skeletal muscle, determined by two or more distinct chemical shifts of water protons within muscle tissue. Further, these water species found in muscle exhibited significantly lowered self-diffusion coefficients, T1 and T2 relaxation times [2].

The results initially caused broad excitement as they seemingly supported long-held views on biological water being a unique phase [3-5]. However, partly due to rapid development of molecular biology, the focus of muscle biology turned to studies of molecules almost exclusively, without much emphasis on muscle water.

Though not widely known, a careful calculations have been made using a standard fluid dynamics model and only about 30% reduction in diffusion of water could be accounted for by geometrical constraint of macromolecules in striated muscle [6]. The lowered NMR diffusion of water within biological systems are now widely accepted to be strictly a consequence of geometrical constraints rather than inherent changes in properties of water itself. Hence the term 'apparent diffusion coefficient (ADC)' is used to describe NMR diffusion of water in biological systems [7].

The topic of biological water was recently rekindled as evidence has shown that surfaces can have extensive effects on nearby water. Water near surfaces has orders of magnitude higher viscosity, lowered NMR T1 relaxation time and diffusion coefficient, negative electrical potential and anomalous 270 nm absorption [8]. Biological systems are rich with surfaces. Surface induced changes in water are necessary components to take into account in better understanding biological water.

To better study the nature of biological water and its role in development of skeletal muscle, we used a standard C2C12 mouse myoblast model to study changes in kinetics of muscle water during skeletal muscle differentiation [9]. The C2C12 model was chosen as it provides robust system to study skeletal muscle differentiation. In addition, the use of well-controllable in-vitro system of living muscle cells alone can simplify the interpretation of data, which was complicated in early NMR studies of muscle, due to

presence of other cell types In this study 1H NMR spectroscopy is employed to study myoblast differentiation into myotubes throughout the course of development.

5.3 Materials and Methods

5.3.1 General

For all experiments, deionized water (type I HPLC grade (18.2 MΩ-cm)) was collected from a Barnstead D3750 Nanopure Diamond purification system.

5.3.2 C2C12 Myoblast Culture

The C2C12 cell line was purchased from ATCC (# CRL 1772). The cells were first thawed slowly and washed in DMEM solution (Life Sciences inc. # 11960) containing 10 % fetal bovine serum (FBS). Following the wash, cells were resuspended in the growth medium composed of DMEM, 10% FBS and 2% Penicillin Streptomycin (Life Sciences inc. #15140148), and seeded onto a cell culture petri dish at concentration of 10 million cells per 1 cm^2. After seeding the cells, the C2C12 cells rapidly proliferated, reaching confluency of ~80% within 3 days.

When C2C12 reached ~80% confluency, growth media was replaced with differentiation media composed of DMEM, 2% horse serum and 2% Penicillin Streptomycin to initiate differentiation of the myoblast cells into myotubes.

5.3.3 Preparation of NMR experimental samples

In order to investigate the water dynamics as a function of developmental stage, the C2C12 cells were collected on day 0, 3 and 7 from initiation of differentiation. Briefly, cells were suspended in 5 mL of 0.05% trypsin-EDTA (Life Sciences, inc. # 25300062) for 5 minutes at 37 °C. After the cells were detached from the bottom surface of the petri dish, 5 mL of DMEM containing 10% FBS was added to stop the breakage of cellular proteins. The resulting cell suspension was then centrifuged at 1500 rpm for 5 minutes to yield the pallet of cells at the bottom, and the supernatant was vacuumed out leaving just the cell pallet. The cell pallet was then re-suspended in PBS and washed twice more. The final cell suspension was then added to Shigimi NMR tube (Shigimi, inc. #BMS-005). The NMR tube was then centrifuged at 1500 rpm for 5 minutes leaving a packed cell pallet at the bottom of the NMR tube. After the supernatant was vacuumed out, the shigimi plug was inserted and the tube was placed inside NMR magnet at 37 °C.

5.3.4 NMR Spectroscopy

The 1H NMR spectra were recorded on a 499 MHz Bruker AVANCE II NMR spectrometer equipped with a 1H {C,N} high-resolution triple resonance probe with Z-gradient. Prior to recording of cells, a spectroscopic standard sample of 1% sucrose in 10% H2O/D2O (v/v) mixture was used to effectively shim the magnet to optimal B_0 field homogeneity. Raw data were collected with 8K time-domain points with a spectral width of 10 ppm centered at 5.0 ppm, recycle delay of 1 s, and acquisition time of 0.55 s. These were then Fourier transformed without zero filling.

A trace quantity of DSS (4,4-dimethyl-4-silapentane-1-sulfonic acid) as external reference was added to one of the samples, and 0 ppm calibration was done by adjusting the reference spectra in subsequent experiments. Three biological replicates were used for measurements in order to establish consistency of the results with statistical significance. The sample temperature was initially set to 298 K +/- 0.1 K and the accuracy of the temperature at the sample was confirmed by measuring the chemical shift separation of the doublet obtained from neat methanol. The chemical shift difference was then cross-correlated with published values to confirm the absolute temperature.

Spin-lattice (T1) relaxation times of water protons in live muscle cells were measured with standard inversion-recovery pulse sequence (π - τ_1 - $\pi/2$). Longitudinal magnetization was collected with 10 varying time delays from 1 ms to 25 s. A standard inversion recovery curve was fitted to the integrated volume of each resonance as a

function of the delay and a single T1-component fit resulted in excellent chi-square statistics. The recorded data had no outliers from the fit.

5.3.5 Temperature Dependence of Cell Water Diffusion Coefficients and Kinetics Studies

In order to measure temperature dependence of spin-lattice relaxation (T1) times and self-diffusion coefficients, both quantities were measured at 5 different temperatures starting with the lowest: 290, 295, 300, 305 and 310 K. Each temperature was set with < 5 mK accuracy.

5.4 Results

In order to investigate skeletal muscle differentiation and induced changes in cell water dynamics and kinetics, C2C12 myoblast cells were induced to differentiate by lowering the serum concentration when cells were ~ 90% confluent. Figure 5.1 shows micrographs of C2C12 cells on day 0, 3 and 8 of differentiation. As shown in the figure, none of the cells were differentiated on day 0, and cells don't show any directionality. On day 3 of differentiation, majority of cells have already started differentiating and morphing together to form myotubes. The myotube lengths varied from about 50 µm up to about 100 µm. In addition, the differentiated myotubes showed much more collective directionality. By day 8 of differentiation, all cells were fully differentiated and

the myotube length reached hundreds of micrometers, indicating mature skeletal muscle phenotype. The widths of myotubes also increased from day 3 to reach about 10 μm.

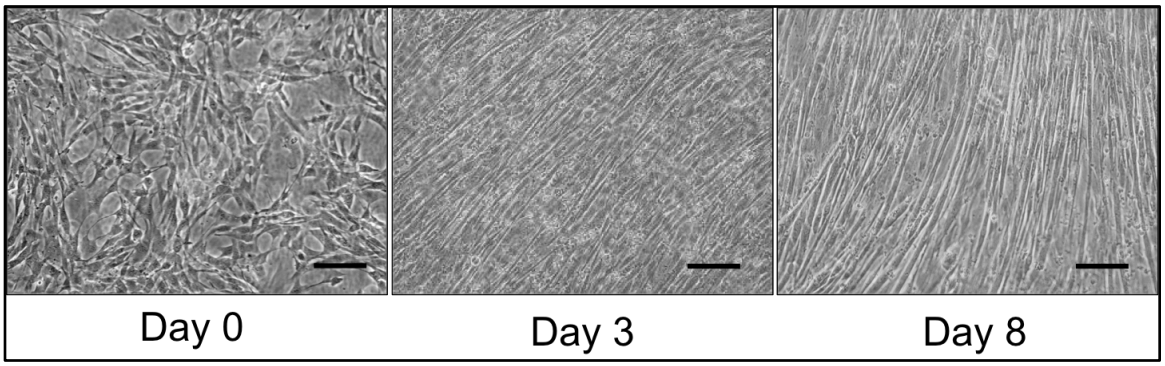

Figure 5.1 Micrographs of C2C12 cells through the course of skeletal differentiation. The scale bar indicates 50 μm.

In order to determine the chemical environment of muscle water at each stage of the skeletal muscle development, live cells were taken from petri dish and pelleted for NMR experiments. 1D experiments were first performed to measure chemical shifts of muscle water on day 0, 3 and 8 of differentiation. Representative fully relaxed 1D spectra of muscle cells on days 0, 3 and 8 at 295K are shown in figure 5.2.

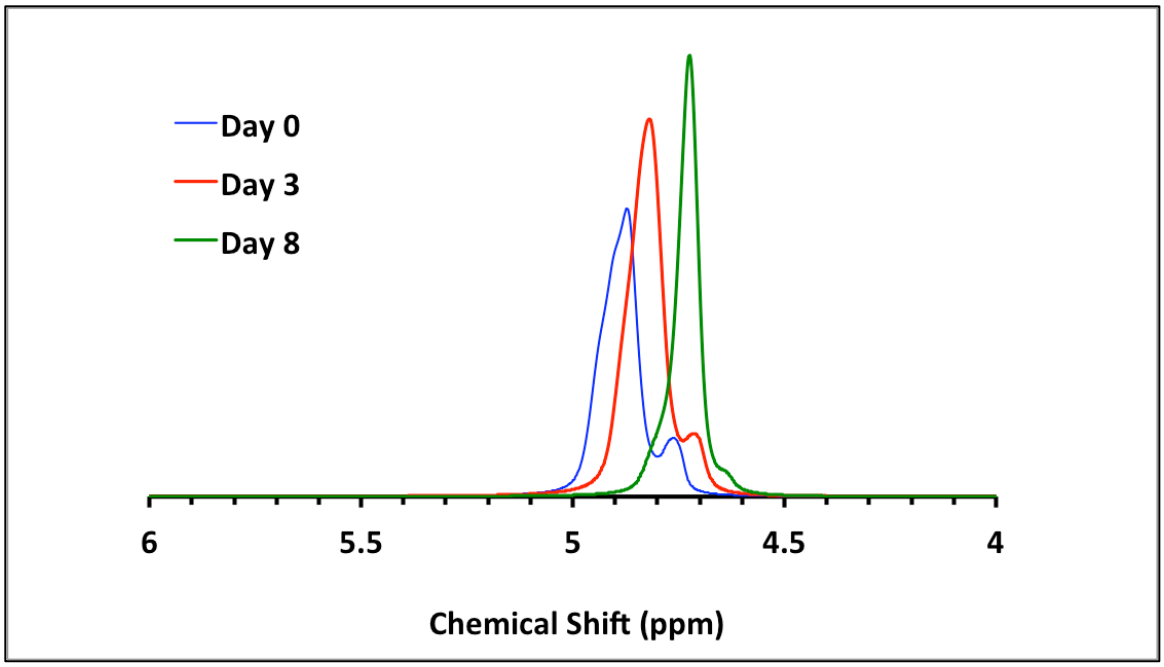

Figure 5.2 Fully relaxed 1H NMR spectra of C2C12 cell pallets on day 0 (blue), day 3 (red) and day 8 (green) with no water suppression

On day 0, shown in blue, there are two distinct chemical shifts of muscle water. The down-field peak at 4.87 ppm represents the tightly-bound component of cell water and represents 88.7% of total water content. The up-field peak at 4.76 ppm is interpreted as the more 'bulk-like' component of cell water and composes 11.3% of cell water. The two peaks are separated by 54.21 Hz.

On day 3 of differentiation, shown in red, there are two distinct chemical shifts of cell water, similar to day 0 spectra. However, both chemical shifts are shifted up-field and this indicates more shielded environment of muscle water induced by differentiation of skeletal muscle. The down-field peak is at 4.82 ppm and comprises 88.9% of cell water.

The up-field peak at 4.72 ppm comprises 11.1 % of the total water content. The separation of the two peaks has decreased from day 0, and 52.17 Hz separates the two peaks.

On day 8 of differentiation, by which time all cells are differentiated to form mature myotubes, the 1D 1H NMR spectra shows that there are still two water resonances, one at 4.72 ppm and another one at 4.64. Compared to day 0 and 3, however, the two resonances are much closer together and the up-field peak shows as a shoulder to the major down-field peak. The two resonances are separated by 42.5 Hz, which is significantly less than those of day 0 and 3.

Further examining figure 5.2, there are several other interesting features associated with skeletal muscle differentiation. First, the echo amplitude increases with developing cell, and this is attributed to growth of cells. As cells differentiate and grow, the total volume of cellular water increases, therefore resulting in larger echo amplitude. The second feature of interest is narrowing of the peak width with developing cell. Taking the down-field major peak as an indicator, it is clearly shown that the full width half maximum of the peak narrows throughout the course of differentiation. The width of 1D peaks are inversely proportional to spin-spin (T2) relaxation times, and therefore indicates that the T2 relaxation times of cell water increases during differentiation of skeletal muscle. The last feature of interest is the decreased separation of two water resonances as differentiation progresses. Such closing proximity shows that chemical

environment of skeletal muscle water goes from heterogeneous to more homogeneous during differentiation.

The changes in dynamics of muscle water throughout the differentiation process was further examined by measuring spin-lattice (T1) relaxation times of muscle water. Figure 5.3 below shows changes in T1 relaxation times for the down-field component of muscle water at 295 K. As muscle cells go from day 0 of differentiation to day 3, the mean T1 relaxation time went up 2.24 s to 2.28. From day3 to 8, the mean T1 relaxation time went up from 2.28 to 2.37. Hence, the farther along developmental state a skeletal muscle cell is the longer T1 relaxation time is. Considering that most of cells were fused into myotubes by day 3, the increase in T1 relaxation from day 0 to 3 can be correlated with both fusion of myoblast cell membranes and partial assembly of filamentous action into muscle fibers. As the muscle develops into more mature and bigger myotubes by day 8, the increase in T1 continued at a faster rate. Hence, skeletal differentiation and maturation of skeletal muscle is characterized by increased spin-lattice relaxation times.

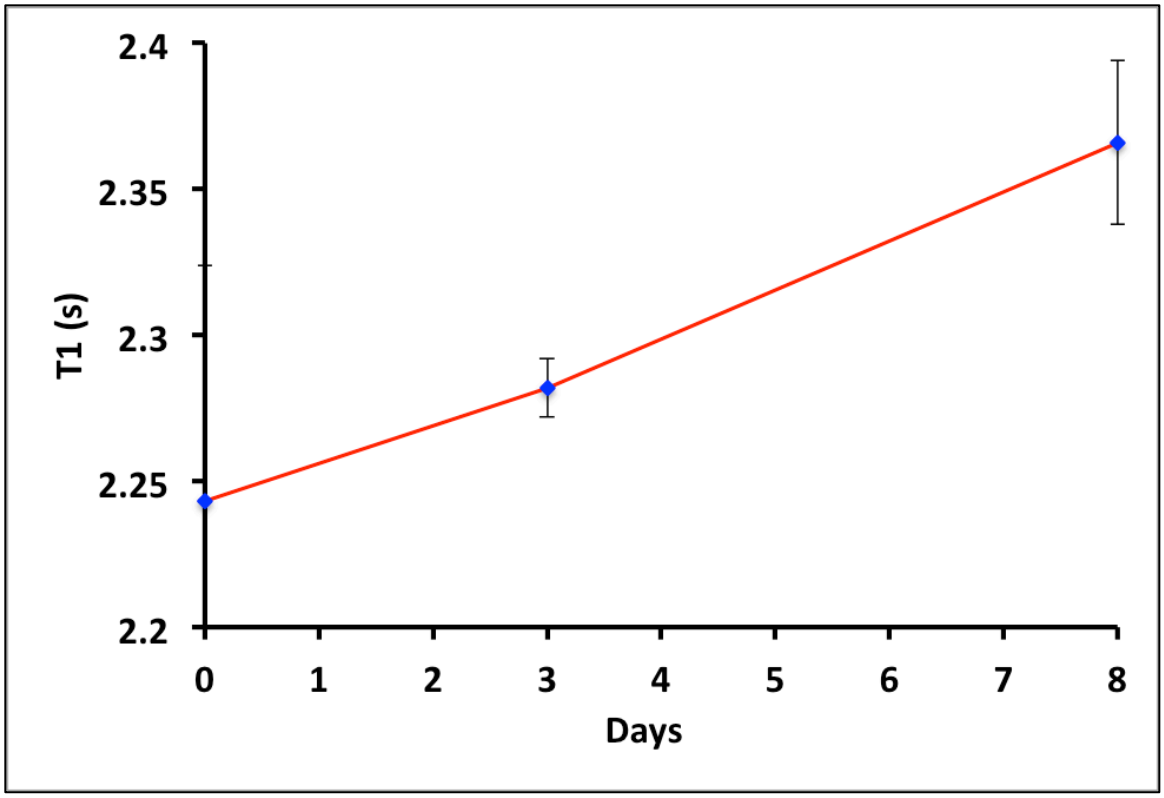

Figure 5.3 Spin-lattice (T1) relaxation times of muscle water proton at 295K on days 0, 3 and 8 after initiating skeletal differentiation.

To characterize the kinetics of muscle water, experiments were carried out to observe temperature dependence of muscle water chemical shift from 290 K to 310 K. Fully relaxed 1D 1H NMR spectra of muscle taken on day 8 are shown in figure 4. Muscle is fully differentiated into myotubes on day 8. These are 1H NMR spectra of myotubes.

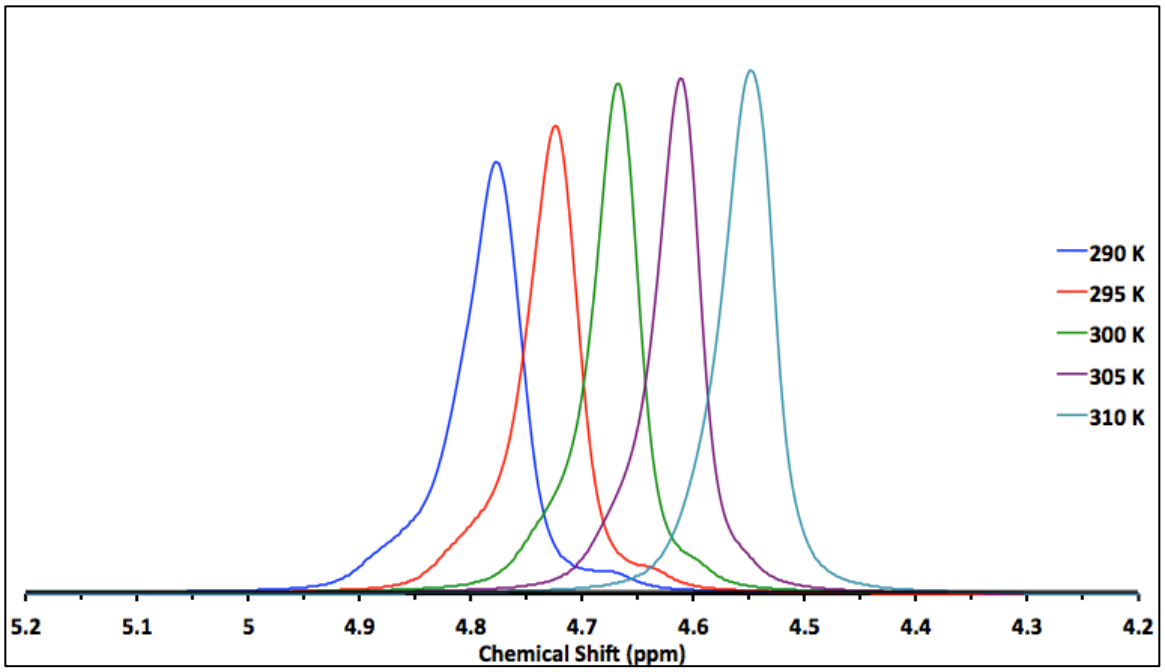

Figure 5.4 Fully relaxed 1D spectra of C2C12 on day 8 of differentiation at 290, 295, 300, 305 and 310 K.

As seen in figure 5.4, the chemical shift of muscle water moves linearly up-field with increasing temperature, with each 5 K temperature jump resulting in ~ 27 Hz shift. At 290K (blue), the major water resonance is at 4.77 ppm. In addition three are two shoulder peaks at 4.88 and 4.68 ppm, indicating three distinguishable chemical environments of muscle water within myotubes at 290 K. At 295 K (red), the main resonance of muscle water is at 4.72 ppm, with less shoulder peaks at 4.81 and 4.64 ppm. Going from 290 to 295 K, all three distinguishable peaks moved up-field while the shoulder peaks became less pronounced. At 300 K (green), the major peak is centered at 4.67 ppm. Interestingly, the left shoulder peak became almost indistinguishable from the main peak, while the up-filed shoulder peak was at 4.60 ppm. At 305 K (purple), the

1H resonance of muscle water became closer to Lorentzian-Gaussian profile with its center at 4.62 ppm. The up-field shoulder was, however, still distinguishable around 4.55 ppm. At 310K (light blue), the major peak showed Lorentian-Gaussian profile with its center at 4.57 ppm. The shoulder peaks were not distinguishable from the major water resonance at 310 K.

These findings indicate that with increasing temperature, the chemical environment of water became more homogeneous, as indicated by a single muscle water resonance. While the three distinguishable resonances show that there are at least three different types of water within skeletal myotube, such compartmentalization of muscle water significantly weakened as the muscle sample was brought to 310K, which is the same as typical physiological temperature of mammals.

Figure 5.4 further shows that the echo amplitude increased with increasing temperature. Since the total volume of water within myotubes remained the same throughout the experiment, the increasing amplitude associated with temperature increase is due to shoulder peaks merging towards the major peak. The peak width, determined by full-width-half-maximum (FWHM) changed slightly as muscle water went from 290 to 310 K with both temperatures showing about 0.5 ppm peak widths. Interestingly, the major water resonance in all temperatures had dramatically bigger peak width compared with that of 'bulk' water and this indicates that the T2 relaxation time is shorter in muscle water compared to bulk water.

In order to study the changes in dynamics of muscle water protons during skeletal differentiation and its energetics, T1 relaxation time was plotted as function of temperature to yield an Arrhenius plot as shown in figure 5.5. All T1 exponential fitting curves used in data analysis showed great chi-square values with one component relaxation models contrary to earlier studies with muscle fiber.

From well-known Arrhenius theory of rate process, the correlation time, τ_c, for rotational molecular motion can be described as the time it takes for a dipole to jump from one equilibrium position to another. In order for this jump to occur, the system needs to overcome the potential barrier and this energy is known as activation energy (ΔE_A). The activation energy can be written in terms of correlation time then:

$$\tau_c = \tau_0 exp\left[\frac{\Delta E_A}{RT}\right]$$

And, it follows from Bloembergen-Purcell-Pound theory (Bloembergen, 1948 #20). that

$$T1 = C\tau_c, for\ \omega_0\tau_c \ll 1$$

Where C is a constant and $\omega_0 = 2\pi\nu_0$, where ν_0 is the resonant frequency. Hence, activation energy, ΔE_A, can be computed from observing temperature dependence of T1 relaxation times:

$$\Delta E_A = 2.303R\left[\frac{\partial \log T_1}{\partial(\frac{1}{T})}\right]$$

Here T is temperature in kelvins and T_1 is in seconds.

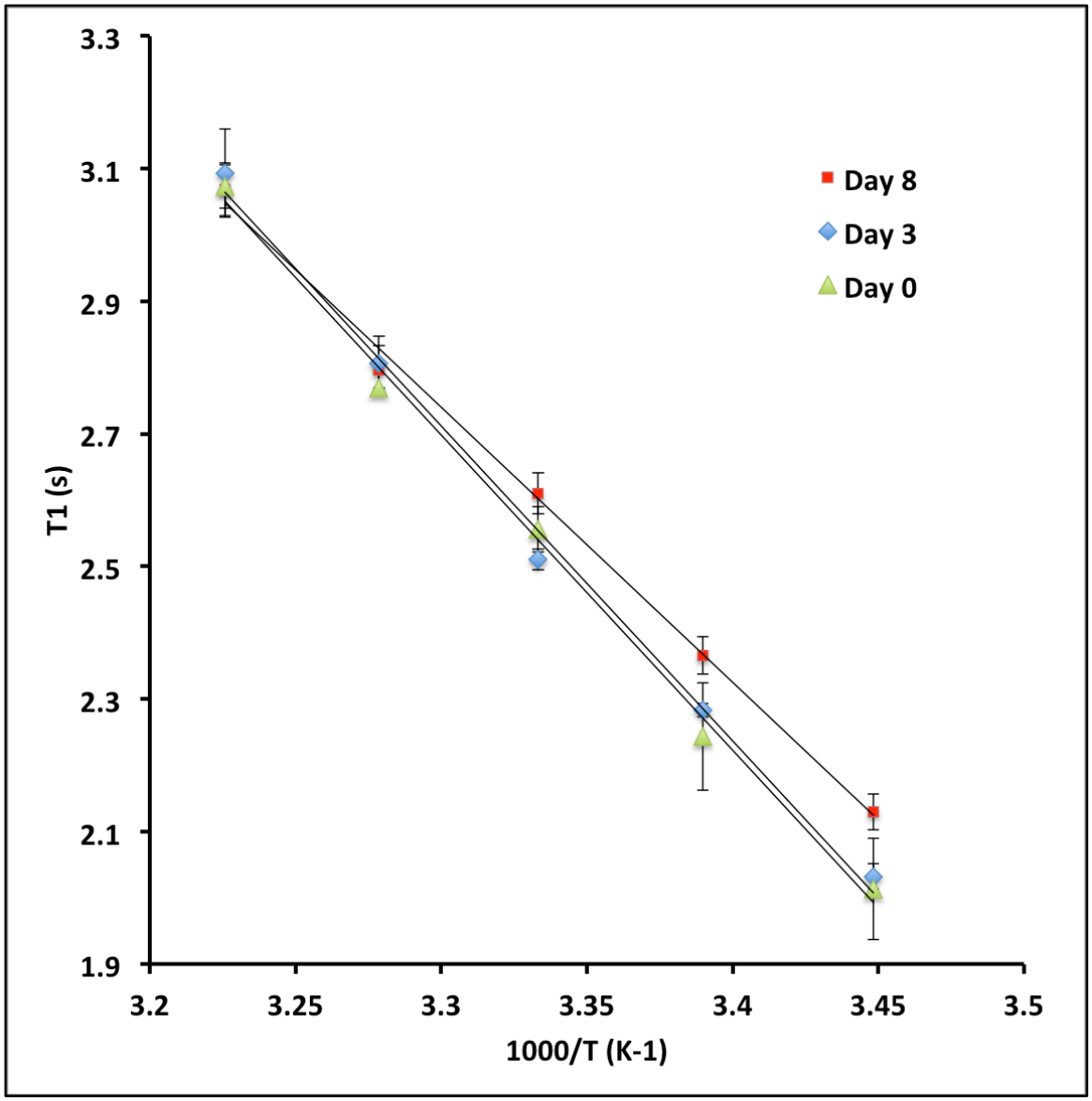

Figure 5.5 Arrhenius plot showing temperature dependence of T1 relaxation of muscle water on day 0, 3 and 8 of skeletal differentiation.

Taking logarithmic values of T1 from the data shown in figure 5.5, we can compute the activation energy of muscle water on day 0, 3 and 8 of differentiation and this is shown in table 5.1.

Table 5.1 Activation energy for T1 relaxation of muscle water on days 0, 3 and 8 of skeletal differentiation

	Day 0	Day 3	Day 8
ΔE_A (kJ/mol)	15.691	15.641	13.427

The activation energy of T1 did not change appreciably going from day 0 to 3. This indicates that fusion of myoblast cells into myotubes does not significantly change activation energy of muscle cell water. However, going from day 3 to day 8, period corresponding to myotube growth resulted in dramatic lowering of activation energy. Hence, the lowering of activation energy is more closely related to growth of myotubes rather than initial stages of skeletal differentiation.

5.5 Discussion

This study was carried out to study changes in muscle water's chemical environment and dynamics associated with skeletal muscle differentiation using C2C12 model. 1D experiments showed two distinguishable chemical shifts of intracellular water at all stages of differentiation. Of the two, the down-field resonant peak constitutes the majority of muscle water, around 90%. As the myoblasts differentiated into myotubes, both the two water proton resonances moved down-field, indicating the more shielded magnetic environment of muscle water as a consequence of muscle development. In

addition the splitting of the two resonances decreased with differentiation. Further studying spin-lattice relaxation (T1) times revealed that the T1 relaxation times of muscle water protons are notably lower than that of 'bulk' water. T1 is the smallest on day 0 of differentiation and further development resulted in increase of T1 relaxation times.

In addition to T1 relaxation measurements, DOSY experiments were carried out to measure self-diffusion coefficients of muscle water protons. Similar to T1 relaxation times, the diffusion constants of muscle water were significantly lower than that of 'bulk' water. In addition, the diffusion coefficient increased as muscle progressed with development. On the contrary to T1 relaxation, however, where a one-component exponential decay was observed, the DOSY data required two-component exponential fitting to yield excellent chi-square statistics. Such results can be understood by considering the exchange of protons between two populations of water. In this case, the exchange time is fast enough to yield only one T1 component, but slow enough to have two muscle water compartments with distinct diffusional characteristics. Similar results have been observed within human brain samples, REF and hence this is not a unique feature of muscle, but a broad range of biological samples exhibit similar characteristics.

To further characterize the muscle water and differentiation associated changes, temperature dependence chemical shifts and T1 relaxation times for the down-field peak were measured between 290 and 310 K at 5 K increments. Similar to behavior of

'bulk' water, T1 increased with increasing temperature, albeit at a smaller rate. Using the temperature dependence of T1, activation energies of T1 in muscle water protons were computed for cells on day 0, 3 and 8 of differentiation. Activation energy for T1 of muscle water proton changed slightly, but with no statistical significance, going from day 0 to 3. However, going from day 3 to 8, activation energy of water dropped more notably by about 15%. Such result is contrary to earlier studies, where inside intact muscle tissue, the activation energy of intracellular water was comparable to that of 'bulk' water [10]. Our findings indicate that not only is the activation energy of water lower than that of 'bulk' water, but also it changes with physiological changes occurring within the muscle cells. The lowered activation energy of muscle water can be best understood by considering rapid proton exchange between water and biomolecules within the muscle cells. The lowered activation energy observed here also agrees other previous studies, where water near proteins showed lower activation energy [11]. The lowered activation energy can mean that biological water may be more catalytic in nature, when compared with bulk water.

Perhaps, one of the biggest challenges for correct interpretation of NMR studies on muscle water is the widely varying experimental data coming from different groups. Several groups have reported multi-component fitting of relaxation data while others reported only one relaxation constant for muscle water. Our study suggests that 1D chemical shift, relaxation and diffusion dynamics are critically dependent on the temperature of the system. Therefore, we suggest that the inconsistent temperature

settings across previous studies were at least one of the factors to be considered when interpreting the data.

Additional difficulty in interpretation of 1H NMR data on muscle water arises when assigning proton resonances to physiologically relevant physical model of water populations. In an intact tissue, there are several different types of cells and connective tissues present inside intact muscle tissues, hence making it difficult to assign water populations unique to muscle. Our approach to using just the myoblast cells to form muscle fiber has simplified the problem in that there is only one kind of cell type in our system. The results gathered in this study indicate that the multi-component T1 relaxation observed in earlier studies of intact muscle may be due to other non-muscle cell components as our system composed of only muscle cells demonstrate one component T1 relaxation.

The nature of significantly lowered diffusion coefficient of water is still under active debate. However, recent general consensus has been that geometrical constraints imposed by biomolecules within cellular environment are the major cause of lowered diffusion of water. Despite this widely accepted view, careful calculations were made on the effects of constrained geometry on diffusion coefficient of water within muscle fibers, and the study concluded that geometrical constraints present in muscle can only account for about 30% reduction in diffusion constant when water is considered to have same intrinsic physical properties as bulk water [6]. An order of magnitude lower diffusion

coefficient found in muscle cells may therefore indicate genuine changes in water in muscular systems.

5.6 References

1 Wernet, P. *et al.* The Structure of the First Coordination Shell in Liquid Water. *Science* **304**, 995-999 (2004).

2 Hazlewood, C. F., Chang, D. C., Nichols, B. L. & Woessner, D. E. Nuclear Magnetic Resonance Transverse Relaxation Times of Water Protons in Skeletal Muscle. *Biophysical Journal* **14**, 583-606, doi:http://dx.doi.org/10.1016/S0006-3495(74)85937-0 (1974).

3 Ling, G. N. THE PHYSICAL STATE OF WATER IN LIVING CELL AND MODEL SYSTEMS*. *Annals of the New York Academy of Sciences* **125**, 401-417, doi:10.1111/j.1749-6632.1965.tb45406.x (1965).

4 Szent-Gyorgyi, A. General views on the chemistry of muscle contraction. *Bibliotheca cardiologica*, 6-51 (1956).

5 Pollack, G. H. *Cells, Gels and Engines of Life*. (Ebner and Sons, 2001).

6 Rorschach, H. E., Chang, D. C., Hazlewood, C. F. & Nichols, B. L. THE DIFFUSION OF WATER IN STRIATED MUSCLE*. *Annals of the New York Academy of Sciences* **204**, 444-452, doi:10.1111/j.1749-6632.1973.tb30797.x (1973).

7 Henkelman, R. M., Stanisz, G. J., Kim, J. K. & Bronskill, M. J. Anisotropy of NMR properties of tissues. *Magnetic Resonance in Medicine* **32**, 592-601, doi:10.1002/mrm.1910320508 (1994).

8 Zheng, J.-m., Chin, W.-C., Khijniak, E., Khijniak Jr, E. & Pollack, G. H. Surfaces and interfacial water: Evidence that hydrophilic surfaces have long-range impact.

Advances in Colloid and Interface Science **127**, 19-27, doi:http://dx.doi.org/10.1016/j.cis.2006.07.002 (2006).

9 Cuenda, A. & Cohen, P. Stress-activated Protein Kinase-2/p38 and a Rapamycin-sensitive Pathway Are Required for C2C12 Myogenesis. *Journal of Biological Chemistry* **274**, 4341-4346 (1999).

10 Chang, D. C., Rorschach, H. E., Nichols, B. L. & Hazlewood, C. F. IMPLICATIONS OF DIFFUSION COEFFICIENT MEASUREMENTS FOR THE STRUCTURE OF CELLULAR WATER*. *Annals of the New York Academy of Sciences* **204**, 434-443, doi:10.1111/j.1749-6632.1973.tb30796.x (1973).

11 Langdon, B. B., Kastantin, M. & Schwartz, D. K. Apparent Activation Energies Associated with Protein Dynamics on Hydrophobic and Hydrophilic Surfaces. *Biophysical Journal* **102**, 2625-2633, doi:http://dx.doi.org/10.1016/j.bpj.2012.04.027 (2012).

Section III

Hydrogen-bonding of Cellular Water and Contraction-induced Changes

Chapter 6. The Structure of Cellular Water in Muscle Fiber and Associated Changes with Activation of Muscle

6.1 Abstract

Protein-water interaction plays a crucial role in protein dynamics, and hence function. To study the chemical environment of water and proteins with high spatial resolution, synchrotron radiation-Fourier transform infrared (SR-FTIR) spectro-microscopy was used to probe skeletal muscle myofibrils. Observing the OH-stretch band showed that water inside relaxed myofibrils is extensively hydrogen-bonded with little or no free OH. In higher resolution measurements obtained with single isolated myofibrils, the water absorption peaks were relatively higher within center region of the sarcomere compared to the I-band region, implying higher hydration capacity of thick filaments compared to the thin-filaments. When specimens were activated, changes in the OH-stretch band showed significant de-hydrogen bonding of muscle water; this was indicated by increased absorption at ~3480 cm^{-1} compared to relaxed myofibrils. These contraction-induced changes in water were accompanied by splitting of the Amide I (C=O) peak, implying that muscle proteins transition from α-helix to β-sheet-rich structures. Hence, muscle contraction can be characterized by a loss of order in the

muscle-protein complex, accompanied by a de-structuring of hydration water. The findings shed fresh light on the molecular mechanism of muscle contraction and motor protein dynamics.

6.2 Introduction

While the importance of water for sustaining life is well recognized, the exact role of water in biological processes remains unclear. On the other hand, an increasing number of studies show that biological processes are heavily influenced by interfacial water dynamics [1].

One such water-mediated process is protein conformational change, which sits at the base of biological function [2-3]. X-ray crystallography studies had initially implied relatively few hydration layers adsorbed onto proteins, which could persist even under high vacuum [4]. However, recent experiments using THz and florescence spectroscopy have reveled that the dynamic hydration shells around proteins can extend out to much longer distances [5-6]. Further, recent dielectric spectroscopy studies have shown that protein folding is largely 'slaved' by dynamics of water beyond the first several hydration layers [7]; i.e., the protein follows the water.

The above-mentioned studies have sparked broad interest in hydration water. However, questions remain as to how such solution systems reflect the intricately ordered and crowded protein-water systems lying inside intact tissues and cells. One such ordered system is muscle. When muscle is activated, proteins undergo synchronous conformational changes over millimeter and centimeter length scales. The protein changes are well studied; however, the changes in muscle-water hydrogen-bonding remain uncharted territory.

Many experimental observations imply that water may play an important role in muscle contraction (for summary, see [8-9]). Several recent findings in particular show that near-surface interfacial water is considerably more viscous than bulk water, with several groups reporting as high as six-fold viscosity elevation near hydrophilic surfaces [10]. This high viscosity implies that the molecular cross-bridge swinging that has been considered central to the contractile process may experience resistance, and correspondingly, that the high energy needed to power such strokes might not be accounted for by ATP splitting alone. This is but one of multiple issues raised by the presence high viscosity interfacial water.

Synchrotron radiation (SR) FTIR spectro-microscopy has lately emerged as a non-invasive probe of biological tissues with unprecedented spectral sensitivity and diffraction-limited spatial resolution, owing to its high brightness and small beam size [11]. This tool has proved especially useful in determination of chemical species and structures [12-14]. IR spectroscopy is also remarkably sensitive to the strength of hydrogen bonding, as OH stretch frequency is linearly related to hydrogen bonding strength (i.e. stronger hydrogen bonding results in lower frequency of OH stretching vibration) [15]. With this technique, we examined possible changes of muscle water and protein structures associated with muscle contraction.

6.3 Materials and Methods

6.3.1 Solutions

Several different solutions were used to simulate different states of contraction. Relaxing solution (pH 7.0) had a composition (in mM) of: 10 MOPS, 64.4 K^+ propionate, 5.23 Mg^{2+} propionate, 9.45 Na_2SO_4, 10 EGTA, 0.188 $CaCl_2$, 7 ATP, and 10 creatine phosphate. Activating solution consisted (in mM) of: 10 MOPS, 45.1 K^+ propionate, 5.21 Mg^{2+} propionate, 9.27 Na_2So_4, 10 EGTA, 9.91 $CaCl_2$, 7.18 ATP, and 10 creatine phosphate. Glycerol solution consisted of half glycerol and half rigor solution, the latter containing (in mM) of: 50 Tris (pH 7.4), 100 NaCl, 2 KCl, 2 $MgCl_2$, and 10 EGTA.

6.3.2 Skeletal myofibril preparation

Two types of specimen were studied: myofibril bundles and single myofibrils. Myofibril bundles were prepared from rabbit psoas muscles. Briefly, muscles were dissected bluntly from the backs of rabbits, along the length of the fibers. They were cut into thin strips, and tied at both ends to a wooden stick in order to maintain their natural length. The prepared muscle strips were placed in glycerol solution and stored in a freezer at -20 °C for long-term storage. To obtain myofibril bundles, the muscle strips stored in glycerol solution were transferred to rigor solution for 60 minutes and then cut into 2 mm segments across the fiber cross-section. A tissue segment was diced using a blender (Sorvall Omni Mixer) in 7 ml of rigor solution using the following protocol: twice X 5 s at 1100 rpm, once x 5 s at 2500 rpm, and once x 1 s at 3100 rpm. The resulting myofibril

bundles were typically about 50 μm in diameter and several hundred micrometers long. Eight myofibril bundles were probed both in relaxed and activated states to confirm the consistency of the data (n=8).

Single honeybee myofibrils were prepared from thorax region of honeybee flight muscles. The dissected specimen was stored at -20 °C in a 50/50 glycerol/rigor solution mixture for long-term storage. To prepare single myofibrils, the muscle tissue was washed in rigor solution and cut using a blender in 2 ml of rigor solution using the following protocol: once X 5 s at 2500 rpm, once X 10 s at 4000 rpm. The resulting myofibrils were typically 4-5 μm in diameter and tens of micrometers long. Ten single myofibril samples were probed in both activated and relaxed states for consistency (n=10).

6.3.3 C2C12 Mouse Myoblast Cell Culture

For maximum infrared transmission, C2C12 cells need to be cultured directly on the CaF2 window. However, CaF2 window is not an ideal cell substrate, and hence, the window needs to be coated with a class of extracellular matrix (ECM) protein, fibronectin to enhance attachment of the cells onto CaF2 window. For culture, C2C12 cells were first plated onto fibronectin coated CaF2 window and expanded in growth media containing DMEM and 10 % fetal bovine serum (FBS). When the cells reach ~90 % confluency, typically after 3 days in culture, they will be cultured in differentiation

media containing DMEM + 2 % horse serum (HS). By day 10, muscle fibers, or myotubes, will form and the CaF2 window containing live cells were fitted to custom-built chamber. The spectra were collected at various developmental stages of C2C12 in order to track changes in cellular water structure associated with muscle development.

6.3.4 Synchrotron Radiation Fourier Transform Infrared (SR-FT-IR) Spectro-microscopy

The SR-FT-IR measurements were made using a Nicolet Magna 760 FTIR bench and a Nicolet Nic-Plan IR microscope with 15X and 32 X objectives, at the Advanced Light Source, Lawrence Berkeley National Laboratory, Infrared Beamline 1.4.3. Myofibril bundle experiments were carried out with a 15X objective, while single myofibril experiments were carried out using a 32X objective. Thirty-two scans of IR spectra were collected between 800 and 4000 cm^{-1} at 4 cm^{-1} resolution, and averaged. SR-FTIR spectra were initially collected to identify the chemical environment of relaxed muscle. To do this, a drop of myofibril bundle suspension was dispensed onto a CaF_2 window and then immersed in relaxing solution for 30 minutes on ice. To collect the SR-FTIR spectra of activated muscle, activating solution was drop dispensed onto the myofibril bundle and measurements were made after the specimen had visibly finished contracting. For obtaining spectral maps of myofibril bundles, total of 8 myofibril bundles were probed in both relaxed and activated states for consistency. Each sample was scanned with a 5 µm step size. For single honeybee myofibrils, 13 myofibrils were probed in both relaxed and activated states. Each sample was scanned with a 1 µm step

size. Second-derivative analysis was performed for enhancement of spectral resolution using the Savitsky-Golay method [37]. To minimize evaporation during data collection, the myofibril bundle was kept in a water-tight custom chamber with a Tefon fitting.

6.4 Results

6.4.1 IR Spectrum of Liquid Water

In order to compare liquid water with muscle water, we first obtained the infrared spectrum of liquid water, as shown in figure 6.1 (top). The OH stretch region of liquid water shows a broad peak due to extensive hydrogen bonding. The second derivative (below) shows that the broad peak resolves into three components: 3230, 3400 and 3620 cm^{-1} corresponding respectively to the symmetric OH stretching mode of ice-like water, partially hydrogen bonded water, and free OH. These are standard assignments. Of the three components, particularly notable is the one at 3400 cm^{-1}, which contains two shoulder peaks at 3480 and 3520 cm^{-1}. These shoulder peaks imply that liquid water may have at least three different arrangements of partially hydrogen-bonded water.

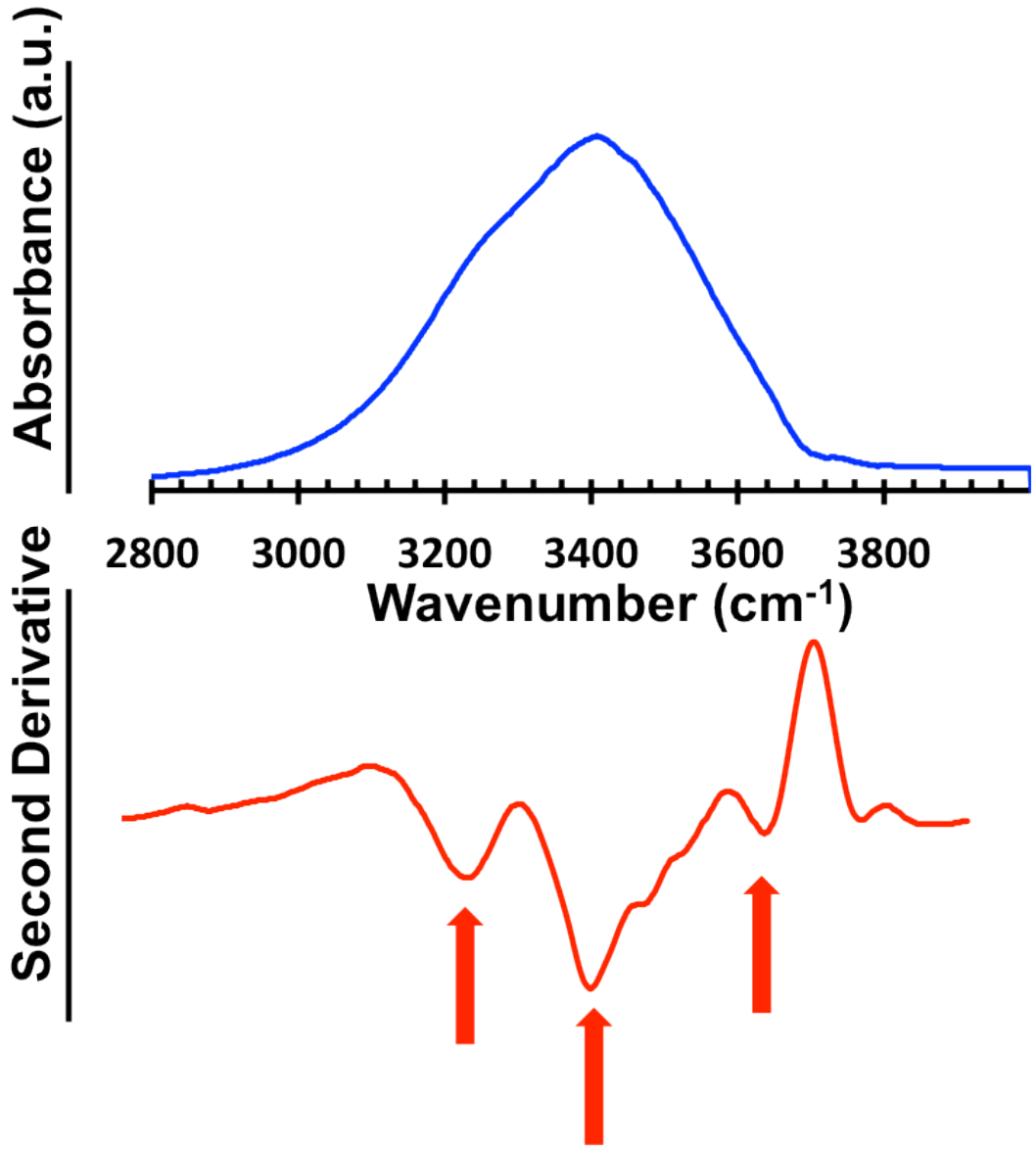

Figure 6.1. Infrared spectrum of liquid water at 22 °C in the OH stretch spectral region (top), and second derivative spectra (bottom). Arrows indicate components resolved with second derivative analysis at 3230, 3400 and 3620 cm^{-1}.

To observe the corresponding hydrogen-bonding environment of muscle water, we collected an infrared map of a single relaxed honeybee myofibril (Figure 6.2). Panel **a**

shows a bright-field image, with visible sarcomeres. The color images in panel **b** show absorption maps obtained at different spectral regions, corresponding to three components of liquid water determined above: fully coordinated ice-like water (3230 cm^{-1}), partially H-bonded water (3400 cm^{-1}), free OH (3620 cm^{-1}). The strong relative absorption at 3230 and 3400 cm^{-1} indicate that the water inside the relaxed myofibril is mostly "ice-like" and partially hydrogen-bonded. The weak absorption at 3620 cm^{-1} indicates little or no free OH. Hence, most of the water molecules inside the relaxed myofibril can be said to be either fully or partially hydrogen-bonded.

A particularly interesting feature of these infrared maps is the inhomogeneous spatial distribution of water along the myofibril. Overlaying the images showed that all three components of water IR absorption were higher in the center of the sarcomere than in the regions around the z-lines. Of those three components, the ice-like water was preferentially present in the middle of the sarcomere. The partially hydrogen bonded water was spread more uniformly over the length of the myofibril, albeit slightly higher in the middle of the sarcomere. Thus, the water content within myofibril shows sarcomeric periodicity. This may mean that the thick-filaments, which are found in the middle of the sarcomere, might have higher water holding capacity than the thin-filaments, which are nearer to the ends of the sarcomere. The stronger absorption of ice-like water may be due to higher negative charge density on the surfaces of thick filaments compared to thin filaments [16-17].

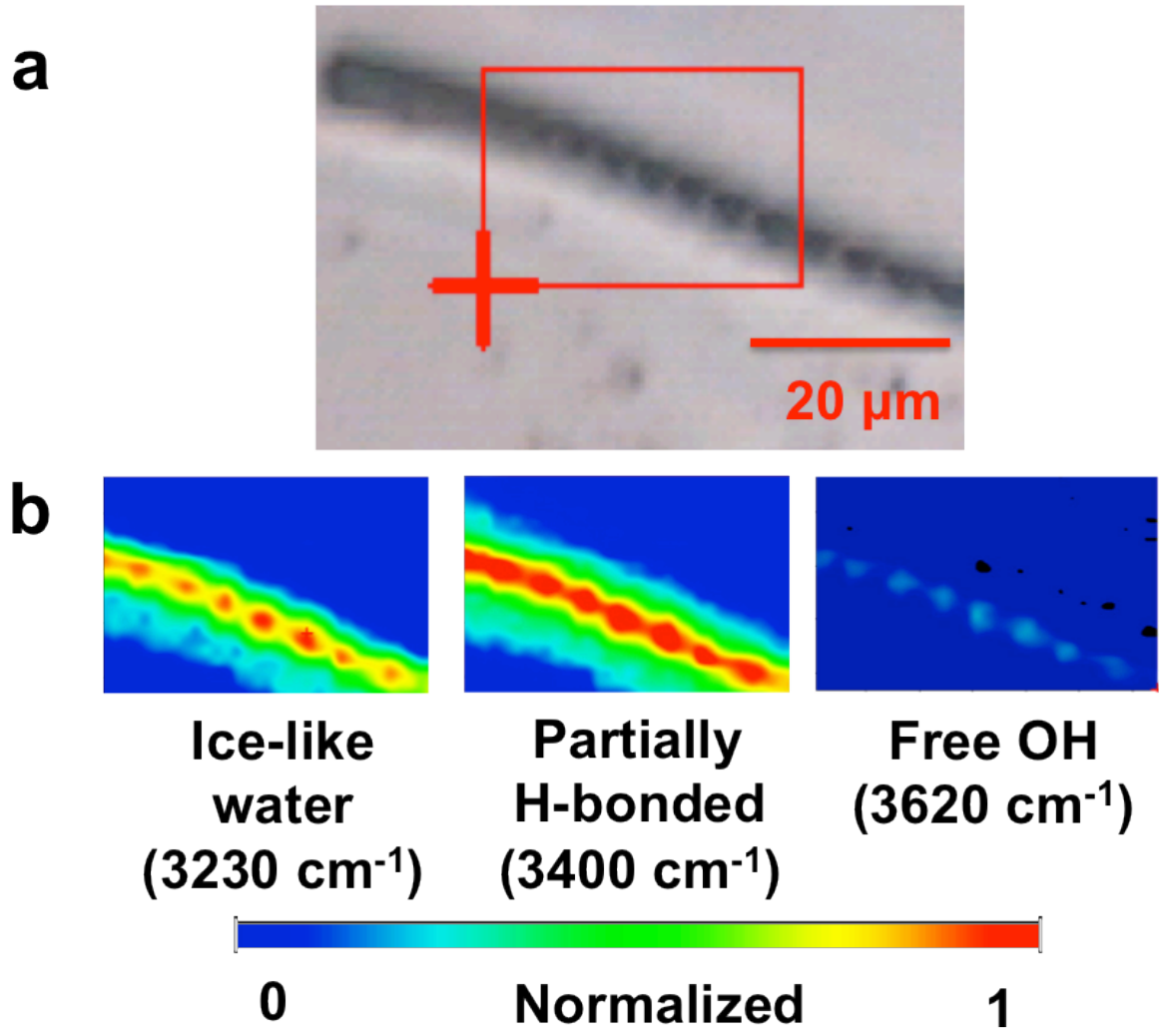

Figure 6.2 a: Bright-field image of a single honeybee myofibril in relaxed state. **b:** IR absorption maps of the same specimen at three wavenumbers, corresponding to ice-like water (3230 cm^{-1}), partially hydrogen bonded water (3400 cm^{-1}), and free OH (3620 cm^{-1}).

In order to investigate the chemical changes associated with contraction, myofibril bundles were studied in relaxed and activated states. To simulate two physiological states of muscle, we used standard model comprising of skinned muscle and two

physiological solutions. The bundle was first bathed in relaxing solution for 30 minutes and an IR map was collected. Next, the same bundle was bathed in activating solution for 30 minutes. By that time, the specimen was fully contracted: all visible signs of contraction development had ceased.

Figure 6.3**a** shows bright-field images and superimposed IR maps of the relaxed and activated bundle. The IR maps were obtained at 3500 cm^{-1}, the spectral region showing the largest changes as the specimen passed from the relaxed state to the contracted state. The activated specimen absorbed significantly more than the relaxed specimen at 3500 cm^{-1}. This increase may be indicative of decreased hydrogen-bonding strength of muscle water during contraction.

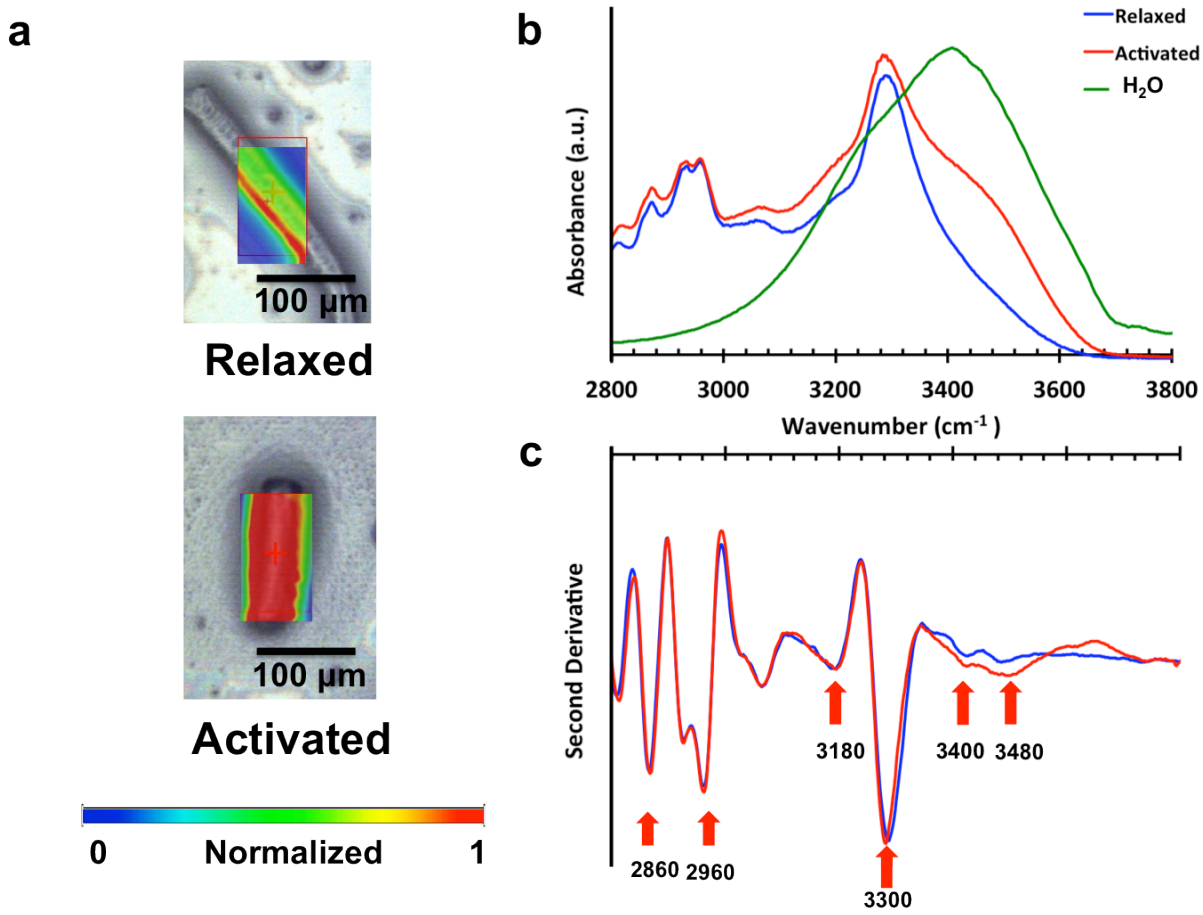

Figure 6.3 ***a***. Bright-field images of relaxed and activated myofibril bundle with overlays of IR images at 3500 cm^{-1} showing significant increase in absorption during contraction. For the color map, absorption of activated muscle at 3550 cm^{-1} is normalized to 1 for comparison. ***b.*** IR spectra of relaxed (blue), activated (red) muscle and deionized water (green). ***c***. Second-derivative spectra of relaxed and activated muscle.

Figure 6.3**b** shows the representative IR spectra from relaxed (blue) and activated (red) specimens. Deionized water (green) is shown for comparison. Consistent with findings in the single myofibril (Figure 1), the spectra of the relaxed bundle shows almost complete

absence of free OH (3620 cm^{-1}) compared to liquid water. This indicates stronger hydrogen bonding strength of muscle water compared with deionized water. The most notable feature of Figure 3b is the shoulder peak near 3500 cm^{-1} that appears upon activation, indicating 'break-up' of the hydrogen-bonding network. However, even with a significant de-hydrogen bonding the activated muscle still largely lacked free OH. The changes seen in the OH stretch region of IR spectra upon activation were reversible at least up to two activate-relaxing cycles, indicated by appearance and disappearance of the shoulder peak at 3500 cm-1 in activated and relaxed states, respectively.

For more detailed spectral analysis of the OH stretch region, second derivative analysis was performed on the original spectra. The results are shown in Figure 3 **c**. They show several peaks corresponding to symmetric and asymmetric CH_2 stretch of lipids (~2852 and 2924 cm^{-1}), asymmetric CH_3 stretch of lipids (2960 cm^{-1}), symmetric NH stretch of amide A and amide B (3300 and 3057 cm^{-1}), besides the water peaks (3180, 3400, 3480 cm^{-1}). Table 1 summarizes those peaks. While other peaks do not show any obvious shifts, the amide A band shows a blue-shift (i.e., to higher frequency) of about 10 cm^{-1}. Such shift has been associated with an α-helix to β-sheet transition [15].

Table 6.1. Assignment of IR bands and their major contributors

Wavenumber (cm^{-1})	Vibrational mode assignment and major contribution
~3620	νOH of Free OH [18]
~3400	νOH of Partially-hydrogen bonded Water [18]

~3300	Amide A, νNH of Proteins [19]
~3230	νOH of Ice-like water [18]
~2960	$\nu_{as}CH_3$ of lipids, proteins and nucleic acids [19]
~2924	$\nu_{as}CH_2$ of lipids [20]
~2860	$\nu_{s}CH_2$ of lipids [20]
~1650	Amide I, *ν*C=O stretch [19]
~1550	Amide II [19]

In Figure 6.3c, second derivative water peaks are seen corresponding to 3180, 3400 and 3480 cm^{1}. Compared with liquid water (Figure 1), the component corresponding to ice-like water occurs at a lower frequency, by about 20 cm^{-1}. This shift indicates that fully coordinated modes of water in muscle contain slower vibrational modes, presumably due to dipolar coupling of water and protein oscillators. Upon activation, the ratio of the amide A peak (3300 cm-1) and the 3480 cm^{-1} water peak increases, showing an increase in the number of broken hydrogen bonds per protein molecule. Thus, the second-derivative analysis confirms the results obtained from the original spectra: a significant 'break-up' of hydrogen bonds during activation. The absence of free OH in both relaxed and activated myofibril bundle shows that the 'break-up' of hydrogen bonding during activation still leaves water molecules hydrogen-bonded to at least one neighboring water molecule.

To confirm that the observed changes in muscle water are not artifacts arising from differences in absorption from the different physiological solutions, we collected infrared spectra of both activating and relaxing solutions (Figure 6.4). Comparison with the spectra of deionized water confirmed that both physiological solutions had IR spectra indistinguishable from that of deionized water.

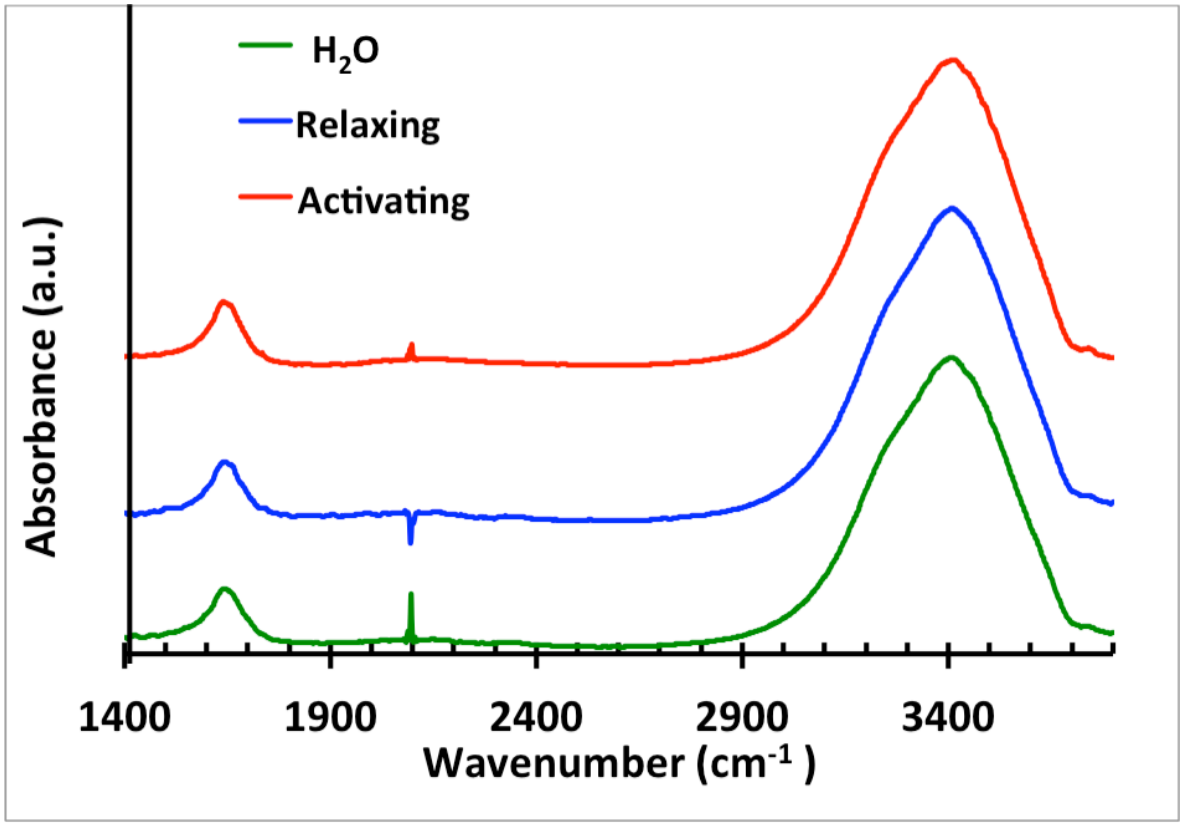

Figure 6.4. IR spectra of deionized water (green), relaxing solution (blue) and activating solution (red), showing no obvious differences.

The amide bands in vibrational spectra of proteins are useful tools for determining the secondary structure of proteins and the proteins' stability [12-13, 20-21]. Specifically, the amide I peak provides sensitive information on protein secondary structures (i.e., α-helix, β-sheets, β-sheet turns, side-chains, etc.). Figure 5**a** shows representative spectra of the corresponding spectral region in relaxed (blue) and activated (red) myofibril bundles. These spectra were taken from the same spectra as figure6.3b. In the relaxed state, the myofibril bundle shows a classic amide I peak centered ~1650 cm^{-1} and amide II peak centered ~1550 cm^{-1}. Upon activation, the amide I peak splits into two (Figure 6.5**a**), the new peak appearing at ~1600 cm^{-1}, over and above the original peak at ~1650 cm^{-1}. Moreover, the centroid of the 1650 cm^{-1} peak is red-shifted to lower frequency by about 15 wavenumbers. While detailed theoretical description of Amide I splitting has posed significant challenges, experimental results indicate that splitting of Amide I peak to lower frequency is associated with β-sheet rich structures [22]. Thus, the red-shifting of the 1650 cm^{-1} peak centroid indicates the formation of intermolecular β-sheets arising out of aggregation of unfolded proteins in activated muscle. The new peak appearing in the amide I region at ~ 1600 cm^{-1} is assigned to the amino acid side-chains of proteins including both hydrogenated and hydroxylated glutamine (H-Gly and OH-Gly), whose transport plays an important role in phosphorylation of muscle and contraction [19, 23]. Thus, increased absorption at ~ 1600 cm^{-1} seen here may be due to formation of side-chains during contraction. Contrary to the amide I band, the amide II band showed less change with activation: diminished absorbance, with no change in the peak location.

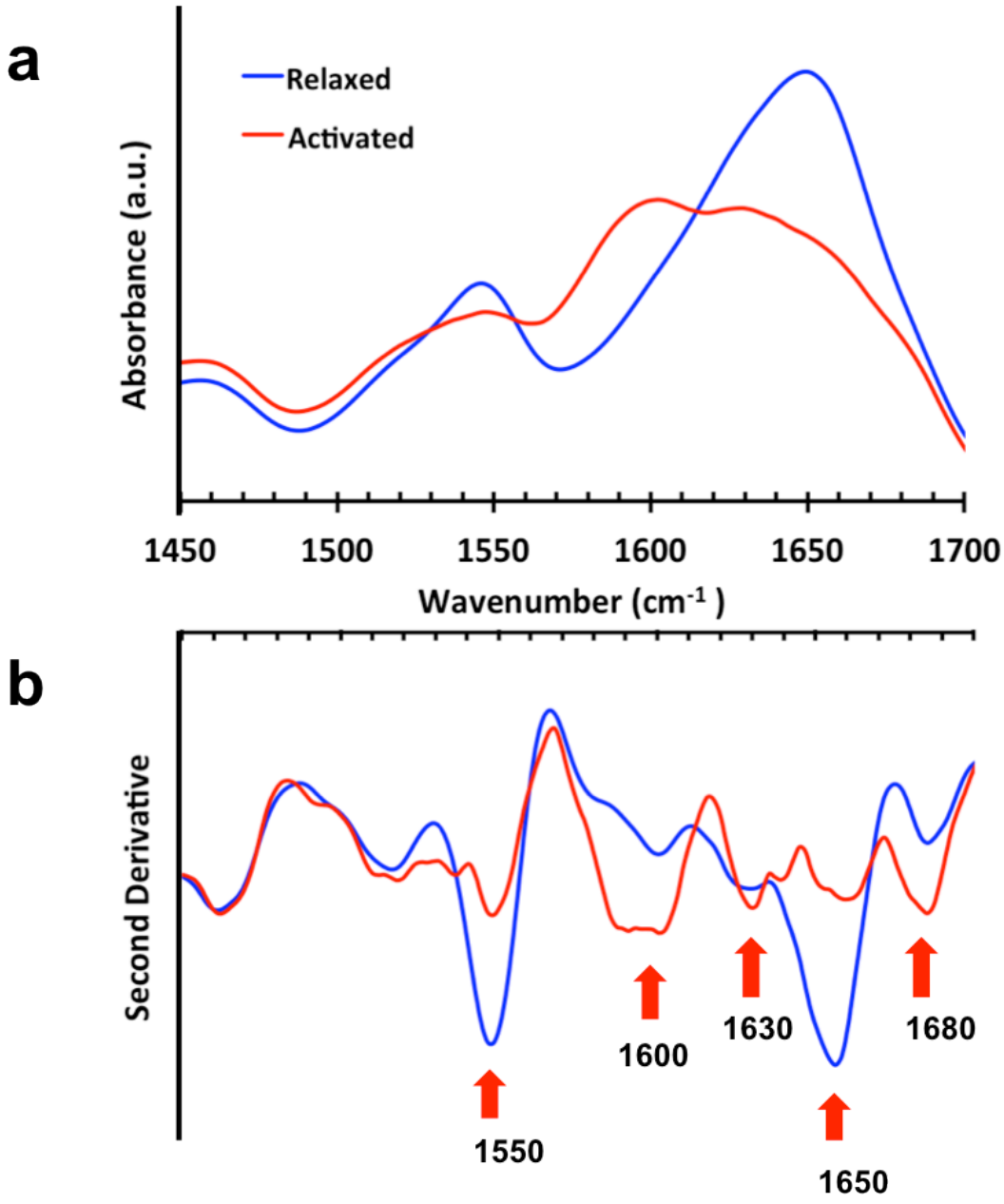

Figure 6.5 ***a***. IR spectra of relaxed (blue) and activated (red) myofibril bundle in amide I and II spectral regions. ***b***. Second-derivative of the IR spectra.

To examine these spectral features in more detail, we looked at the second derivative spectra. Figure 6.5 **b** shows the second derivative of the original spectra in the amide I and II region. Several features are of interest. First, the relaxed muscle has markedly higher composition of α-helix (1652 cm^{-1}) than activated muscle. Second, the peak centered at ~1630 cm^{-1} and ~1680 cm^{-1} increased significantly in amplitude when muscle went from relaxed to activated. These peaks represent β-sheets and β-turns respectively [19]. Taken together, these findings show that muscle proteins lost helical order during activation, similar to the conclusions drawn earlier from x-ray diffraction studies [24].

The activation-associated changes of muscle water are appreciable (Fig. 6.3 **b**). However, the myofibril bundle contains water both inside the myofibril and between the myofibrils. To ensure that the observed changes in hydrogen bonding are indeed due to changes within the myofibrils, i.e. associated with myosin, actin, etc., we probed single myofibrils, where the only water present in the sample lies within the contractile apparatus. Contraction is ordinarily less pronounced in honeybee myofibrils, but was confirmed by monitoring shortening of sarcomeres in bright-field images. The statistics are summarized in figure 6.6.

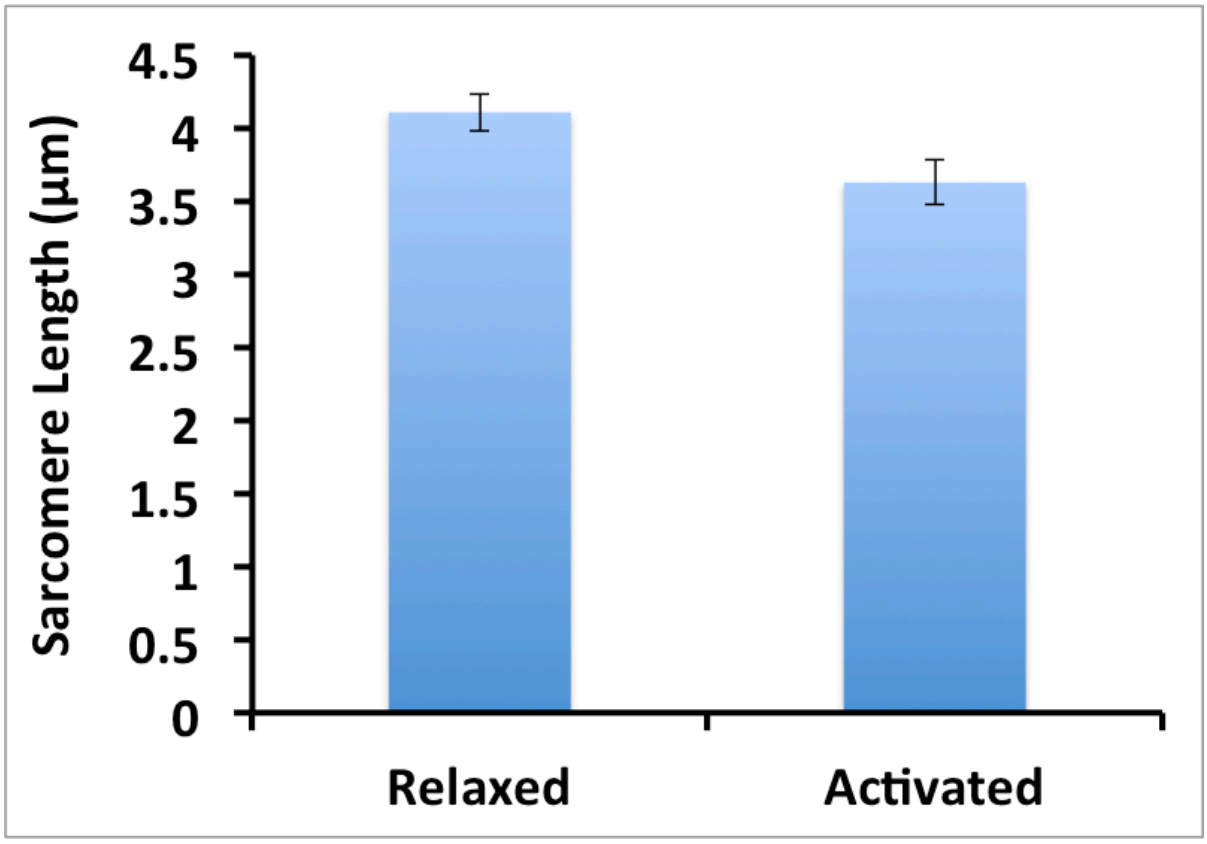

Figure 6.6 Length of sarcomeres in relaxed and activated single honeybee myofibrils with standard error of mean.

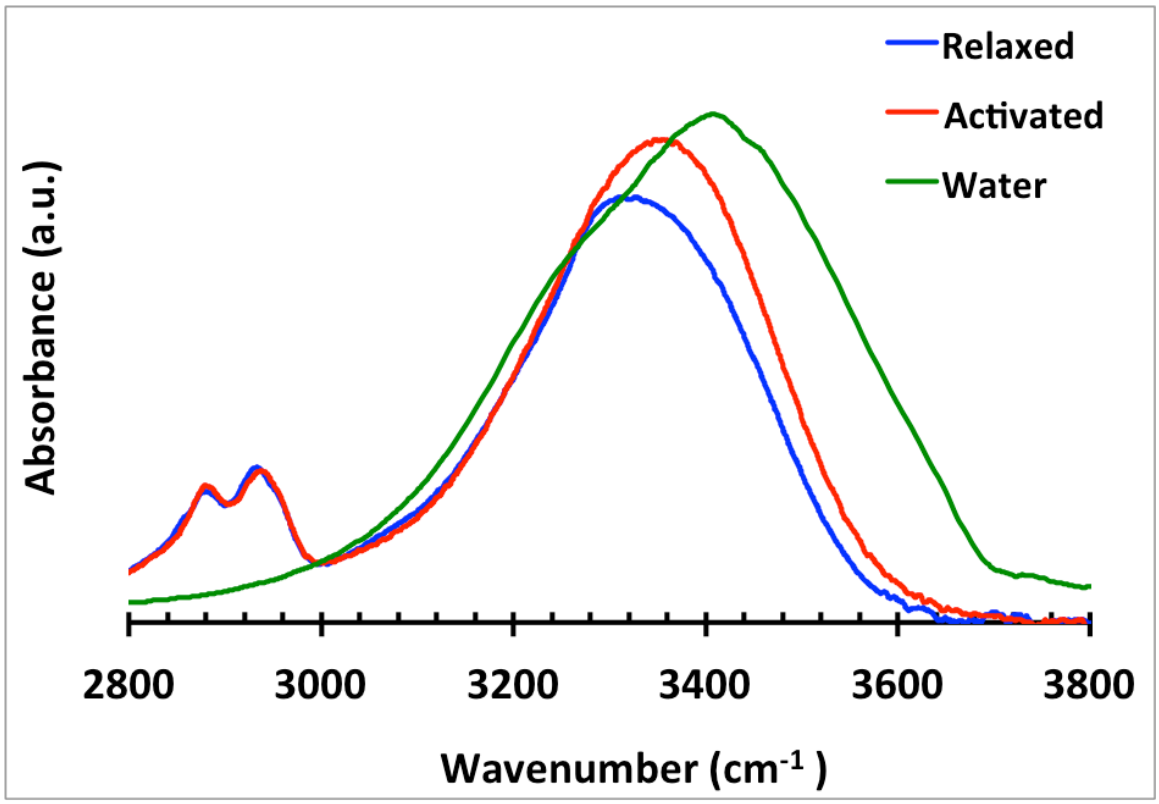

Figure 6.7 IR spectra of relaxed (blue) and activated single myofibril (red). The IR spectra of liquid water are shown for comparison (green).

The results obtained with the single myofibril largely concur with those obtained with the myofibril bundles (Figure 6.3). As seen above with rabbit myofibril bundles, the representative spectrum of relaxed single myofibril in figure 6.7 shows an OH stretch peak significantly red-shifted from that of deionized water. This shift indicates stronger hydrogen bonding than liquid water. Moreover, as the specimen passed from relaxed (blue) to activated (red) hydrogen bonding strength decreased, as indicated by a ~25 cm^{-1} blue-shifting of the centroid of water OH stretch peak. The de-hydrogen bonding agrees with results obtained from myofibril bundles. Hence, the major findings in

muscle water hydrogen bonding are consistent in both single myofibrils and myofibril bundles, indicating that those changes occur within the acto-myosin complex.

While glycerinated muscle fibers offer a standard model to study muscle contraction, the abundance of holes punctured on cell membranes alter osmotic properties of the cell when compared with living cells having intact cell membranes. In order to study the water hydrogen-bonding environment of live muscle fiber, C2C12 cells were cultured and differentiated to form skeletal myotubes.

The cells proliferated and differentiated well on CaF2 window well, and fused into muscle fiber with no significant problem as shown in figure 6.8. Similar to earlier studies with explanted muscle fiber, Infrared maps were also collected on live skeletal muscle fibers. As with single myofibrils and myofibril bundles, water inside muscle cells absorb more preferentially at 3230 and 3400 cm-1, while very little abosorption is observed at 3620 cm-1. This indicates that water in live skeletal muscle cell is either fully or partially hydrogen bonded, and contains little or no free OH. Another interesting result of the study is higher overall absorption of water peaks in fused muscle cell, compared with un-fused myoblast cells. Thus, muscle cell may have higher water-holding capacity, or more hydrophilic as it goes from precursor myoblast to fully differentiated myotubes.

The studies with live muscle cell confirm that the well hydrogen-bonded water environment is general for muscle fibers, hence confirming earlier studies.

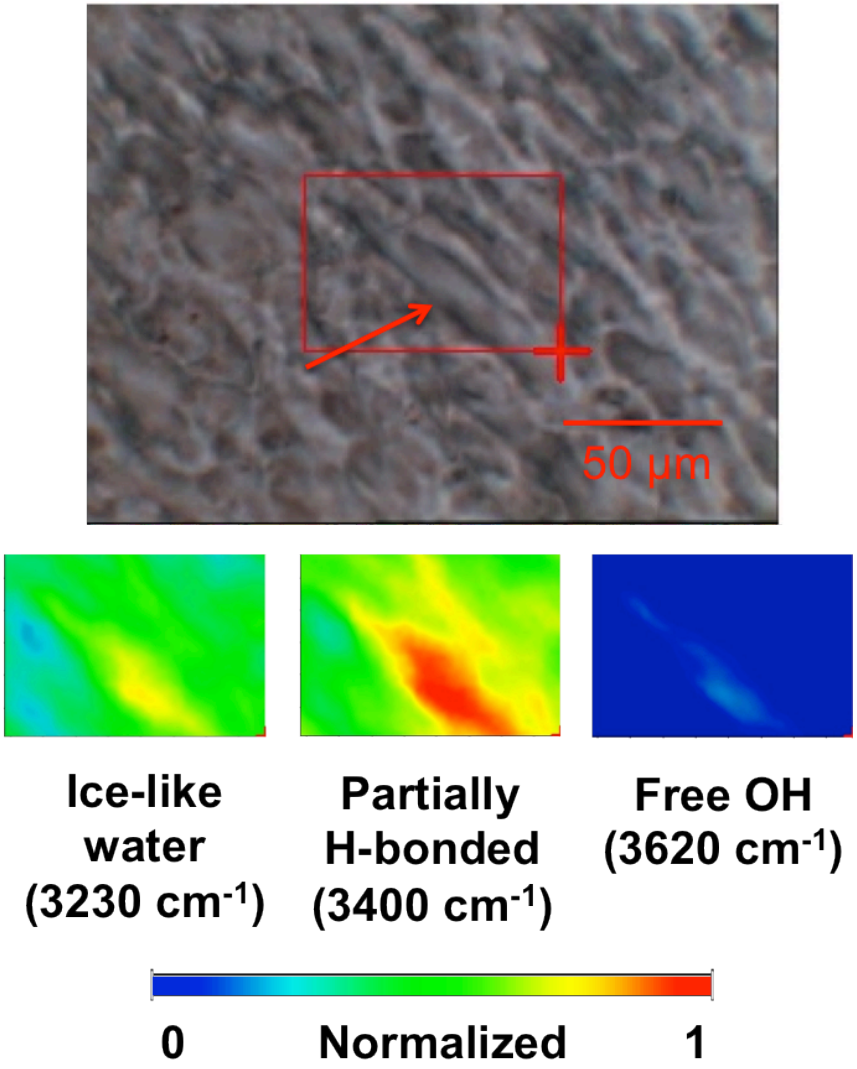

Figure 6.8 (top) bright-field image of C2C12 cells on day 5. By day 5, myoblasts are fused to form muscle fiber indicated by the arrow. (bottom) IR absorption maps at three water components: 3230, 3400 and 3620 cm-1.

6.5 Discussion

This study was carried out to understand the chemical environment of skeletal muscle water and its possible role in contraction. Our results show that water in relaxed muscle

is significantly more structured than bulk water, with little or no free-OH present. This was found inside myofibril bundles as well as inside single myofibrils. The most notable result of this study was the sensitivity of the water hydrogen-bonding environment to distinct physiological states. When the myofibril was activated, the well-hydrogen-bonded muscle water lost order as the muscle proteins changed conformation. Water evidently plays some role in the contractile process.

It is widely believed that water inside biological tissues is similar to bulk water, except for the first two or three protein hydration layers. However, more recent results have shown that hydrophilic surfaces can extensively order nearby water [25-27]. Further, recent NMR measurements show that in confined geometries such as inside reverse-micelles, protein hydration shells can extend out to several dozens of layers [28]. Considering the confined geometry inside the myofilament lattice, it is no surprise that most of the muscle water is well structured. Thus, muscle water differs substantially from bulk water.

While modern understanding of muscle contraction is largely dominated by the 'cross-bridge' theory originally proposed by Sir Andrew Huxley and H.E. Huxley [29-30], many experimental results remain at odds with that theory. The most notable are shortening of thick filaments during contraction [31] and generation of force even with no apparent overlap of thick and thin filaments [32], where no attachment of myosin heads to actin filaments can occur. Both findings indicate the need for reconsideration of that mechanism [9, 33]. On the other hand, the breakup of water structure during contraction

implies that the high viscosity issue mentioned in the Introduction may be less of a problem for the prevailing theory than initially considered. If the water remained highly viscous, not only could cross-bridges fail to swing, but also any kind of filamentary motion might confront substantial difficulty.

Several physical changes occur immediately following stimulation but prior to force generation. These include changes in thick filament length [31], sudden decreases in viscoelasticity [34], loss of axial and helical order in myosin [35], and latency relaxation [36]. All of those changes occur within milliseconds after stimulation and well before the onset of force generation. While these changes are seemingly necessary preconditions for force generation, their mechanisms have remained unclear. Changes in water structure might potentially explain some or all of those changes and help provide better understanding of the molecular mechanism of muscle contraction.

Given the breakup of water structure during contraction, a lingering question is which of the two events comes first: changes in protein conformation or break-up of ordered hydration water? Time-resolved studies will be needed to answer this important question, which may have relevance also for other biological systems.

6.6 References

1. Chaplin, M. Do we underestimate the importance of water in cell biology? *Nat Rev Mol Cell Biol* **2006,** *7* (11), 861-866.

2. Cheung, M. S.; Garcia, A. E.; Onuchic, J. N. Protein folding mediated by solvation: water expulsion and formation of the hydrophobic core occur after the structural collapse. *Proceedings of the National Academy of Sciences of the United States of America* **2002,** *99* (2), 685-90.

3. Makarov, V.; Pettitt, B. M.; Feig, M. Solvation and hydration of proteins and nucleic acids: a theoretical view of simulation and experiment. *Accounts of chemical research* **2002,** *35* (6), 376-84.

4. Svergun, D. I.; Richard, S.; Koch, M. H. J.; Sayers, Z.; Kuprin, S.; Zaccai, G. Protein hydration in solution: Experimental observation by x-ray and neutron scattering. *Proceedings of the National Academy of Sciences* **1998,** *95* (5), 2267-2272.

5. Born, B.; Kim, S. J.; Ebbinghaus, S.; Gruebele, M.; Havenith, M. The terahertz dance of water with the proteins: the effect of protein flexibility on the dynamical hydration shell of ubiquitin. *Faraday Discussions* **2009,** *141* (0), 161-173.

6. Ebbinghaus, S.; Kim, S. J.; Heyden, M.; Yu, X.; Heugen, U.; Gruebele, M.; Leitner, D. M.; Havenith, M. An extended dynamical hydration shell around proteins. *Proceedings of the National Academy of Sciences* **2007,** *104* (52), 20749-20752.

7. Frauenfelder, H.; Chen, G.; Berendzen, J.; Fenimore, P. W.; Jansson, H.; McMahon, B. H.; Stroe, I. R.; Swenson, J.; Young, R. D. A unified model of protein

dynamics. *Proceedings of the National Academy of Sciences of the United States of America* **2009,** *106* (13), 5129-34.

8. Oplatka, A. Critical review of the swinging crossbridge theory and of the cardinal active role of water in muscle contraction. *Critical reviews in biochemistry and molecular biology* **1997,** *32* (4), 307-60.

9. Pollack, G. H. *Muscles & molecules : uncovering the principles of biological motion*. Ebner & Sons Publishers: Seattle, Wash., 1990; p x, 300 p.

10. Goertz, M. P.; Houston, J. E.; Zhu, X. Y. Hydrophilicity and the Viscosity of Interfacial Water. *Langmuir* **2007,** *23* (10), 5491-5497.

11. Levenson, E.; Lerch, P.; Martin, M. C. Spatial resolution limits for synchrotron-based infrared spectromicroscopy. *Infrared Physics & Technology* **2008,** *51* (5), 413-416.

12. Holman, H.-Y. N.; Bechtel, H. A.; Hao, Z.; Martin, M. C. Synchrotron IR Spectromicroscopy: Chemistry of Living Cells. *Analytical Chemistry* **2010,** *82* (21), 8757-8765.

13. Holman, H.-Y. N.; Hao, Z.; Martin, M. C.; Bechtel, H. A. Infrared Spectromicroscopy: Probing Live Cellular Responses to Environmental Changes. *Synchrotron Radiation News* **2010,** *23* (5), 12-19.

14. Holman, H.-Y. N.; Miles, R.; Hao, Z.; Wozei, E.; Anderson, L. M.; Yang, H. Real-Time Chemical Imaging of Bacterial Activity in Biofilms Using Open-Channel Microfluidics and Synchrotron FTIR Spectromicroscopy. *Analytical Chemistry* **2009,** *81* (20), 8564-8570.

15. Falk, M.; Ford, T. A. INFRARED SPECTRUM AND STRUCTURE OF LIQUID WATER. *Canadian Journal of Chemistry* **1966,** *44* (14), 1699-1707.

16. Noble, M. I.; Pollack, G. H. Molecular mechanisms of contraction. *Circulation Research* **1977,** *40* (4), 333-342.

17. Yu, L. C.; Dowben, R. M.; Kornacker, K. THE MOLECULAR MECHANISM OF FORCE GENERATION IN STRIATED MUSCLE. *Proceedings of the National Academy of Sciences* **1970,** *66* (4), 1199-1205.

18. Falk, M.; Ford, T. A. Infrared Spectrum and Structure of Liquid Water. *Can J Chemistry* **1966,** *44* (14), 1699-&.

19. Barth, A. Infrared spectroscopy of proteins. *Biochimica et Biophysica Acta (BBA) - Bioenergetics* **2007,** *1767* (9), 1073-1101.

20. Birarda, G.; Grenci, G.; Businaro, L.; Marmiroli, B.; Pacor, S.; Piccirilli, F.; Vaccari, L. Infrared microspectroscopy of biochemical response of living cells in microfabricated devices. *Vibrational Spectroscopy* **2010,** *53* (1), 6-11.

21. Vaccari, L.; Birarda, G.; Businaro, L.; Pacor, S.; Grenci, G. Infrared Microspectroscopy of Live Cells in Microfluidic Devices (MD-IRMS): Toward a Powerful Label-Free Cell-Based Assay. *Analytical Chemistry* **2012,** *84* (11), 4768-4775.

22. Litvinov, R. I.; Faizullin, D. A.; Zuev, Y. F.; Weisel, J. W. The ±-Helix to ≤-Sheet Transition in Stretched and Compressed Hydrated Fibrin Clots. *Biophysical journal* **2012,** *103* (5), 1020-1027.

23. Rennie, M. J.; Low, S. Y.; Taylor, P. M.; Khogali, S. E.; Yao, P. C.; Ahmed, A. Amino acid transport during muscle contraction and its relevance to exercise. *Advances in experimental medicine and biology* **1998,** *441*, 299-305.

24. Reconditi, M.; Brunello, E.; Linari, M.; Bianco, P.; Narayanan, T.; Panine, P.; Piazzesi, G.; Lombardi, V.; Irving, M. Motion of myosin head domains during activation and force development in skeletal muscle. *Proceedings of the National Academy of Sciences* **2011,** *108* (17), 7236-7240.

25. Yoo, H.; Paranji, R.; Pollack, G. H. Impact of Hydrophilic Surfaces on Interfacial Water Dynamics Probed with NMR Spectroscopy. *The Journal of Physical Chemistry Letters* **2011,** *2* (6), 532-536.

26. Zheng, J.-m.; Pollack, G. H. Long-range forces extending from polymer-gel surfaces. *Physical Review E* **2003,** *68* (3), 031408.

27. Pollack, G. H. *The Fourth Phase of Water: Beyond Solid, Liquid, and Vapor*. Ebner and Sons: Seattle, WA, 2013.

28. Nucci, N. V.; Pometun, M. S.; Wand, A. J. Site-resolved measurement of water-protein interactions by solution NMR. *Nat Struct Mol Biol* **2011,** *18* (2), 245-249.

29. Huxley, H.; Hanson, J. Changes in the Cross-Striations of Muscle during Contraction and Stretch and their Structural Interpretation. *Nature* **1954,** *173* (4412), 973-976.

30. Huxley, A. F. Muscle structure and theories of contraction. *Progress in biophysics and biophysical chemistry* **1957,** *7*, 255-318.

31. Nagornyak, E. M.; Blyakhman, F. A.; Pollack, G. H. Stepwise Length Changes in Single Invertebrate Thick Filaments. *Biophysical journal* **2005,** *89* (5), 3269-3276.

32. Carlsen, F.; Knappeis, G. G.; Buchthal, F. Ultrastructure of the Resting and Contracted Striated Muscle Fiber at Different Degrees of Stretch. *The Journal of Biophysical and Biochemical Cytology* **1961,** *11* (1), 95-117.

33. Pollack, G. H. *Cells, gels and the engines of life : a new, unifying approach to cell function*. Ebner & Sons: Seattle, WA, 2001; p xiv, 305 p.

34. Ford, L. E.; Huxley, A. F.; Simmons, R. M. Tension responses to sudden length change in stimulated frog muscle fibres near slack length. *The Journal of Physiology* **1977,** *269* (2), 441-515.

35. Brunello, E.; Bianco, P.; Piazzesi, G.; Linari, M.; Reconditi, M.; Panine, P.; Narayanan, T.; Helsby, W. I.; Irving, M.; Lombardi, V. Structural changes in the myosin filament and cross-bridges during active force development in single intact frog muscle fibres: stiffness and X-ray diffraction measurements. *The Journal of Physiology* **2006,** *577* (3), 971-984.

36. Lännergren, J. The Effect of Low-Level Activation on the Mechanical Properties of Isolated Frog Muscle Fibers. *The Journal of General Physiology* **1971,** *58* (2), 145-162.

37. Savitzky, A.; Golay, M. J. E. Smoothing and Differentiation of Data by Simplified Least Squares Procedures. *Analytical Chemistry* **1964,** *36* (8), 1627-1639.

Effect of Radiant Energy on Near-Surface Water

Binghua Chai, Hyok Yoo, and Gerald H. Pollack*

Department of Bioengineering, Box 355061, University of Washington, Seattle, Washington 98195

Received: August 24, 2009

While recent research on interfacial water has focused mainly on the few interfacial layers adjacent to the solid boundary, century-old studies have extensively shown that macroscopic domains of liquids near interfaces acquire features different from the bulk. Interest in these long-range effects has been rekindled by recent observations showing that colloidal and molecular solutes are excluded from extensive regions next to many hydrophilic surfaces [Zheng and Pollack *Phys. Rev. E* **2003**, *68*, 031408]. Studies of these aqueous "exclusion zones" reveal a more ordered phase than bulk water, with local charge separation between the exclusion zones and the regions beyond [Zheng et al. *Colloid Interface Sci.* **2006**, *127*, 19; Zheng and Pollack *Water and the Cell: Solute exclusion and potential distribution near hydrophilic surfaces*; Springer: Netherlands, 2006; pp 165−174], here confirmed using pH measurements. The main question, however, is where the energy for building these charged, low-entropy zones might come from. It is shown that radiant energy profoundly expands these zones in a reversible, wavelength-dependent manner. It appears that incident radiant energy may be stored in the water as entropy loss and charge separation.

Introduction

For many years and from many old studies, it has been known that liquids behave differently from bulk in the region of interfaces. A summary of this older evidence can be found in a comprehensive review written more than a half-century ago by Henniker.[1] Henniker cites more than 100 papers showing that, for many liquids, the physical chemical behavior in the regions near interfaces diverges from the physical chemical behavior farther away, the near-surface liquid taking on different structural forms. Among the cited studies are those of Hardy,[2] who emphasized structural differences extending up to hundreds of micrometers from the surface. Included among the liquids cited to show such structural differences was water.

By and large, however, the existence and putative functional roles of these extensive interfacial zones have been forgotten. This has been at least partly due to technological advances that have permitted exploration of the few water layers closest to the material surface, which have confirmed the presence of icelike layers.[3−5] Because of the compelling nature of these observations, the field's emphasis has focused on those intimate layers, while interest in possible long-range effects, not addressed by those methods, has dwindled.

A notable exception is the work of Green and Otori,[6] which considered whether such long-range effects might be responsible for the biological phenomenon known as the "unstirred layer". Surrounding many biological tissues is a zone of extremely slow diffusion extending up to hundreds of micrometers from the surface.[7] Postulating some role of extended near-surface water, Green and Otori exposed biological tissues and gels to microsphere suspensions and found that the microspheres were excluded from regions on the order of 200 to 300 μm from the respective surfaces, speculating that some feature of near-surface water might be different and might thereby account for the slow diffusion.

* To whom correspondence is addressed. E-mail: ghp@u.washington.edu. Tel.: (206)685-1880. Fax: (206)685-3300.

More recently, a series of systematic studies confirmed and extended these observations. The first experiments largely duplicated those of Green and Otori (which had been unknown to the authors at the time) with different surfaces. Thus, aqueous microsphere suspensions were exposed to hydrophilic gel surfaces, and the microspheres were excluded from zones extending 100−200 μm from the respective surfaces. Multiple controls were tested for possible artifacts, and all results were negative for artifact or trivial explanations.[8]

Subsequent studies confirmed profound exclusion of microspheres from a series of hydrophilic surfaces and went on to show that it was not only microspheres that were excluded but also various small molecules; hence, the zone of exclusion, labeled hereafter as the "exclusion zone" or EZ, appeared to behave much like an ordered liquid that broadly excluded many molecules.[9] By various physical chemical methods, this zone was further shown to be both more stable and more ordered than bulk water, albeit less ordered than the icelike zones of the first few layers immediately adjacent to the surface.[9] (An example of such an EZ is shown below in Figure 2A.)

A notable feature of the EZ is its negative charge. Microelectrodes placed within the zone showed large potential differences relative to the water lying beyond, as high as 100−200 mV negative.[10] Since the potential difference is reckoned between contiguous water regions, the result implies charge separation within the water, and the question arises as to where the energy might come from for driving such charge separation and increased ordering. The fact that the more ordered zone is as large as it is implies that substantial energy might be required, well beyond that available from ordinary surface energy. The question of energy source is the focus of the studies reported here.

Materials and Methods

Sample Preparation. The hydrophilic substances used in the experiments included Nafion tubing (TT-050 with 0.042 in. diameter, Perma Pure LLC) and Nafion 117 per-fluorinated membrane (0.007 in. thick, Aldrich). Before use, they were

10.1021/jp908163w CCC: $40.75
Published on Web 09/29/2009

immersed in deionized water for 10 min. All experiments were carried out at 22−23 °C and in a dark room to minimize background noise.

All experiments used deionized water, which was obtained from a NANOpure Diamond ultrapure water system. The purity of water from this system is certified by a resistivity value up to 18.2 mΩ·cm, which exceeds ASTM, CAP, and NCCLS type I water requirements. In addition, the deionized water was passed through a 0.2-μm hollow fiber filter for ensuring bacteria- and particle-free water.

Polybead carboxylate microspheres (2.65% solids-latex, Polysciences Inc.), hydrophilic silica microspheres (SiO_2, Polysciences Inc.), and sulfate microspheres (2.65% solids-latex, Polysciences Inc.) were used to delineate the extent of the exclusion zone. The volume fractions of these aqueous microsphere suspensions were set to 1 to 500.

pH Measurements. Two types of pH measurement were carried out: one using miniature pH probes for tracking the time course of pH change at various distances from the Nafion surface; and another for measuring the pH distribution as a function of distance from the Nafion surface.

For the former, a micro pH probe (catalog no.: PHR-146U, Lazar Research Laboratories, Inc., Los Angeles, CA) connected to a standard pH meter (catalog no.: 6230N, Jenco, San Diego, CA) was used to measure local pH. A 1-cm-high chamber was built with floor dimension 1 cm × 4 cm. The floor was fully covered by a sheet of Nafion. Distilled, deionized water (5 mL) was added slowly enough to avoid disturbing the Nafion sheet. The pH probe was then lowered to the desired height (1, 5, or 10 mm above the sheet), and pH readings were taken at 5 s intervals.

For the pH-dye experiments, a thin 75 mm × 1 mm Nafion film (Sigma Aldrich, Inc.) was first cut and glued at the base of a chamber made out of standard microscope slides. The glass chamber had a 75 mm × 1 mm base and height of 25 mm. Standard pH dye (Sigma Aldrich) was then diluted per manufacturer's recommendation and poured slowly into the chamber. The local pH change next to Nafion was recorded using a charge coupled device (CCD) camera (Scion Corporation) and image.

Effects of Radiant Energy. A Zeiss Axiovert-35 microscope was used for all observations. A high-resolution single chip color digital camera (CFW-1310C), well-suited for bright-field and low-light color video microscopy, as well as for photo documentation was used for color imaging. It has a pixel resolution of 1360 × 1024 with a dynamic range of 10 bits. The CCD sensor of that camera employs the widely used Bayer color-filter arrangement.

Two types of chamber were used. The first was made using a thin cover glass stuck to the bottom of a 1-mm thick cover slide with a 9-mm circular hole in the center; that chamber was used for experiments with Nafion tubing. The second was the same except that the hole was a rectangle of length 3.15 cm × width 1.2 cm × height 1.5 mm, which was for experiments with Nafion membrane, secured with a "microvessel" clip to stand up in the middle of the chamber (0.75 × 4-mm jaws, World Precision Instruments).

Light Source and Incident Power Measurement. For sample illumination, a series of LEDs were used. Infrared LEDs (Gistopics) came in TO-18 packages with parabolic reflectors for reducing the beam-divergence angle. For the visible range, the LED Φ5 series (Nichia) was used. And, for illumination in the UV region, we used LED NSHU590 (Nichia) emitting at 365 nm, and LEDs UVTOP 265 and UVTOP 295 (Sensor Electronic Technology) encapsulated in metal−glass TO-39 packages with UV-transparent hemispherical lens optical windows, emitting, respectively, at 270 and 300 nm. All LEDs were driven at 2 kHz by a Model D-31 LED driver (Gistoptics). Output power was regulated for consistency using a Newport 1815-C optical power meter with Newport 818-UV, 818-SL, and 818-IR probes.

To obtain an incident beam of small diameter, a pinhole 50 μm in diameter and 0.25 mm thickness (Edmund Optics) was used. An integrated holder was built to keep the pinhole and LED together as a single unit, the LED positioned as close as possible to the pinhole. In order to maximize incident power, the unit almost touched the chamber's edge.

Temperature Measurements. To measure the temperature at various points within the chamber, an OMEGAETTE datalogger thermometer HH306 with compact transition ground-junction probe (TJC36 series) was used. This is a compact dual-input thermometer whose stainless steel-sheathed probe is small enough (250 μm) to fit within the EZ. Its range extends from −200 to 1370 °C ± 0.2% and its resolution is 0.1 °C. The datalogger can store up to 16 000 records at programmed intervals as short as once per second.

Results

Initial experiments followed earlier studies[8−10] showing a negatively charged EZ. A lingering question was whether the negative charges of the EZ might be balanced by complementary positive charges beyond the EZ, namely by protons or hydronium ions.

To explore this possibility, the time course of pH change in the vicinity of Nafion was measured. Figure 1A shows that as the EZ was built, the pH in the zone beyond went sharply downward; it then recovered to a value lower than the initial value. Farther from the Nafion surface, the phasic downturn began later. The results implied a wave of protons emerging from the direction of the EZ, leaving the water at lower pH than prior to the time the EZ had begun building.

To confirm and extend these pH measurements to longer distances, pH-sensitive dyes were added, and the results are shown in Figure 1B. The clear zone just above the Nafion surface implies that the pH-sensitive dyes are excluded from the EZ. Beyond the EZ, the color is red-orange, indicating a pH less than 3. Farther from the Nafion, the pH was lower than the Nafion-absent control, and eventually, at 10 mm from the Nafion surface and beyond, pH values were similar to controls. Hence, the results imply that the zone beyond the EZ is indeed populated by abundant protons that appear to be associated with EZ buildup.

A clue for the source of energy for EZ buildup came after having inadvertently left the experimental chamber on the microscope stage overnight. The EZ size had diminished overnight; but after turning on the microscope lamp to full intensity, the EZ size began to increase, restoring itself within minutes to its former size, ~300 μm. With preliminary evidence that light could expand the EZ, we investigated systematically whether the energetic source for EZ buildup might indeed be radiant energy.

Liquid water absorbs strongly at wavelengths of 2.9−3.25 μm, which corresponds to the fundamental O−H stretching mode.[11−13] In this spectral range, the most accessible commercially available source was an LED radiating at 3.1 μm with full width at half-maximum (fwhm) of 0.55 μm; hence, the first light source used was LED31-PR.

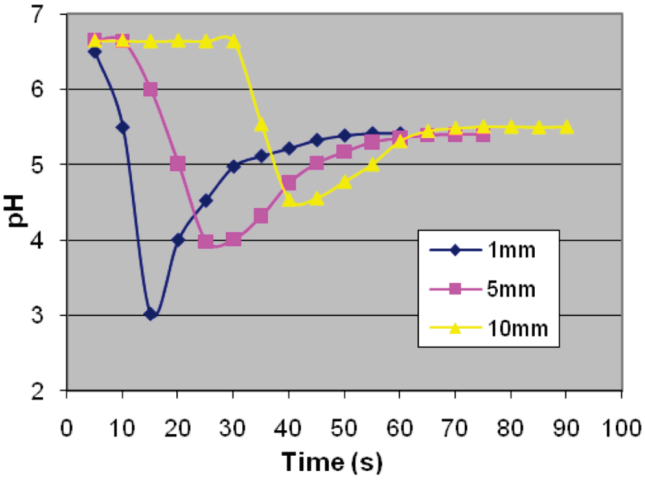

(A)

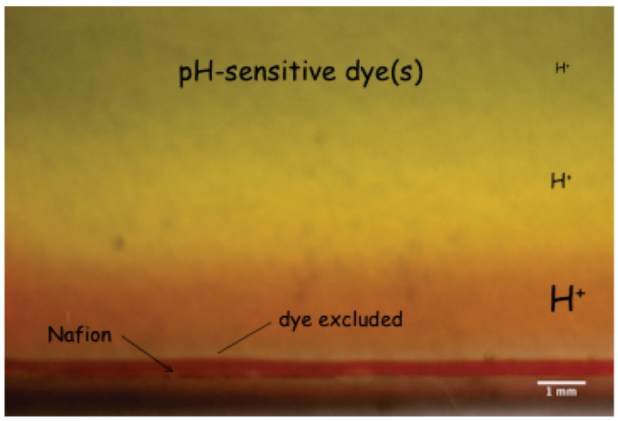

(B)

Figure 1. (A) Time course of pH change following addition of water to Nafion sheet. Values of pH were measured at 5 s intervals using a miniature pH probe positioned at three distances from the Nafion surface, as indicated in the legend. A wave of protons is generated as the EZ forms, giving lower pH. At a distance of 1 mm, the pH drop transiently exceeds 3 pH units, which represents a H^+ increase in excess of 1000 times. (B) Chamber containing Nafion tube (bottom) filled with water containing pH-sensitive dye. The view is normal to the wide face of a narrow chamber. The image obtained 5 min after dye-containing solution was added to Nafion. The red color indicates pH < 3; the colors above indicate progressively higher pH levels, with near neutrality at the top.

Nafion tubing was suffused with a 1-μm carboxylate-microsphere suspension with a 1:500 volume fraction, to a depth of ~1 mm. The chamber was made using a thin cover glass stuck to the bottom of a 1-mm thick cover slide with a 9-mm circular hole cut in the center and was placed on the stage of the microscope. A pinhole was used to obtain an incident beam of restricted diameter. A fabricated holder integrated the pinhole and LED into a single unit with the LED mounted close to the pinhole. The LED−pinhole axis was vertically oriented.

Basic Observations. The baseline EZ size was first established before measuring IR-induced EZ expansion. The sample was prepared and initially left in the dark. Once enough time had passed for the EZ to stabilize, approximately 5 min, the microscope lamp was turned on briefly to take photomicrographs showing the baseline EZ size. The EZ size after IR irradiation was compared to this baseline size to compute the expansion ratio in each run.

To minimize any effects of microscope illumination on EZ size, the microscope lamp was turned on only when necessary

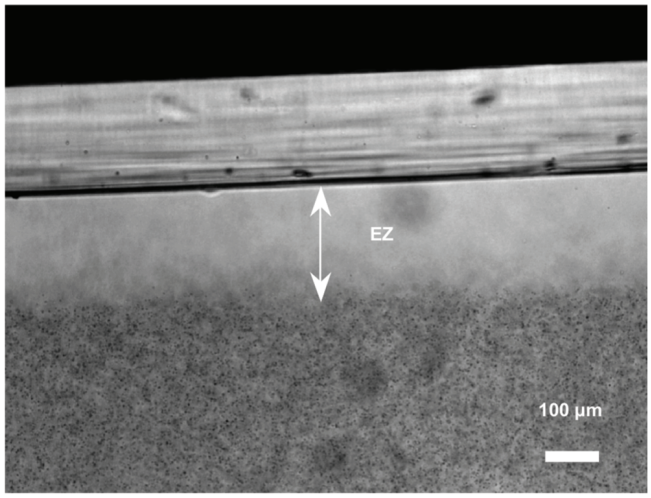

(A)

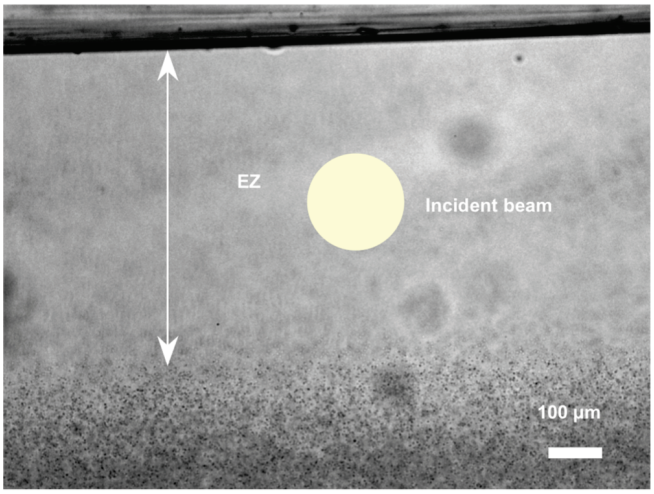

(B)

Figure 2. EZ in control experiment (A) and after 5 min of exposure to light from LED31-PR (B). EZ denotes the region in which microspheres are absent. The approximate size of the incident beam is shown in panel B.

for visualizing the EZ, and then immediately turned off. A green filter with a sharp peak at 550 nm was used to further minimize incident radiation. Immediately following the baseline measurements, the incident IR source was turned on. Optical power output was 33 μW, and the estimated power incident on the sample through the pinhole was ~2.4 nW. After 5 min of exposure, the IR LED assembly was removed and the EZ was immediately photographed through the microscope. From the representative records shown in Figure 2, it is apparent that even with modest IR exposure, the EZ grew to approximately three times its control size.

Aware of the potential for contamination by even brief microscope-light illumination, appropriate controls were carried out. The sample was left for 5 min with and without the microscope light turned on. The intensity of incident light was kept the same as in all other experiments, including the green filter. The EZ size was 280 ± 24.1 μm with light and 260 ± 13.3 μm without (n = 5). Hence, even with microscope illumination of a far longer duration than in actual experiments (5 min vs several seconds), the effect on EZ size was modest. Apparently, the extensive expansion effects observed were due solely to the incident IR radiation.

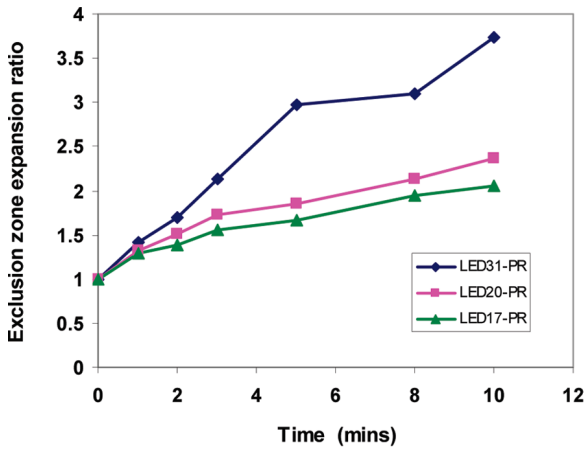

(A)

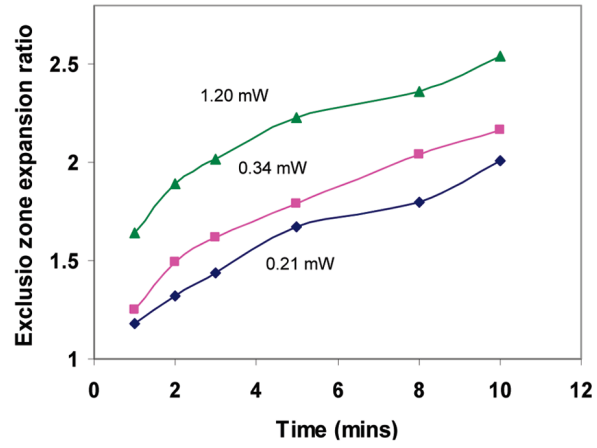

(B)

Figure 3. (A) EZ expansion as a function of exposure time, for three IR sources (lower power for LED31-PR). (B) EZ expansion ratios as a function of time during 10 min exposure at different intensities using LED20-PR.

We also tracked the EZ width's time course. This was carried out not only with the 3.1-μm source, but also with the 2.0-μm and 1.75-μm sources (fwhm = 0.16 and 0.18 μm, respectively). For the latter two sources, intensities were maintained at approximately 190 μW; but for the 3.1-μm source, power was kept at the maximally attainable value, 33 μW.

During a 10-min exposure at all three wavelengths, EZs continued to expand approximately linearly (Figure 3A). The largest effect was seen at 3.1 μm, despite lower incident power. To determine whether the EZ continues to expand beyond the 10-min exposure, the 3.1-μm source was left on at the same intensity as above for up to 1 h. The ratios increased from 3.7 $\pm$ 0.10 (10 min) to 4.7 $\pm$ 0.12 (30 min) and to 6.1 $\pm$ 0.17 (1 h), respectively. Hence, the EZ continues to expand with continued exposure for up to at least one hour. Longer durations were deemed unreliable, as evaporation became noticeable; hence measurements were suspended.

Postillumination EZ-size dynamics were examined as well. When the infrared light was turned off after 5 min of exposure, the EZ width remained roughly constant with fluctuations for about 30 min; then, it began decreasing noticeably, reaching halfway to baseline levels in typically ~15 min.

To determine the effect of beam intensity on EZ expansion, the 2-μm source was employed at three power levels, 0.21, 0.34, and 1.20 mW. The rate of EZ expansion increased with an increase of incident power (Figure 3B).

TABLE 1: Temperature Increases Measured at Different Distances from the Nafion Surface after 10 min of Exposure to 3.1-μm Radiation (n = 3)

distance from Nafion	mean temperature increase
175 μm	1.1 °C
250 μm	0.91 °C
350 μm	0.92 °C
4 mm	0.91 °C
6 mm	0.92 °C

The results of Figure 3A and B show that, at a given wavelength, EZ expansion is a function of both time and intensity. Hence, EZ growth depends on the cumulative amount of incident energy induced charge separation.

To test whether the expansion might arise out of some unanticipated interaction between the incident radiation and the particular type of microsphere probe, microspheres of different size and composition were tested. For carboxylate microspheres of diameters 0.5, 1, 2, and 4.5 μm at the same volume concentrations (1:500), mean expansion ratios for 5 min of exposure of 3.1-μm radiation were the following: 2.41, 2.97, 3.08, and 3.34, respectively (n = 6). For 1-μm microspheres made of carboxylate, sulfate, and silica under conditions the same as above, expansion ratios were 2.97, 3.10, and 1.50. Hence, some material-based and size-based variations are noted—the latter arising possibly because of different numbers of particles per unit volume—but appreciable radiation-induced expansion was nevertheless seen under all circumstances and with all materials. Hence, the existence of the light-induced expansion effect is not material-specific.

We also explored the effect of IR illumination at different depths relative to the water/air interface. Interestingly, EZ expansion was observed well below the water surface. This result is unexpected given the previously reported short penetration depth of IR in water.[14,15] Nevertheless, IR effects extending far beyond the expected penetration depth have been reported and attributed to coherent energy redistribution of IR-induced excitation of surface layers via pressure waves.[16,17] A more systematic time-correlated approach will be needed to determine whether any such mechanism might apply here.

Controls for Temperature. Infrared absorption in water causes a temperature elevation. Hence, we considered the possibility that the expansion might arise from an appreciable increase of chamber temperature. To measure local temperatures, an OMEGAETTE datalogger thermometer HH306 was used, with a stainless-steel-sheathed, compact transition ground-junction probe (TJC36 series), small enough (250 μm) to fit within the EZ. With the incident beam positioned to elicit the maximum expansion, i.e., centered 175 μm from the Nafion surface, the measured temperature increases are shown in Table 1. Radiation-induced temperature increases were modest at all positions and fairly uniform over the chamber. We also found little temperature variation with depth, implying that the thermal mass of the probe itself, immersed by varying extents for measurements at varying depths, did not introduce any serious artifact.

Further to this point, we recorded the dynamics of temperature rise. The temperature increase occurred steadily, reaching a plateau of ~1 °C at 10−15 min after turn-on. This plateau was attained at a time that the EZ continued to expand (Figure 3A and associated text). Hence, not only was the temperature increase modest, but also the time course of temperature rise and EZ expansion were not correlated.

Spectral Analysis. A principal objective was to determine EZ-expansion's spectral sensitivity. The experimental setup was

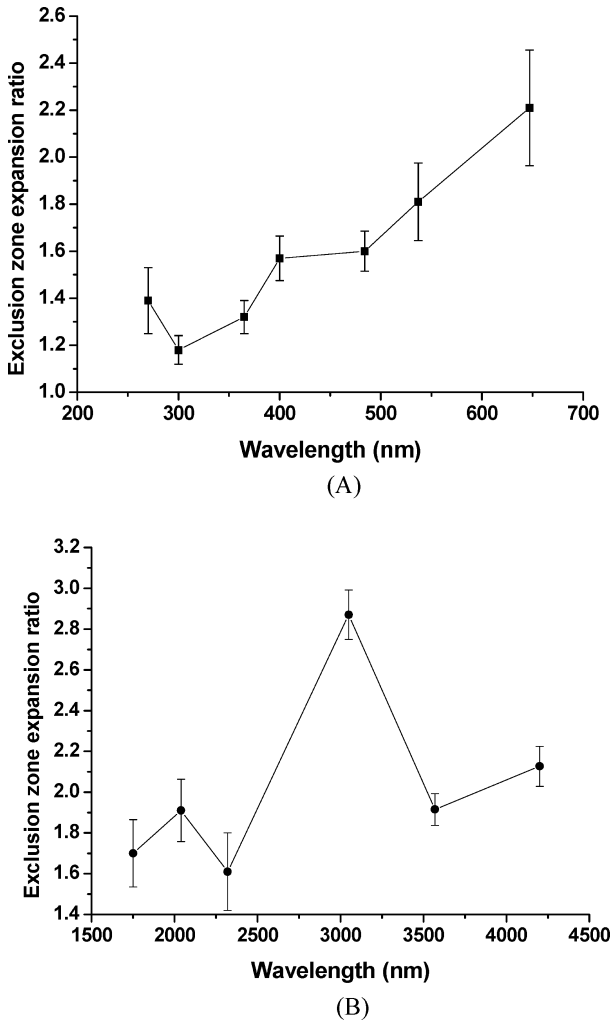

Figure 4. (A) Exclusion-zone expansion ratio under illumination for 5 min in the UV−vis spectral region. (B) Exclusion-zone expansion ratio under illumination for 5 min at IR wavelengths.

similar to that described above. The ~200-μm wide light beam emerging from the pinhole was directed to the middle of EZ, and expansion was measured 300 μm below solution surface. For the UV and visible sources, maintaining consistent optical power output at all wavelengths was achievable within ±10% by adjusting the driver current. But IR sources were considerably weaker; hence, output power was maintained at a lower level, 3 orders of magnitude lower than in the UV−visible ranges. Spectral results are therefore plotted separately.

For UV and visible ranges, all incident wavelengths brought appreciable expansion (Figure 4A). The degree of expansion increased with increasing wavelength, the exception being the data point at 270 nm, which was higher than the local minimum at 300 nm. The higher absorption may reflect the signature absorption peak at 270 nm characteristic of the EZ.[18] Clear wavelength sensitivity was also found in the IR region, the most profound expansion occurring at 3.1 μm (Figure 4B). Recognizing that the optical power available for use in the IR region was 1/600 of that in the visible and UV regions, one can assume that with comparable incident power, the IR curve would shift considerably upward—continuing the upward trend evident in Figure 4A. Hence, the most profound effect is in the mid-IR region, particularly at 3.1 μm.

Discussion

The most significant result of this study is that the near-surface exclusion zone expands extensively in the presence of incident radiant energy. That is, growth of this more ordered, negatively charged zone is dependent on incident electromagnetic energy.

A secondary result is that growth of this negatively charged zone is associated with buildup of a zone of high proton concentration beyond (Figure 1). Those protons or hydronium ions may facilitate the current flow that can be observed through an external load connected between electrodes placed in the EZ and the zone beyond.[19]

Regarding the light-dependent EZ expansion, the overall spectral sensitivity of expansion (Figure 4) follows closely the spectral sensitivity of water absorption. In both cases, there is an overall minimum in the near-UV region, plus a local maximum at 2.0 μm, and a peak in the vicinity of 3.1 μm. If not by coincidence, then a connection is implied between IR absorption and EZ expansion—although the linkage is apparently not through temperature increase, which was both modest and temporally uncorrelated. Further to this point, increasing the bath temperature actually *diminishes* EZ size (unpublished observations). Hence, the effect of incident electromagnetic energy is apparently nonthermal.

Mechanistic Considerations. One question is how radiant energy could augment EZ size. This question rests on the more basic question of the energy responsible for the original EZ buildup, because buildup and augmentation may be driven from the same energetic source. It is apparent from the data of Figure 4 that mid-IR has a significantly more profound impact than other regions of the spectrum. Since infrared energy is consistently available under ambient conditions, IR energy is likely to be the major agent responsible for both the initial buildup and the augmentation.

To build the EZ, bulk water must undergo some kind of change. We found that as the negatively charged EZ builds, the concentration of protons in the region beyond the EZ likewise builds. Hence, it appears that the mechanism involves radiant energy-induced splitting of bulk water into negative and positive entities. The negative entity forms the ordered EZ, while the positive entity distributes itself broadly over the bulk. The negative−positive combination forms a battery-like entity, fueled by radiant energy.

While the energy of an IR photon is generally considered lower than the dissociation energy of the O−H bond, some dissociation of water occurs even under ambient conditions; i.e., the dissociation constant of water, $K_w = [H^+][OH^-]$, underlies all pH measurement, and implies that there is some dissociation even under ambient conditions. Incident IR would merely augment the naturally occurring dissociation. Once dissociated—either through excitation via ambient IR exposure or augmented IR—the negatively charged component would then go on to form the more ordered EZ.

IR-induced reorganization of water is not a new result; IR-induced clathrate formation in liquid water has been reported previously.[20,21] Another study found an unexpectedly low energy required to delocalize a proton between two neighboring water molecules of liquid water when in the second excited state of O−H stretch vibration; this energy corresponds to less than 20% of the energy for dissociating the water O−H bond in the gas phase.[22] Hence, there is precedent for IR-induced molecular rearrangement in liquid water.

The question then becomes: by what mechanism does such ordering take place? Classical thermodynamics prohibits splitting of water by IR due to the low energy of an IR photon. On the other hand, quantum mechanical considerations of liquid water, along with IR and Raman spectra, imply that mid-infrared radiation corresponding to the fundamental OH stretch has

strong resonant effects on water, thereby resonantly exciting the system's vibrational energy. Several studies have reported a vibrational excitation that reorganizes hydrogen-bonded liquid water. These studies show the formation of ion-pair-state ($H^+ \cdots OH^-$) water clusters following mid- and near-IR irradiation resonant to the fundamental and fourth harmonic of the O−H stretch.[16,17,23] Thus, the IR-induced dissociation of water implied here has both precedent and physical rationale, although the exact mechanism is not yet worked out.

In summary, the long-ignored issue of extensive near-surface water ordering may be slightly less enigmatic than thought. The present studies make clear that the buildup of this more ordered near-surface zone involves charge separation and that the underlying energy source is incident radiant energy. Interestingly, the wavelengths most responsible for building this zone are the very wavelengths most strongly absorbed by water. Hence, in a more general context, it may be that a good fraction of the electromagnetic energy absorbed by water is used to build order and separate charge.

Acknowledgment. We thank Drs. H. Ishiwatari and D. Schmidt for technical suggestions, Drs. H. Ishiwatari, B. Liu, R. Stahlberg, and J. Watterson for their comments on the manuscript, and Jeff Magula for building the apparatus. This study was supported by NIH Grants AT-002362 and AR-44813 and ONR Grant N00014-05-1-0773.

References and Notes

(1) Henniker, J. C. *Rev. Mod. Phys.* **1949**, *21*, 322.
(2) Hardy, W. B. *Proc. R. Soc. London* **1912**, *86*, 610.
(3) Yalamanchili, M. R.; Atia, A. A.; Miller, J. D. *Langmuir* **1996**, *12*, 4176.
(4) Nihonyanagi, S.; Ye, S.; Uosaki, K.; Dreesen, L. *Surf. Sci.* **2004**, *573*, 11.
(5) Noguchi, H.; Hiroshi, M.; Tominaga, T.; Gong, J. P.; Osada, Y.; Uosaki, K. *Phys. Chem. Chem. Phys.* **2008**, *10*, 4987.
(6) Green, K.; Otori, T. *J. Physiol.* **1970**, *207*, 93.
(7) Pollack, G. H.; Clegg, J. *Phase Transitions in Cell Biology: Unexpected linkage between unstirred layers, exclusion zone, and water*; Springer: New York, 2008; pp 143−152.
(8) Zheng, J.-M.; Pollack, G. H. *Phys. Rev. E* **2003**, *68*, 031408.
(9) Zheng, J.-M.; Chin, W.-C.; Khijniak, E.; Pollack, G. H. *Adv. Colloid Interface Sci.* **2006**, *127*, 19.
(10) Zheng, J.-M.; Pollack, G. H. *Water and the Cell: Solute exclusion and potential distribution near hydrophilic surfaces*; Springer: Netherlands, 2006; pp 165−174.
(11) http://www.lsbu.ac.uk/water/vibrat.html (accessed September 24, 2009).
(12) Venyaminov, S. Y.; Prendergast, F. G. *Anal. Biochem.* **1997**, *248*, 234–245.
(13) Bertie, J. E.; Ahmed, M. K.; Eysel, H. H. *J. Phys. Chem.* **1989**, *93*, 2210–2218.
(14) Hale, G. M.; Querry, M. R. *Appl. Opt.* **1973**, *12*, 555.
(15) Wieliczka, D. M.; Weng, S.; Querry, M. R. *Appl. Opt.* **1989**, *28*, 1714.
(16) Toyama, N.; Kohno, J.; Kondow, T. *Chem. Lett.* **2006**, *35*, 966–967, No. 8.
(17) Toyama, N.; Kohno, J. Y.; Kondow, T. *Chem. Phys. Lett.* **2006**, *420*, 77.
(18) Chai, B.-H.; Zheng, J.-M.; Zhao, Q.; Pollack, G. H. *J. Phys. Chem. A* **2008**, *112*, 2242.
(19) Pollack, G. H. http://uwtv.org/programs/displayevent.aspx?rID=22222, 2008 (accessed September 24, 2009).
(20) Yokono, T.; Shimokawa, S.; Mizuno, T.; Yokono, M.; Yokokawa, T. *Jpn. J. Appl. Phys.* **2004**, *43*, 1436.
(21) Shimokawa, S.; Yokono, T.; Yokono, T.; Yokokawa, T.; Arais, T. *Jpn. J. Appl. Phys.* **2007**, *46*, 333.
(22) Bakker, H. J.; Nienhuys., H.-K. *Science* **2002**, *297* (5581), 587.
(23) Klochkov, D. V.; Kotkovskil, G. E.; Nalobin, A. S.; Tananina, E. S.; Chistyakov, A. A. *JETP Lett.* **2002**, *75* (1), 22–24.

JP908163W

Chapter 7

CHARACTERISTICS OF WATER ADJACENT TO HYDROPHILIC INTERFACES

Hyok Yoo, David R. Baker, Christopher M. Pirie, Basil Hovakeemian, and Gerald H. Pollack
Department of Bioengineering, Box 355061,
University of Washington,
Seattle WA 98195
ghp@u.washington.edu

7.1 INTRODUCTION

Water molecules contiguous with hydrophilic interfaces are organized into ordered arrays. Such ordering is thought to project out by several molecular layers from the interface, the molecules lying beyond them undergoing thermal motion intense enough to preclude much additional ordering. Hence, beyond those few layers, water molecules are widely considered to lie within the bulk [1].

On the contrary, recent findings imply that some degree of ordering may project out from the surface by up millions of water layers or more [2, 3]. Much of the evidence and rationale for this view is presented in a recent award lecture: http://uwtv.org/programs/displayevent.aspx?rID=22222 (contents outlined and reviewed in http://www.i-sis.org.uk/liquidCrystallineWater.php), where the reader may obtain a deeper appreciation for the basis of these claims.

The core observation is a counterintuitive surprise: colloids and solutes of varied size are profoundly excluded from the region adjacent to hydrophilic materials. The EZ commonly extends up to hundreds of micrometers from the surface. An example is shown in Fig. 7.1.

Water: The Forgotten Biological Molecule
Edited by Denis Le Bihan and Hidenao Fukuyama

www.panstanford.com

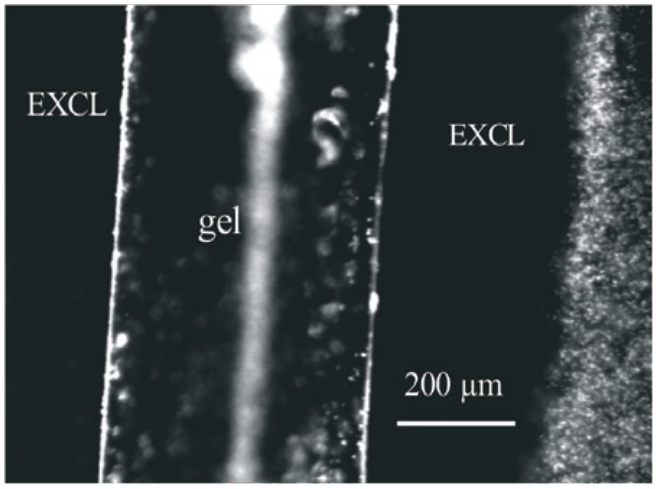

Figure 7.1 Solute exclusion (EXCL) in the vicinity of polyacrylic acid gel. The gel runs vertically. The blurred vertical white element to the right of "gel" is an optical artifact. The gel was placed on a coverslip, superfused with a suspension of 1 µm carboxylate-coated microspheres, and observed in an inverted microscope equipped with a 20x objective. The image was obtained 20 min after superfusion. Microspheres (seen on the right edge) undergo active thermal motion but do not enter the exclusion zone.

These core observations are largely detailed in two papers [2, 3]. The first deals with the question of whether the finding of long-range exclusion may have some trivial explanation. Plausible candidates were tested and ruled out by an extensive series of controls. Since then, multiple groups have informally tested and confirmed the basic finding, which is easily replicable using any of a wide range of hydrophilic surfaces, both biological and nonbiological. In fact, a similar result had been published four decades ago: in addressing the origin of the so-called "unstirred layer" adjacent to biological tissues—a region where mixing is known to be extremely slow—Green and Otori (1970) showed in both corneal tissue and contact lenses that the unstirred layer excludes microspheres; EZs several hundred micrometers wide were found, essentially the same as that in Fig. 7.1 [4].

Hence, there is little question of the existence of unexpectedly large EZs next to hydrophilic surfaces. The question is what such zones might mean, and the second paper [3] shows that the physical–chemical properties of the EZ differ from those of bulk water. Four sets of results were presented: nuclear magnetic resonance rotational relaxation time is shorter in the EZ than in bulk water, indicating a decreased degree of freedom of EZ water; infrared radiation from the EZ is less intense than from bulk water, indicating increased stability of this zone; potential gradients exist in the EZ but not in bulk water; and ultraviolet–visible spectroscopy absorption spectra are markedly different in the EZ relative to bulk water.

Hence, four independent approaches show that EZ water differs from the water beyond the EZ. Collectively, these approaches imply that EZ water may well be more ordered than, and more stable than, bulk water. This difference in physicochemical properties is what appears to lead to the observed exclusion of solutes.

Here we extend these findings in four ways. We explore the possibility of ultra-long-range EZ propagation and find examples extending in length up to 1 m. We then examine the chemoelectrical features, finding charge separation that is intimately associated with the EZ. We also consider the viscosity of the EZ relative to that of bulk water and find it is much higher. And, finally, preliminary differential interference contrast data show birefringence at the Nafion–water interface extending up to hundreds of micrometers.

7.2 METHODS

For experiments on long-range EZs, a meter-long glass tube, 2.5 cm in diameter was used. A polyacrylic acid gel (or Nafion sheet) was secured with a pin to the inside of a rubber stopper that sealed one end of the tube. The other end of the tube was sealed with another rubber stopper. The tube was filled with a suspension of 0.45 μm–diameter carboxylate-coated microspheres in deionized high-performance liquid chromatography–grade water from a Barnstead Nanopure Diamond unit (Model D11931) and held horizontally.

For the pH experiments, a universal pH indicator dye (Sigma #36803) was added to the water at the recommended concentration.

For the viscosity experiments, falling-ball viscometry was used. To track the descent of spheres, a chamber with transparent glass walls was constructed using ordinary 1 mm thick, 50 × 73 mm glass microscope slides held apart by 1 mm glass spacers, which formed the sides of the chamber. Epoxy glue (Cat. #14250, Devcon, MA) was applied around the resulting boxlike chamber to prevent water leakage. At the bottom of the chamber, we glued either a sheet of Nafion (Sigma-Aldrich #274674) or, as a control, a strip of aluminum or steel, which generated little or no EZ. Polystyrene microspheres, 5, 10, and 15 μm diameter (Bangs Laboratory, Cat. #5623, 6955, 6716, respectively) were used as falling balls. These spheres are nearly neutral, thereby minimizing any electrostatic interaction among the spheres.

To carry out experiments, the chamber was first filled with deionized water (see earlier). To make sure that the Nafion was fully hydrated, the microspheres were added several minutes after the chamber had been filled.

A small loop, diameter ~600 μm, was constructed out of a 100 μm–diameter copper wire for suspending microspheres into the chamber. By

dipping the loop into the prepared microsphere suspension, it was possible to obtain a thin film of microsphere suspension (<0.5 μL) containing only a few microspheres. This loop was then dipped into the top of the chamber. Typically 10–20 microspheres were seen to descend.

As microspheres descended, downward displacement was tracked using a Nikon bright-field microscope with a 5x objective (Model 76023) and a Scion CCD digital camera (Model CFW-1310C). A green *light-emitting diode* (Phillips Luxeon R5JG) with a narrow localized peak at 530 nm was used as a light source. Minimizing intensity tended to minimize thermal convection. To compute the vertical component of descent (some sideways motion was often present), screens showing 1,200 μm high zones were examined using ImageJ at one frame every five seconds, and velocity was computed. This was done at a series of heights—4,800, 3,300, and 1,800, 1,000, 500, 200, 100, and 50 μm. Five runs were made at each height for microspheres of each size.

Polarizing microscopy was used to examine birefringence at the Nafion–water interface. A Nafion 117 film (Aldrich, Inc.) was placed in a 1 mm thick water chamber made of two 0.17 mm thick coverslips. The chamber was observed with a 5×/0.12NA objective lens with a maximally reduced condenser NA. Five raw polarization images were captured with an LC-polscope (CRI, Woburn, MA) and processed using a five-frame algorithm [5].

7.3 RESULTS AND DISCUSSION

7.3.1 Character of Exclusion Zones

The simplest way of envisioning a stable, ordered array is to consider it in terms of a liquid crystal, in which molecules show more alignment than a liquid but less than a solid. Like crystals of ice, liquid crystals of water could be expected to exhibit growth in any and all directions. If the EZ is liquid crystalline, then it is expected that growth would not necessarily be confined to the zone adjacent to the nucleating surface, as in Fig. 7.1. Under appropriate circumstances such as geometrical asymmetry, growth could be directed elsewhere, in odd and perhaps unpredictable directions.

Figure 7.2a shows a segment of a ribbon-shaped solute EZ that grew to extend the full length of a meter-long glass tube. A polyacrylic acid gel was positioned at one end, and the tube was filled with a microsphere suspension. Initially, a disklike EZ grew uniformly from the face of the gel surface; within 10 minutes it extended ~1 mm into the aqueous phase. The entire microsphere-free zone then shifted upward along the gel surface, creating a surge into the microsphere-containing zone. At or near the top of the surge,

a thin ribbon of EZ began growing into the aqueous phase, parallel to the tube's axis (Fig. 7.2b). After several hours this ribbon extended the entire length of the meter-long tube and persisted indefinitely (i.e., for at least the maximum observation time of two weeks). During this time, microspheres undergoing rapid thermal motion just outside the ribbon failed to penetrate into the ribbon, and the ribbon retained its integrity.

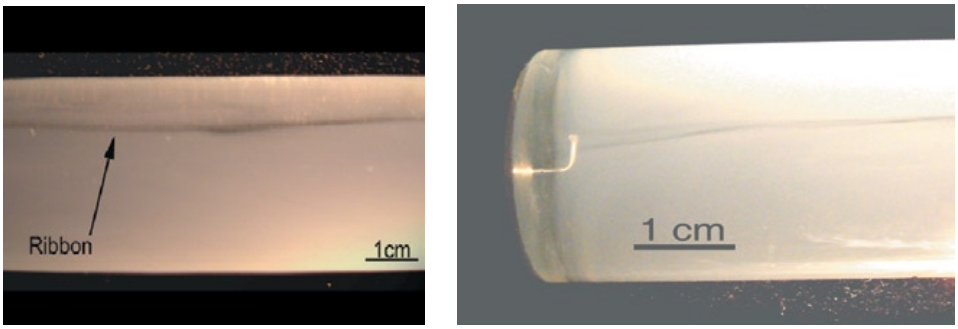

Figure 7.2 (a) Section of exclusion "ribbon" running along the length of a cylindrical tube, nucleated at the surface of the polyacrylic acid gel beyond the left side of the panel. The tube was filled with a solution containing distilled water and 15 drops of stock solution of 0.45 μm–diameter carboxylate-coated microspheres, yielding an estimated concentration of 6×10^8 microspheres per ml. (b) Top view of the chamber showing the wedge-shaped origin of the exclusion ribbon. The wedge grows out of the original disc-shaped exclusion zone adjacent to a polyacrylic acid gel surface. The prominent white object on the left is a pin used to hold the gel against the stopper.

The ribbon did not grow by adding to its tip but apparently by adding from its origin near the gel's surface. This supposition came from the behavior of ribbon defects, which maintained both their shapes and their distances from the tip while translating away from the originating surface. Generally, the ribbon remained almost linear, focusing itself along a line that formed the upper edge of the cylindrical tube, although in one out of six cases, the ribbon formed elsewhere. An alternative chamber with a square cross section was made of acrylic sheets. In this case several ribbons formed simultaneously, mainly but not always along the top surface. These latter ribbons were typically wavy wisps, sometimes branched, and undergoing seemingly random fluctuations. Fluctuations notwithstanding, the structure maintained itself. Ribbon character did not appear to depend on whether it was nucleated by the polyacrylic acid gel or by a similarly positioned sheet of Nafion, a hydrophilic ionomer.

Occasionally, ribbonlike structures could also be seen in the absence of a nucleating surface. These structures were generally shorter, thinner, and less predictably evident than the ones above and could be seen only in

situations in which microsphere stock had been freshly diluted immediately before use. These structures may be analogous to the solute-free "voids" seen in pure microsphere suspensions [6, 7]. Such voids were stable, and were amorphously shaped, with a characteristic dimension on the order of 100 μm. Possibly the more extended shapes seen here reflect the long chamber geometry in the present studies.

The evidence depicted in Fig. 7.2 (similar when the gel or Nafion was replaced by a hydrophilic monolayer) confirms that the EZ is a distinct phase, coexisting with the ordinary solute-containing phase. Microspheres undergoing active thermal motion just outside the ribbon phase do not penetrate into the ribbon, even for several weeks. Phase coexistence of colloidal suspensions of differing composition is well recognized [8], as is phase coexistence of mixtures of microsphere solutes of different size [9]. The current experiments show similar phase separation, one phase containing colloidal solutes, the other not.

The existence of the ribbonlike extensions is consistent with liquid crystalline behavior. Growth can be anticipated in multiple directions for extended distances; this is what was observed. On the contrary, the presence of such ribbons does not seem compatible with the alternative hypothesis that the EZ is created by some kind of electrostatic repulsive force between the gel–polymer surface and the microspheres, for meter-long extensions are difficult to envision under such a hypothesis, as electrostatic force diminishes as the square of distance. These apparently liquid crystalline structures, as mentioned, are quite stable over long periods of time, reinforcing the idea of some kind of crystal.

7.3.2 Charge Separation

A significant aspect of the EZ is its negative electrical potential [3]. The potential is most negative next to the nucleating surface and diminishes toward zero at the EZ–bulk water boundary. The implication of the negative potential is that the EZ may contain a negative charge—which would not be surprising for a liquid crystalline array of molecules. But, if the EZ were negatively charged, then a positively charged counterpart ought to exist somewhere, and we considered whether the bulk water might have excess unbound protons.

Figure 7.3 shows an image of a narrow water-containing chamber with a Nafion sheet placed at the bottom. A universal pH indicator dye was added to the water in concentration as per the manufacturer's recommendation. The Nafion sheet appears dark red because of local acidity. Just above and below the Nafion are clear zones, from which the dye is excluded in much the same

way as microspheres are excluded (see earlier). Above this EZ is a rainbow of colors, indicating a steep pH gradient. The red color indicates pH < 3; the colors above indicate progressively higher pH levels, with near neutrality at the top.

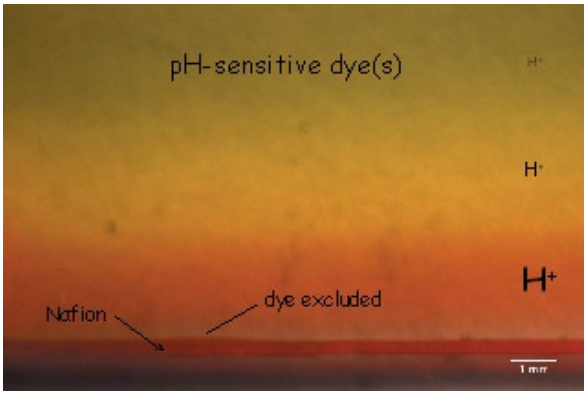

Figure 7.3 Chamber containing a Nafion tube (bottom) filled with water containing a pH-sensitive dye. View is normal to the wide face of a narrow chamber. Image obtained 5 min after dye solution poured into chamber.

A result similar to that of Fig. 7.3, but taken at a later time, is shown in Fig. 7.4. Several features are of interest. First, the Nafion at the bottom is looped in several places; this results from expansion of the Nafion sheet as it hydrates. Second, the EZ projects nearly vertically, extending into the solution in several regions. The extensions are very much like those in Fig. 7.2. Of most interest is the fact that the red color surrounds each one of those projections, indicating a low pH even around the projecting entities. This implies that whether the EZ is closely adjacent to the nucleating surface or projects far away from it, a zone of high proton concentration surrounds it. Inevitably, a region of high proton concentration is juxtaposed next to the negatively charged EZ.

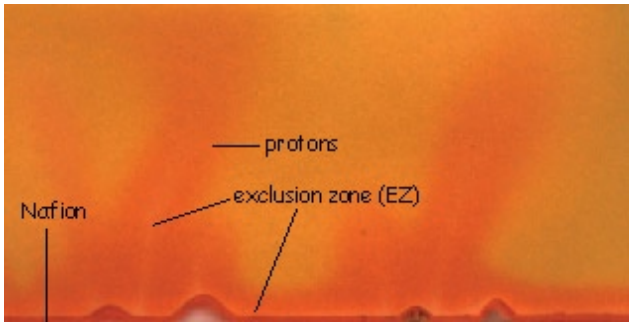

Figure 7.4 Similar to Fig. 7.3 but taken 20 min after the water with pH indicator dye is poured into the chamber. Note the exclusion zone growth perpendicular to the Nafion surface, surrounded by areas of low pH.

From the latter observation, it seems likely that the free protons come from the EZ water and not from the Nafion. Nafion is an ionomer, which is expected to conduct and donate protons. Compatible with this expectation is the image of Fig. 7.3, where a region of high proton concentration lies adjacent to the Nafion. The protons could have come either from the Nafion or from the EZ water next to the Nafion, and deciding between the two options is not possible from this experiment alone. However, Fig. 7.4 implies that it may well come largely from the water, for the vertically oriented high-proton zones are far from any Nafion-proton source. Rather, those zones lie immediately adjacent to EZ water.

Another difference between Figs. 7.3 and 7.4 is that in the latter image, the pH is lower overall; the image is dominated mainly by the red color, with green (neutral pH) virtually absent. The probable reason is that the image was obtained later, after the EZ had grown substantially and included many vertical projections. The substantially larger EZ volume implies a much larger release of protons, which would diffuse out to bulk water, lowering the pH overall and accounting for the largely red-looking image.

The results imply that negative and positive zones exist side by side. It would not be surprising if the release of protons were a necessary condition for creating the negatively charged EZ. The negative–positive configuration is much like that of a capacitor or battery. Indeed, we have found (unpublished data) that when electrodes are placed in the EZ and in the region beyond, sustained currents can be obtained. Such currents provide evidence of the presence of separated charges—the EZ being negative and the region beyond being positive.

7.3.3 Time Course of Proton Discharge

To measure the time course of proton discharge, a miniature pH probe was positioned at each of a series of distances from the Nafion surface. At each distance, measurements were taken immediately after the water was added, recorded manually at 5-second intervals, for the duration of one minute or more. Representative results obtained from three sets of readings are shown in Fig. 7.5.

Consistent with the dye experiments, the pH value dropped rapidly and as a function of distance. At a distance of 1 mm, the pH drop was more than 3 pH units, which represents an H^+ increase in excess of 1,000 times. At larger distances the drop began progressively later and was of lower magnitude. Eventually, the pH at all three distances reached a similar value—reduced

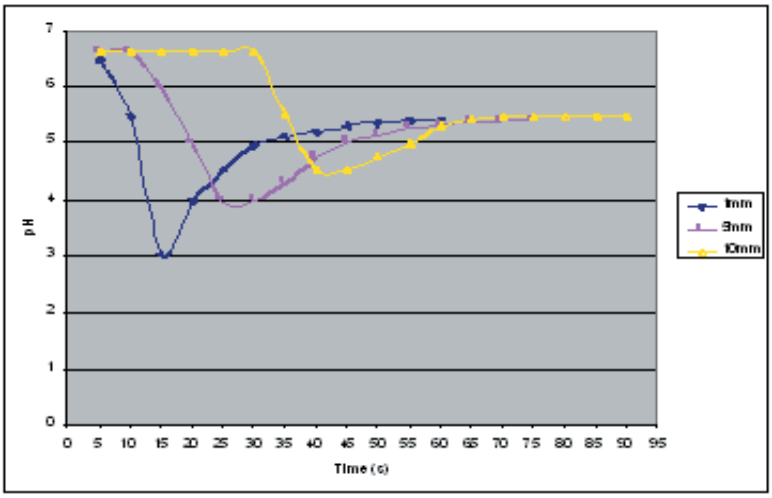

Figure 7.5 Time course of pH following addition of water to a sheet of Nafion. The pH was measured at three distances, indicated to the right, from the Nafion surface. A wave of protons appears to be generated.

considerably from the original water's pH, seemingly as a result of diffusion of protons or hydronium ions released from the EZ. This result is similar to the result shown in Fig. 7.4 with the pH indicator dye: eventually, the solution pH diminishes substantially from its initial value, although the time scales may differ somewhat because of geometrical and other differences.

It appears from Fig. 7.5 that as the EZ builds, a wave of protons is generated and "pushed" outward, leaving the region beyond the EZ with a high concentration of H^+. The time course and final level would be very much dependent on both the size and the shape of the container, as well as the exposed area of the nucleating surface. Indeed, in some instances we could find pH values that on occasion fell to stable values as low as 2 or 1 with gels that occupied the majority of relatively small chambers.

7.3.4 Viscosity

The EZ's liquid-crystalline-like nature implies a cohesiveness among constituent elements, which in turn implies that the ensemble should have higher viscosity than bulk water. To test this expectation, we used falling-ball viscometry. A strip of Nafion was glued to the bottom of an experimental chamber, which was filled with water. The velocity of the descent of spheres was tracked to determine whether the spheres might slow down as they descended into the EZ.

Representative results are shown in Fig. 7.6. A reduction of velocity near the Nafion surface was found for both the 10 and 15 μm spheres. For the 5 μm spheres the fall was most pronounced, reaching a value less than 0.01 μm/sec at heights less than 1,000 μm.

From the values of velocity, it was possible to compute the viscosity from the simplified version of the Navier–Stokes equation. Thus,

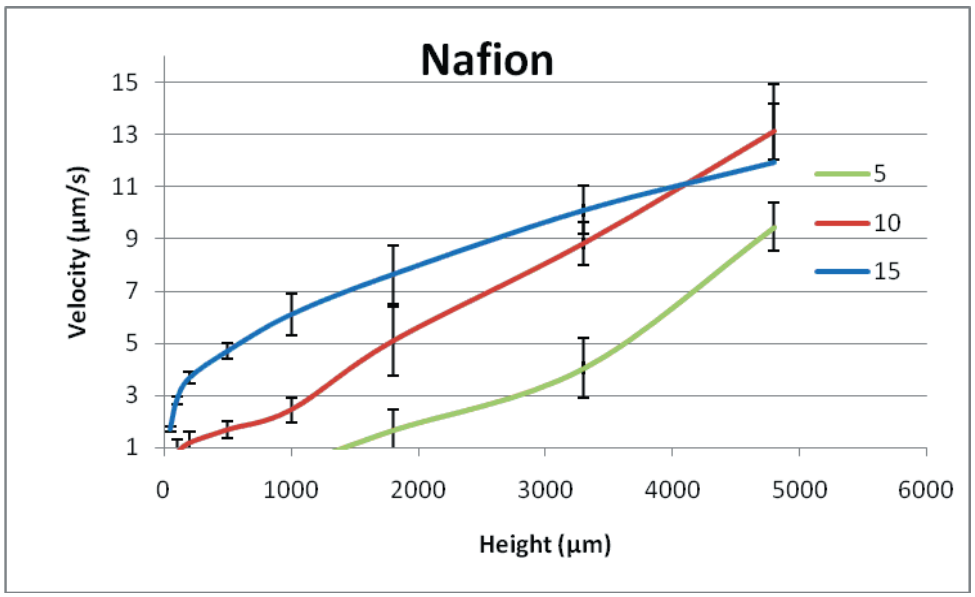

Figure 7.6 Velocity as a function of height above the Nafion surface, for 5, 10, and 15 μm–diameter polystyrene microspheres.

$$V_S(y) = \frac{2}{9}\frac{r^2\, g(\rho_P - \rho_f)}{\eta}\vec{y}$$

Here V_s is the particle's settling velocity (m/s), r is the Stokes radius of the particle, g is the gravitational acceleration, ρ_p is the density of the particles, ρ_f is the density of the fluid, and η is the fluid viscosity. For simplicity, nonlinear convective forces were not considered and fluid density was assumed constant. It was also assumed that the microspheres were falling at their terminal velocity.

Results are shown in Fig. 7.7. Note that computed viscosity increases markedly near the Nafion surface. By contrast, results of Fig. 7.8 show that the near-surface viscosity increase is absent for substances that have little or no EZ. Hence, the EZ is considerably more viscous compared with regions next to non-EZ-generating surfaces.

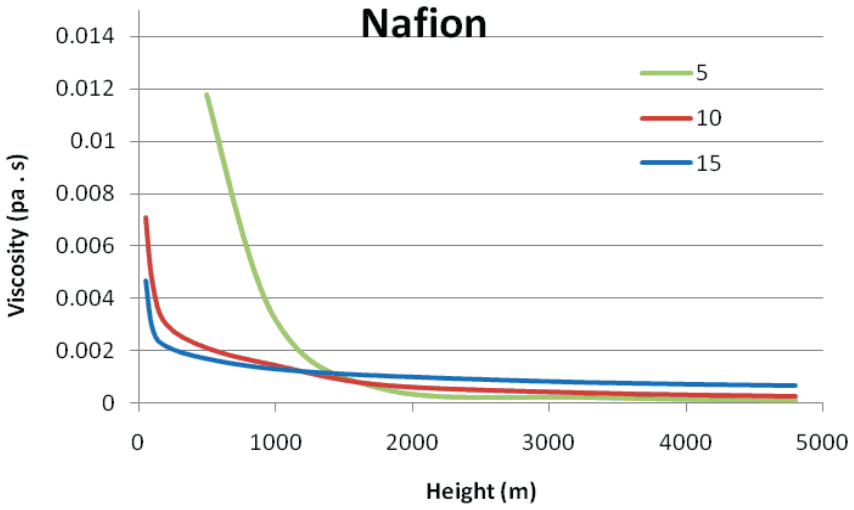

Figure 7.7 Computed viscosity as a function of distance from the Nafion surface for 5, 10, and 15 μ m–diameter polystyrene microspheres.

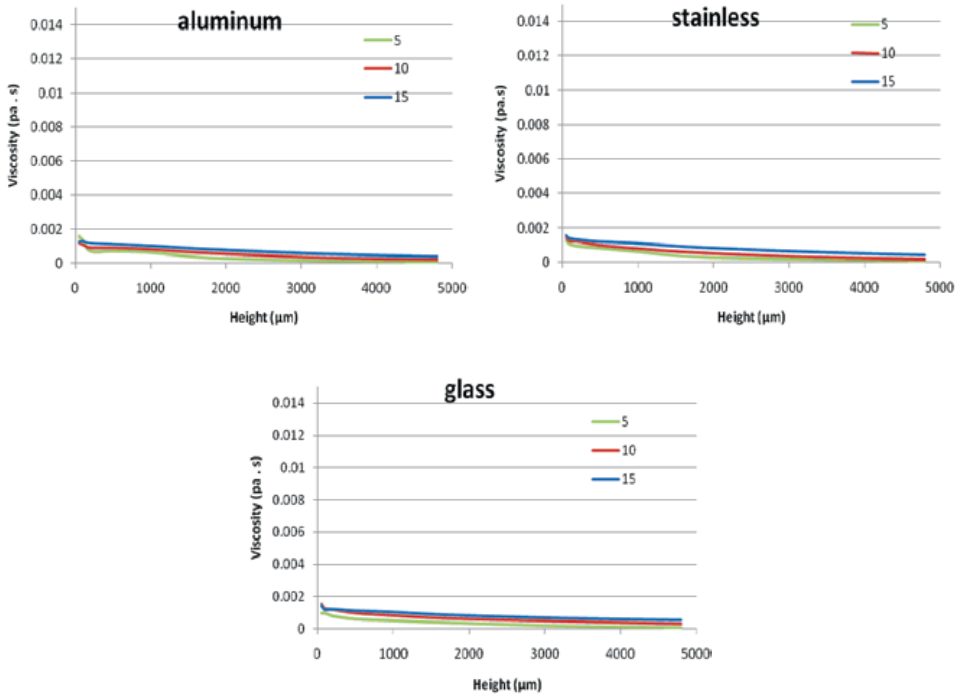

Figure 7.8 Computed viscosity as a function of distance from the surface for 5, 10, and 15 µm–diameter polystyrene microspheres, for aluminum, glass, and stainless steel.

7.3.5 Polarizing Microscopy

The possible liquid crystalline nature of EZ was further explored by measuring birefringence of the water near the Nafion surface using polarizing microscopy. Preliminary experiments have been carried out in the laboratory of Michael Shribak at Woods Hole, and the results are shown in Figs. 7.9a,b.

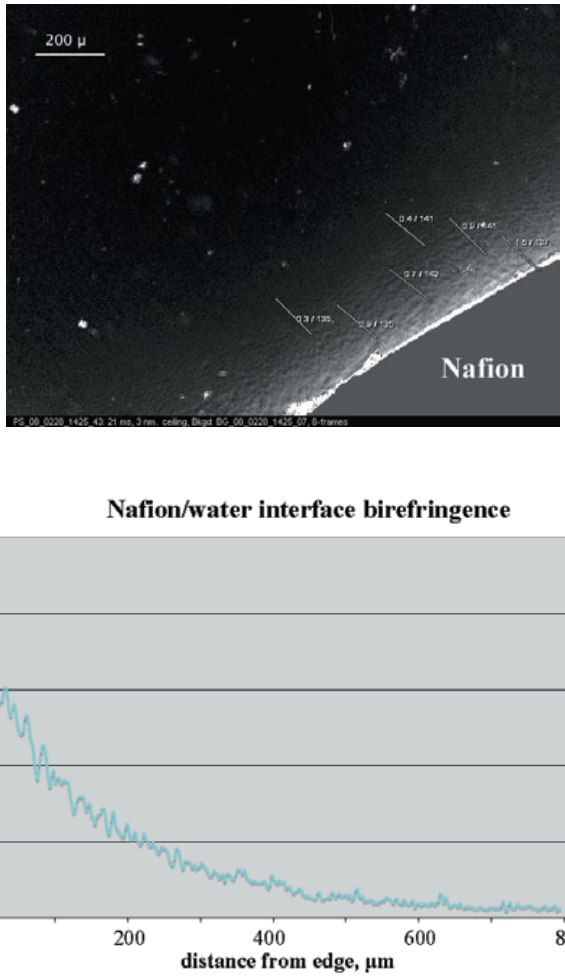

Figure 7.9 (a) Birefringent zone (bright) extends approximately 200 µm from the Nafion surface. The lines indicate the direction of the highest refractive index. Nafion sample covered by grey. (b) Optical retardation near Nafion–water interface.

A few interesting features are shown in Fig. 7.9a, which should be considered preliminary. The image brightness is linearly proportional to retardance, where the white level corresponds to 3 nm. The Nafion film itself is very birefringent; it introduces retardance of about 160 nm, which is beyond

of the chosen grey scale. This is expected inasmuch as interfacial water is caged within the polymer. Perhaps, the more striking feature appears in the aqueous zone next to the Nafion. The interfacial water shows a birefringent zone with smoothly diminishing retardation extending out to about 200 μm from the edge of the Nafion (Fig. 7.9b). The dimension observed here matches nicely with the size of the EZ measured with other methods.

Another interesting finding lies in the direction of the slow axis shown in Fig. 7.9a. It was observed that the slow-axis direction within the EZ always followed the slow-axis direction of the Nafion, independent of the orientation of the Nafion edge. This implies a continuity between the water in the Nafion and the water in the EZ.

7.4 CONCLUSIONS

A near-hydrophilic aqueous zone, first identified on the basis of its proclivity to exclude solutes, shows characteristics of a liquid crystal. Previous observations have shown this zone to be more stable than bulk water [3], while current observations show that the zone not only exists contiguously with the nucleating surface, but it may also project out like stalactites, to great distances. This is one of the characteristics of crystals.

Furthermore, this liquid-crystal-like zone is negatively charged; this was shown earlier [3]. It is apparent from the present results (Figs. 7.4 and 7.5) that this negatively charged zone is contiguous with a region rich in protons and hence positively charged. This juxtaposition of negative and positive is apparent whether the EZ lies contiguously with the nucleating surface or projects out at right angles to that surface.

A possibility, then, is that the negatively charged, liquid crystalline zone arises from bulk-water molecules that are reorganized into positive and negative entities. The negatively charged species would coalesce into the stable, cohesive liquid-crystal-like structure making up the EZ, while the positive entities would remain in the bulk, free to diffuse as protons, hydronium ions, or other large-scale positively charged water-based structures. The negative entity is stable, while the positive entity is free to diffuse.

As anticipated for a liquid crystalline substance, the viscosity is considerably higher than that of bulk water. The data of Figs. 7.6–7.8 show viscosity that is an order of magnitude larger than in the vicinity of nonexcluding surfaces. The increased viscosity of EZ water may help explain the gel-like character of the cell and of various gels, where interfacial water is commonplace. If EZ water is present in abundance in these entities, then their macroscopic mechanical behavior would be more like that of a liquid

crystal than that of a liquid. The implied liquid crystalline nature is further supported by preliminary polarizing microscopic data.

Although the tentative conclusions drawn here seem out of accord with generally held views, they seem the simplest interpretation of previous and current results. They imply a structural and functional aqueous framework considerably different from what is generally accepted and perhaps raise more questions than they answer. Nevertheless, they imply that aqueous behavior at interfaces may be far different than that implied by standard textbook views.

References

1. Israelachvili, J. (1992) *Intermolecular and Surface Forces*, Academic Press, San Diego.
2. Zheng, J.-M., and Pollack, G. H. (2003) Long range forces extending from polymer surfaces, *Phys. Rev. E*., **68** (031408), 1–7.
3. Zheng, J.-M., Chin, W.-C, Khijniak, E., Khijniak, E., Jr., and Pollack, G. H. (2006) Surfaces and interfacial water: evidence that hydrophilic surfaces have long-range impact, *Adv. Colloid Interface Sci*., **127**, 19–27.
4. Green, K., and Otori, T. (1970) Direct measurement of membrane unstirred layers, *J. Physiol. London*, **207**, 93–102.
5. Shribak, M., and Oldenbourg, R. (2003) Techniques for fast and sensitive measurements of two-dimensional birefringence distributions, *Appl. Opt.*, **42** (16), 3009–3017.
6. Ito, K., Yoshida, H., and Ise, N. (1994) Void structure in colloidal dispersions, *Science*, **263,** 66–68.
7. Yoshida, H., Ise, N., and Hashimoto, T. (1995) Void structure and vapor-liquid condensation in dilute deionized colloidal dispersions, *J. Chem. Phys*., **103** (23), 10146–10151.
8. Albertsson, P.-A. (1960) *Partition of Cell Particles and Macromolecules*, John Wiley, New York.
9. Kaplan, P. D., Rouke, J. L., Yodh, A. G., and Pine, D. J. (2004) Entropically driven surface phase separation in binary colloidal mixtures, *Phys Rev. Lett*., **72** (4), 582–585.

THE JOURNAL OF PHYSICAL CHEMISTRY Letters

LETTER

pubs.acs.org/JPCL

Impact of Hydrophilic Surfaces on Interfacial Water Dynamics Probed with NMR Spectroscopy

Hyok Yoo,[†,§] Rajan Paranji,[‡,§] and Gerald H. Pollack[*,†]

[†]Department of Bioengineering, University of Washington, Seattle, Washington 98195, United States

[‡]Department of Chemistry, University of Washington, Seattle, Washington 98195, United States

ABSTRACT: In suspensions of Nafion beads and of cationic gel beads, NMR spectroscopy showed two water−proton resonances, one representing intimate water layers next to the polymer surface, the other corresponding to water lying beyond. Both resonances show notably shorter spin−lattice relaxation times (T1) and smaller self-diffusion coefficients (D) indicating slower dynamics than bulk water. These findings confirm the existence of highly restricted water layers adsorbed onto hydrophilic surfaces and dynamically stable water beyond the first hydration layers. Thus, aqueous regions on the order of micrometers are dynamically different from bulk water.

SECTION: Surfaces, Interfaces, Catalysis

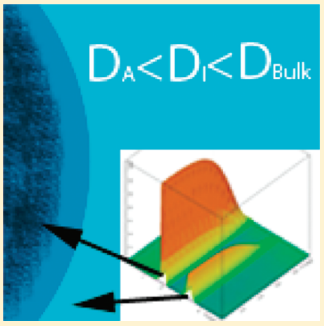

Water is arguably the most important liquid on earth. Despite its significance and abundance, water remains mysterious in many ways, and many anomalous features remain incompletely understood.[1] Among the lingering mysteries are the dynamics at interfaces. Interfacial water is of critical importance to biology, chemistry, and geo-climatic and atmospheric processes, as many catalytic reactions occur at interfaces.[2,3] Yet the properties of interfacial water are poorly understood.

It is commonly accepted that in the vicinity of hydrophilic interfaces water organizes into ice-like water, which project from the surface by a few nanometers.[4−6] Partly due to the rapid development of surface-characterization techniques, most recent work has focused almost exclusively on near-surface dynamics, i.e., dynamics of the first few molecular layers. Consequently, possible macroscopic effects have not been widely studied.

On the other hand, decades of early work has demonstrated that water can exhibit physical properties quite different than those of bulk water, out to distances on the order of micrometers.[7] Further, such an extensive surface water zone near many biological surfaces, known as the unstirred layer, has been observed to significantly impact the rate of colloidal diffusion across cell membranes.[8,9]

Work begun several years ago in our group indicates that the interfacial water zone may extend unexpectedly far from hydrophilic surfaces.[10] Those surfaces include a wide range of materials such as ion-exchange resins, polymers, hydrogels, functionalized monolayers, biological tissues and metal oxides. The near-surface aqueous zones exhibit a number of unique properties, the most notable being that suspended particles (e.g., monodisperse colloids) are excluded from the surface to distances of several hundred micrometers; thus, these particle-free zones have been termed exclusion zones (EZs). EZs exhibit a variety of physical properties differing from those of bulk water. They bear negative charge, as much as 150−200 mV near the nucleating surface, they exhibit increased dynamic viscosity, and they show diminished infrared emissivity and retarded T2 relaxation times.[11,12] These properties imply that the water within EZs may be more ordered than bulk water.

Nuclear magnetic resonance (NMR) spectroscopy is a well-established technique for determining the chemical structure and environment in aqueous systems.[13] NMR chemical shift, relaxation, and self-diffusion measurements have proved especially successful for probing interfacial water structure and dynamics near various biological and polymeric surfaces.[14−16] In the present study, high-resolution NMR spectroscopy was employed to measure the chemical shift, spin−lattice (T1) relaxation, and self-diffusion coefficient of interfacial water in order to obtain a more detailed physical picture of the molecular environment within the EZ.

Figure 1 is a representative 1H NMR spectrum of cationic resin/water system at 298° K in thermal equilibrium. Two water−proton resonances are evident, at 4.63 ppm and 6.00 ppm, indicating two distinct and magnetically unique water species, as observed within the NMR time scale. The standard chemical shift value of 1H resonance at 298 K for the HOD peak in an H_2O:D_2O mixture is 4.8 ppm.[17] Since the frequency axis was referenced to an external standard, i.e., 4,4-dimethyl-4-silapentane-1-sulfonic acid (DSS), it is reasonable to identify the upfield resonance at 4.6 ppm as that of less restricted water in the interstitial region between the beads. The downfield shift to the resonance at 6.00 ppm is indicative of a more "deshielded" environment of the water, and therefore corresponds to highly restricted water layers adsorbed onto polymer surfaces inside and around the resin. Integrating the fully relaxed 1H spectrum

Received: January 12, 2011
Accepted: February 10, 2011
Published: February 18, 2011

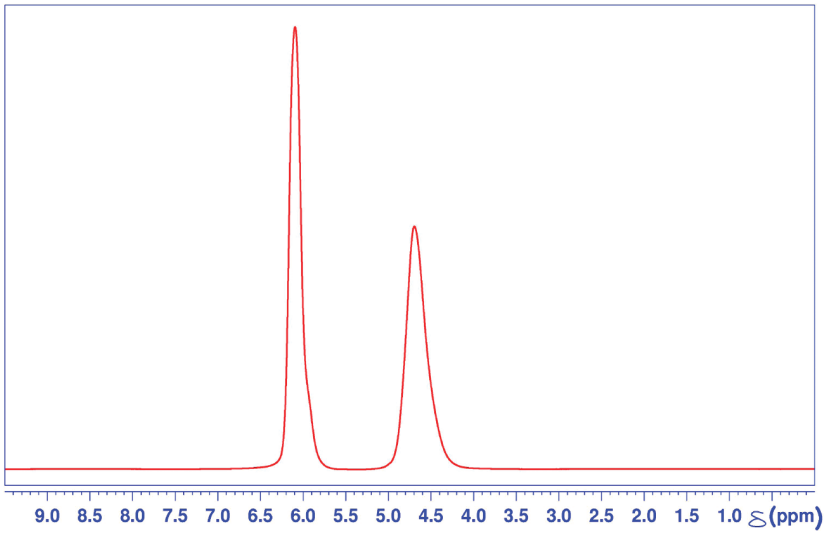

Figure 1. A fully relaxed one-dimensional (1D) 1H NMR spectrum of a cationic resin/water system. Two water proton resonances are observed at 6.0 ppm and 4.63 ppm, each corresponding to internal and interstitial water, respectively.

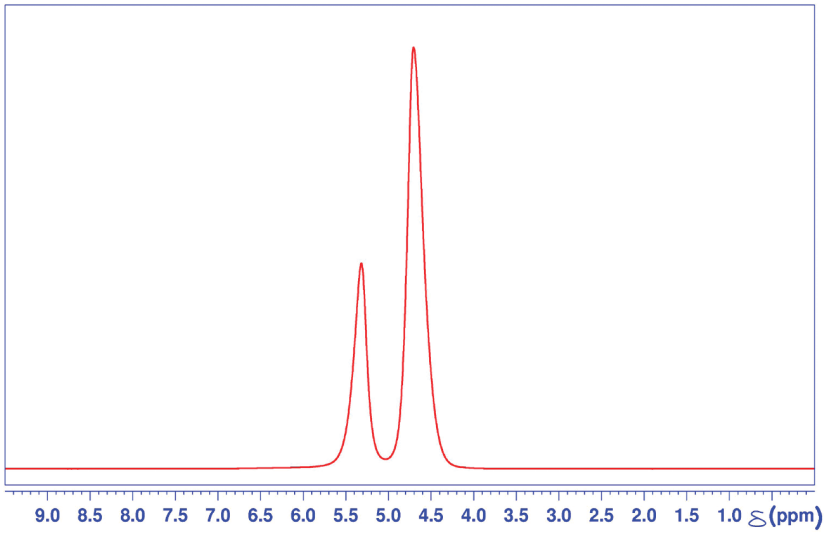

Figure 2. A fully relaxed 1D 1H NMR spectra of Nafion bead/water system. Two water proton resonances are observed at 5.35 ppm and 4.61 ppm, each corresponding to internal and interstitial water, respectively.

shown in Figure 1 yielded a 1:1 ratio of area under the peaks corresponding to internal water and the interstitial water, respectively. Full width at half-maximum (fwhm) line widths of the downfield-shifted peak are approximately 80% of the peak for interstitial water at 4.63 ppm.

Figure 2 shows a representative 1H NMR spectrum of a Nafion bead/water system at 298° K in thermal equilibrium. As in the cationic resin/water system, two chemical shifts of water protons are observed. The upfield resonance at 4.61 ppm is assigned as interstitial water lying between the Nafion beads, while the downfield resonance at 5.35 is assigned to adsorbed water inside and around Nafion beads. The integrated area under each resonance peak shows an intensity ratio of 7:3, interstitial-to-internal water, respectively. The fwhm line widths of the two resonances are roughly the same.

To further characterize the observed water species in each system, longitudinal relaxation (T1) and self-diffusion coefficients were measured for the respective chemical shifts. Five samples were used for T1 relaxation and self-diffusion measurements to verify the robustness and consistency of the results.

T1 relaxation and diffusion coefficients of the two water proton resonances in cationic resin/water system are shown in Table 1. T1 relaxation for interstitial water identified by the peak at 4.63 ppm was measured to be 1.82 s, which is significantly shorter than the T1 relaxation time of bulk water at 298 K.[18] The corresponding self-diffusion coefficient of interstitial water, 14.91×10^{-10} m^2/s, was measured to be about 60% of the known diffusion coefficient of bulk water at 298 K, namely, 23.00×10^{-10} m^2/s.[19]

Corresponding results for the Nafion resin/water system are shown in Table 2. T1 relaxation of upfield peak at 4.61 ppm corresponding to interstitial water was 1.34 s at 298 K, indicating faster longitudinal relaxation than bulk water as in the

dx.doi.org/10.1021/jz200057g |J. Phys. Chem. Lett. 2011, 2, 532–536

Table 1. Longitudvinal Relaxation (T1) Times and Self-Diffusion Coefficients of Water Species in a Cationic Exchange Bead/Water System

	T1 (s)		
δ_{HOD} (ppm)	component 1	component 2	D_{HOD} (1×10^{-10} m^2/s)
6.00	0.532	1.511	6.47
4.63	1.82		14.91

Table 2. Longitudinal Relaxation (T1) Times and Self-Diffusion Coefficients of Water Species in a Nafion Bead/Water System

	T1 (s)		
δ_{HOD} (ppm)	component 1	component 2	D_{HOD} (1×10^{-10} m^2/s)
5.35	0.190	2.053	5.39
4.61	1.34		16.91

case of the cationic resin/water system. The diffusion coefficient of interstitial water in the Nafion resin/water system was determined to be 16.91×10^{-10} m^2/s, about 25% smaller than that of bulk water. In order to rule out radiation damping as the cause of the observed shorter T1 values, the same measurements were made with 300 and 500 MHz spectrometers, and relaxation times on the same order of magnitude were confirmed.

In both systems, the T1 curve-fitting procedure for the downfield water peak yielded rather poor results if only a single exponential recovery curve was employed, indicating that a single T1 component cannot explain the data accurately. In contrast, when a two-component fit was used, the same set of experimental data gave excellent fit statistics without the necessity to remove even a single data point. This indicates that there are two distinct relaxation times. Thus, both tables show a faster and a slower T1 component for the downfield peaks, which correspond to highly restricted water adsorbed on the hydrophilic sulfonate-group sites within the polymer matrix.

The self-diffusion coefficient of water inside the cationic resin matrix at 298 K was 6.47×10^{-10} m^2/s. The self-diffusion coefficient of water inside the Nafion resin matrix at 298 K was slightly smaller, albeit on the same order of magnitude, 5.39×10^{-10} m^2/s. The fact that both D values of internal water were significantly lower than that of bulk water is self-consistent with the observed shorter T1 values compared to that of bulk. At room temperature, T1 relaxation is mainly mediated by translational and rotational diffusion in a solution, and the relaxation efficiency is inversely proportional to the rate of diffusion. The shorter diffusion constants of both internal and interstitial waters are indicative of the restricted environments that the water molecules experience. Fundamental NMR relaxation theory of liquids indeed stipulates that the T1 relaxation times are correspondingly shorter than that of water in bulk in slow-diffusing environments.

The most notable finding in this study is that there is no bulk water present in both bead suspensions, as indicated by T1 relaxation and self-diffusion measurements. The adsorbed water in and around both Nafion and ion-exchange beads is shown to be anisotropic due to confined geometry within polymer matrix,[20−22] and therefore it is expected that internal water has much slower self-diffusion and shorter T1 relaxation than bulk, indicating highly restricted molecular environment.

Interestingly, our experimental data show that the interstitial water as well has notably shorter T1 relaxation and smaller self-diffusion coefficient than bulk water. This was true in both experimental systems. In the case of the cationic resin system, maximal packing of 180 μm diameter spherical beads in face center cubic lattice-like arrangement would leave the interstitial region to be on the order of tens of micrometers in size. Assuming that the packing was not ideal and taking into account the variability in ion-exchange resin size, one can expect even larger dimensions of interstitial water region. For the Nafion system, this interstitial region is expected to be even larger due to the beads' irregular shape and larger dimensions, and this is demonstrated by larger interstitial to internal water peak area ratio shown in Figure 2 versus Figure 1.

While such extensive effects of the surface on nearby water dynamics may seem counterintuitive, previously observed characteristics of the EZ near hydrophilic surfaces indicates that nearby water can take on a more stable form out to distances of tens of micrometers.[11] Further, convergence of EZs extending from two neighboring nucleating surfaces within 100 μm, as in this case, has been observed. It is then reasonable to assume the interstitial water in both systems to be composed of mostly EZ water, and thus, the restricted water dynamics within the interstitial region observed here complements other known EZ characteristics.

T1 relaxation time and the self-diffusion coefficient of solutions can be profoundly affected by the solute that is dispersed in the medium, and the presence of trace impurities could in theory account for observed changes in T1 relaxation and diffusion coefficient of water. However, the 1H chemical shift spectrum of a given compound is a robust fingerprint of what is present in a solution. One may then state with reasonable certainty that there are no impurities of unknown origin in our experimental system, evidenced by the absence of any anomalous peaks present other than water proton peaks.

Invoking impurities as the cause of change in water dynamics also lacks theoretical rationale. No well-established theory of chemical shifts in solution NMR can account for the observed "multiple resonance" spectra of water found in two distinct sample preparations studied here, as due to the effect of "trace impurities" of unknown origin. Indeed, to our knowledge, there are no aqueous NMR spectra that exhibit anything other than a single bulk water NMR peak in and around 4.8 ppm at 298 K. This is true, independent of the kind of solute that is dissolved in water, ranging from small organic molecules to large biomolecules such as proteins or nucleic acids.

The only reports found in literature that had recorded such multiple resonances of water are associated with biological tissues or polymer systems that are quite similar to the ion exchange resins or Nafion that were used in this study.[23−26] These studies, however, did not address the dynamics of water lying outside the polymers or tissues.

Thus, the unique dynamic properties of water presented in this study are evidently not due to the presence of impurities, but rather caused by the presence of hydrophilic surfaces. While chemical shift provides unique structural identification of a molecule, it does not report the possible existence of intermolecular interactions and the resulting long-range ordering of a solution system. In contrast, T1 relaxation and self-diffusion measurements do provide this crucial information, as shown

here. In fact, although the chemical shift of EZ water is quite similar to that of bulk water, albeit the small difference of 0.2 ppm, the T1 and *D* values turn out to be clear identifiers of the more restricted and long-range coupled nature of EZ water.

Hence, the most interesting implications of this study may be that, in the presence of Nafion, resin beads, or other hydrophilic surfaces, water is readily organizing and changing its otherwise bulk dynamic properties extensively. The results of this study therefore underscore the organizational and dynamic complexity of water juxtaposed next to certain classes of surface.

EXPERIMENTAL SECTION

For all experiments, deionized water (Type I HPLC Grade (18.2 MΩ·cm)) was collected from a Barnstead D3750 Nanopure Diamond purification system. A 5% D_2O/H_2O (v/v) solution was used in all experiments, and was prepared by diluting 99.9% deuterium oxide (Cambridge Isotopes DLM-4-100) with deionized water.

Two types of polymer beads were used as EZ-nucleating surfaces. One was analytical-grade cationic ion-exchange resin, 180−425 μm diameter, in H-form (AG 50W-X8, Bio-Rad, CA) with cross-linking of 8% divinylbenzene (DVB). The other was Nafion, a sulfonated tetrafluoroethylene based fluoropolymer, with dimensions on the order of 300−500 μm in H-form (495786, Sigma-Aldrich, MO). Both types of polymer have abundant sulfonic acid sites, providing highly hydrophilic environments.

Beads were first hydrated in experimental solvent for 1 h to ensure sufficient level of hydration. Once hydrated, the beads were placed in a standard 5 mm OD NMR tube (WG-1241-7, Wilmad Glass, NJ) and left to settle in 100 mL of 5% D_2O/H_2O (v/v). For both types of bead systems, the final height of tightly packed beads was 3 cm as measured from the bottom of the tube.

The 1H NMR spectra were recorded on a 750 MHz Bruker AVANCE II NMR spectrometer equipped with a 1H {C,N} high-resolution triple resonance probe with Z-gradient. A spectroscopic standard sample of 1% sucrose in 10% H_2O/D_2O (v/v) solvent mixture was used to shim the magnet to optimal B_0 field homogeneity prior to recording the spectra from the resin beads and Nafion beads. Raw data were collected with 8K time-domain points with a spectral width of 10 ppm centered at 5.0 ppm, recycle delay of 1 s, and acquisition time of 0.55 s. These were then Fourier transformed without zero filling.

Proper referencing of spectra was ensured by adding a trace quantity of DSS as external reference for one sample and the ensuing spectrum reference frequency was used for calibrating the 0 ppm in subsequent sample preparations. Five identical NMR sample tubes were prepared for repeating the measurements and establishing consistency of the results. The sample temperature was set to 298 K ± 0.1 K and the accuracy of this value at the sample was confirmed by measuring the chemical shift difference of the doublet of neat methanol and cross checking against published values.

Spin−lattice (T1) relaxation of water in the polymer/water system was measured using inversion−recovery ($\pi - \tau_1 - \pi/2$) pulse sequence. Longitudinal magnetization was collected with 10 time delays varying from 1 ms to 25 s. A standard inversion recovery curve with three unknowns was fitted to the integrated volume of each resonance as a function of the delay. When a single T1-component fit exhibited a substantial number of outliers leading to poor χ^2 statistics, a two-component fit was employed, leading to excellent fits with no outliers from the recorded set of data points.

Self-diffusion measurements of the two chemical shifts of water in polymer/water system were carried out using the stimulated spin−echo pulse sequence ($(\pi/2) - g(\delta) - (\pi/2) - \Delta - (\pi/2) - g(\delta)$). The attenuation in spin−echo amplitude was recorded as a function of increasing gradient strength, *g*. In an isotropic system, where diffusion is unrestricted, the echo attenuation is given by the Stejskal−Tanner equation:

$$\psi(\delta, g, \Delta) = \exp\left(- \gamma^2 \delta^2 g^2 D \left(\Delta - \frac{\delta}{3} \right) \right) \qquad (1)$$

Here γ is the gyromagnetic ratio, δ and *g* are duration and amplitude of the magnetic-field gradient, respectively, Δ is the duration for phase encoding the diffusing magnetization, and *D* is the bulk self-diffusion coefficient of the solvent. *D* was computed from the slope obtained by fitting eq 1 as a function g^2 to the echo amplitude decay. Prior to making measurements with the bead systems, the bulk self-diffusion coefficient of deionized water was measured at 298 K and confirmed to agree with literature values.

AUTHOR INFORMATION

Author Contributions

[§]Equal contributing authors.

ACKNOWLEDGMENT

This study was supported by a grant from the NIH (5R01 GM093842).

REFERENCES

(1) Finney, J. L. Water? What's so Special about It? *Philosophical Transactions: Biological Sciences* **2004**, *359*, 1145–1165.

(2) Senadheera, L.; Conradi, M. S. Rotation and Diffusion of H_2 in Hydrogen - Ice Clathrate by ^{1}H NMR. *J. Phys. Chem. B* **2007**, *111*, 12097–12102.

(3) Catalano, J. G.; Fenter, P.; Park, C. Water Ordering and Surface Relaxations at the Hematite (110)−Water Interface. *Geochim. Cosmochim. Acta* **2009**, *73*, 2242–2251.

(4) Noguchi, H.; et al. Interfacial water structure at polymer gel/quartz interfaces investigated by sum frequency generation spectroscopy. *Phys. Chem. Chem. Phys.* **2008**, *10*, 4987–4993.

(5) Tian, C.; Ji, N.; Waychunas, G. A.; Shen, Y. R. Interfacial Structures of Acidic and Basic Aqueous Solutions. *J. Am. Chem. Soc.* **2008**, *130*, 13033–13039.

(6) Smith, J. D.; et al. Energetics of Hydrogen Bond Network Rearrangements in Liquid Water. *Science* **2004**, *306*, 851–853.

(7) Henniker, J. C. The Depth of the Surface Zone of a Liquid. *Rev. Mod. Phys.* **1949**, *21*, 322–341.

(8) Green, K.; Otori, T. Direct Measurements of Membrane Unstirred Layers. *J. Physiol. (London)* **1970**, *207*, 93–102.

(9) Wilson, F. A.; Sallee, V. L.; Dietschy, J. M. Unstirred Water Layers in Intestine: Rate Determinant of Fatty Acid Absorption from Micellar Solutions. *Science* **1971**, *174*, 1031–1033.

(10) Zheng, J. M.; Pollack, G. H. Long-Range Forces Extending from Polymer−Gel Surfaces. *Phys. Rev. E: Stat., Nonlinear, Soft Matter Phys.* **2003**, *68*, 031408.

(11) Zheng, J. M.; Chin, W. C.; Khijniak, E.; Khijniak, E., Jr.; Pollack, G. H. Surfaces and Interfacial Water: Evidence That Hydrophilic Surfaces Have Long-Range Impact. *Adv. Colloid Interface Sci.* **2006**, *127*, 19–27.

(12) Hyok Yoo, D. R. B.; Pirie, C. M.; Hovakeemian, B.; Pollack, G. H. In *Water: The Forgotten Biological Molecule*; Denis Le Bihan, H. F. , Ed.; Pan Stanford Publishing: Singapore, 2011.

(13) Levitt, M. H. *Spin Dynamics: Basics of Nuclear Magnetic Resonance*; Wiley: New York, 2002.

(14) Duval, F. P.; Porion, P.; Van Damme, H. Microscale and Macroscale Diffusion of Water in Colloidal Gels. A Pulsed Field Gradient and NMR Imaging Investigation. *J. Phys. Chem. B* **1999**, *103*, 5730–5735.

(15) Perrin, J.-C.; Lyonnard, S.; Guillermo, A.; Levitz, P. Water Dynamics in Ionomer Membranes by Field-Cycling NMR Relaxometry. *J. Phys. Chem. B* **2006**, *110*, 5439–5444.

(16) Topgaard, D.; Söderman, O. Self-Diffusion in Two- and Three-Dimensional Powders of Anisotropic Domains: An NMR Study of the Diffusion of Water in Cellulose and Starch. *J. Phys. Chem. B* **2002**, *106*, 11887–11892.

(17) Gottlieb, H. E.; Kotlyar, V.; Nudelman, A. NMR Chemical Shifts of Common Laboratory Solvents as Trace Impurities. *J. Org. Chem.* **1997**, *62*, 7512–7515.

(18) Simpson, J. H.; Carr, H. Y. Diffusion and Nuclear Spin Relaxation in Water. *Phys. Rev.* **1958**, *111*, 1201–1202.

(19) Holz, M.; Heil, S. R.; Sacco, A. Temperature-Dependent Self-Diffusion Coefficients of Water and Six Selected Molecular Liquids for Calibration in Accurate ^{1}H NMR PFG Measurements. *Phys. Chem. Chem. Phys.* **2000**, *2*, 4740–4742.

(20) Webber, J. B. W.; Dore, J. C.; Strange, J. H.; Anderson, R.; Tohidi, B. Plastic Ice in Confined Geometry: The Evidence from Neutron Diffraction and NMR Relaxation. *J. Phys.: Condens. Matter* **2007**, 415117.

(21) Webber, J. B. W.; Anderson, R.; Strange, J. H.; Tohidi, B. Clathrate Formation and Dissociation in Vapor/Water/Ice/Hydrate Systems in SBA-15, Sol−Gel and CPG Porous Media, As Probed by NMR Relaxation, Novel Protocol NMR Cryoporometry, Neutron Scattering and Ab Initio Quantum-Mechanical Molecular Dynamics Simulation. *Magn. Reson. Imaging* **2007**, *25*, 533–536.

(22) Liu, E.; et al. Neutron Diffraction and NMR Relaxation Studies of Structural Variation and Phase Transformations for Water/Ice in SBA-15 Silica: I. The Over-Filled Case. *J. Phys.: Condens. Matter* **2006**, *18*, 10009–10028.

(23) Gough, T. E.; Sharma, H. D.; Subraman., N Proton Magnetic Resonance Studies of Ionic Solvation in Ion-Exchange Resins 0.1. Sulfonated Cation-Exchange Resins. *Can. J. Chem.* **1970**, *48*, 917–923.

(24) Lenk, R.; Bonzon, M.; Greppin, H. Dynamically Oriented Biological Water as Studied by NMR. *Chem. Phys. Lett.* **1980**, *76*, 175–177.

(25) OConnor, P. J.; et al. H-1 NMR characterization of swelling in cross-linked polymer systems. *Macromolecules* **1996**, *29*, 7872–7884.

(26) Howery, D. G.; Shore, L.; Kohn, B. H. Proton Magnetic Resonance Studies of the Structure of Water in Dowex 50W. *J. Phys. Chem.* **1972**, *76*, 578–581.

THE JOURNAL OF PHYSICAL CHEMISTRY Letters

Letter

pubs.acs.org/JPCL

Open Access on 02/25/2015

Contraction-Induced Changes in Hydrogen Bonding of Muscle Hydration Water

Hyok Yoo,[†] Ekaterina Nagornyak,[†] Ronnie Das,[†] Adam D. Wexler,[‡] and Gerald H. Pollack*,[†]

[†]Department of Bioengineering, University of Washington, Box 355061, Seattle, Washington 98195, United States

[‡]Wetsus Center for Sustainable Water Technology, Agora 1, 8900CC Leeuwarden, The Netherlands

Supporting Information

ABSTRACT: Protein−water interaction plays a crucial role in protein dynamics and hence function. To study the chemical environment of water and proteins with high spatial resolution, synchrotron radiation-Fourier transform infrared (SR-FTIR) spectromicroscopy was used to probe skeletal muscle myofibrils. Observing the OH stretch band showed that water inside of relaxed myofibrils is extensively hydrogen-bonded with little or no free OH. In higher-resolution measurements obtained with single isolated myofibrils, the water absorption peaks were relatively higher within the center region of the sarcomere compared to those in the I-band region, implying higher hydration capacity of thick filaments compared to the thin filaments. When specimens were activated, changes in the OH stretch band showed significant dehydrogen bonding of muscle water; this was indicated by increased absorption at ~3480 cm^{-1} compared to relaxed myofibrils. These contraction-induced changes in water were accompanied by splitting of the amide I (C═O) peak, implying that muscle proteins transition from α-helix to β-sheet-rich structures. Hence, muscle contraction can be characterized by a loss of order in the muscle−protein complex, accompanied by a destructuring of hydration water. The findings shed fresh light on the molecular mechanism of muscle contraction and motor protein dynamics.

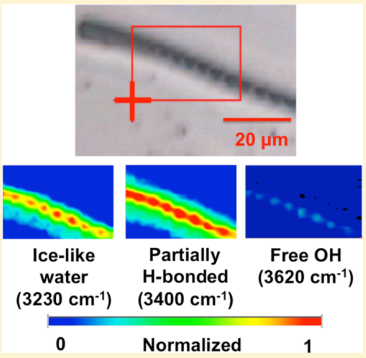

SECTION: Biophysical Chemistry and Biomolecules

While the importance of water for sustaining life is well-recognized, the exact role of water in biological processes remains unclear. On the other hand, an increasing number of studies show that biological processes are heavily influenced by interfacial water dynamics.[1]

One such water-mediated process is protein conformational change, which sits at the base of biological function.[2,3] X-ray crystallography studies had initially implied relatively few hydration layers adsorbed onto proteins, which could persist even under high vacuum.[4] However, recent experiments using THz and fluorescence spectroscopy have reveled that the dynamic hydration shells around proteins can extend out to much longer distances.[5,6] Further, recent dielectric spectroscopy studies have shown that protein folding is largely "slaved" by dynamics of water beyond the first several hydration layers,[7] that is, the protein follows the water.

The above-mentioned studies have sparked broad interest in hydration water. However, questions remain as to how such solution systems reflect the intricately ordered and crowded protein−water systems lying inside of intact tissues and cells. One such ordered system is muscle. When muscle is activated, proteins undergo synchronous conformational changes over millimeter and centimeter length scales. The protein changes are well studied; however, the changes in muscle water hydrogen bonding remain uncharted territory.

Many experimental observations imply that water may play an important role in muscle contraction (for a summary, see refs 8 and 9). Several recent findings in particular show that near-surface interfacial water is considerably more viscous than bulk water, with several groups reporting as high as 6-fold viscosity elevation near hydrophilic surfaces.[10] This high viscosity implies that the molecular cross-bridge swinging that has been considered central to the contractile process may experience resistance, and correspondingly, that the high energy needed to power such strokes might not be accounted for by ATP splitting alone.[11] This is but one of multiple issues raised by the presence of high-viscosity interfacial water.

Synchrotron radiation (SR) FTIR spectromicroscopy has lately emerged as a noninvasive probe of biological tissues with unprecedented spectral sensitivity and diffraction-limited spatial resolution, owing to its high brightness and small beam size.[12] This tool has proved especially useful in determination of chemical species and structures.[13−15] IR spectroscopy is also remarkably sensitive to the strength of hydrogen bonding as OH stretch frequency is linearly related to hydrogen bonding strength (i.e., stronger hydrogen bonding results in lower frequency of the OH stretching vibration).[16] With this technique, we examined possible changes of muscle water and protein structures associated with muscle contraction.

Received: January 14, 2014
Accepted: February 25, 2014
Published: February 25, 2014

In order to compare liquid water with muscle water, we first obtained the infrared spectrum of liquid water, as shown in Figure 1 (top). The OH stretch region of liquid water shows a broad peak due to extensive hydrogen bonding. The second derivative (below) shows that the broad peak resolves into three components, 3230, 3400, and 3620 cm^{-1} corresponding, respectively, to the symmetric OH stretching mode of ice-like water, partially hydrogen-bonded water, and free OH. These are standard assignments. Of the three components, particularly notable is the one at 3400 cm^{-1}, which contains two shoulder peaks at 3480 and 3520 cm^{-1}. These shoulder peaks imply that liquid water may have at least three different arrangements of partially hydrogen-bonded water.

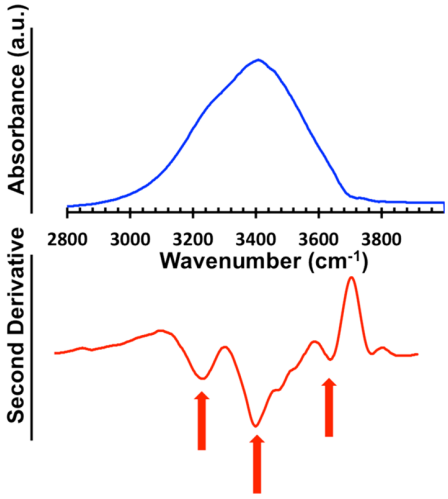

Figure 1. Infrared spectrum of liquid water at 22 °C in the OH stretch spectral region (top) and the second-derivative spectrum (bottom). Arrows indicate components resolved with second-derivative analysis at 3230, 3400, and 3620 cm^{-1}.

To observe the corresponding hydrogen bonding environment of muscle water, we collected an infrared map of a single relaxed honeybee myofibril (Figure 2). Panel (a) shows a bright-field image, with visible sarcomeres. The color images in panel (b) show absorption maps obtained at different spectral regions, corresponding to three components of liquid water determined above, fully coordinated ice-like water (3230 cm^{-1}), partially H-bonded water (3400 cm^{-1}), and free OH (3620 cm^{-1}). The strong relative absorptions at 3230 and 3400 cm^{-1} indicate that the water inside of the relaxed myofibril is mostly "ice-like" and partially hydrogen-bonded. The weak absorption at 3620 cm^{-1} indicates little or no free OH. Hence, most of the water molecules inside of the relaxed myofibril can be said to be either fully or partially hydrogen bonded.

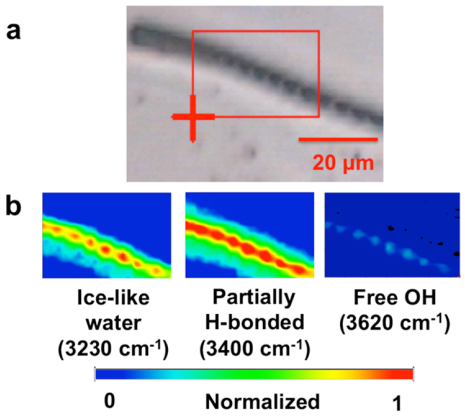

Figure 2. (a) Bright-field image of a single honeybee myofibril in the relaxed state. (b) IR absorption maps of the same specimen at three wavenumbers, corresponding to ice-like water (3230 cm^{-1}), partially hydrogen-bonded water (3400 cm^{-1}), and free OH (3620 cm^{-1}).

A particularly interesting feature of these infrared maps is the inhomogeneous spatial distribution of water along the myofibril. Overlaying the images showed that all three components of water IR absorption were higher in the center of the sarcomere than in the regions around the z-lines. Of those three components, the ice-like water was preferentially present in the middle of the sarcomere. The partially hydrogen-bonded water was spread more uniformly over the length of the myofibril, albeit slightly higher in the middle of the sarcomere. Thus, the water content within the myofibril shows sarcomeric periodicity. This may mean that the thick filaments, which are found in the middle of the sarcomere, might have higher water holding capacity than the thin filaments, which are nearer to the ends of the sarcomere. The stronger absorption of ice-like water may be due to higher negative charge density on the surfaces of thick filaments compared to that for thin filaments.[17,18]

In order to investigate the chemical changes associated with contraction, myofibril bundles were studied in relaxed and activated states. To simulate two physiological states of muscle, we used a standard model composed of skinned muscle and two physiological solutions. The bundle was first bathed in relaxing solution for 30 min, and an IR map was collected. Next, the same bundle was bathed in activating solution for 30 min. By that time, the specimen was fully contracted; all visible signs of contraction development had ceased.

Figure 3a shows bright-field images and superimposed IR maps of the relaxed and activated bundle. The IR maps were obtained at 3500 cm^{-1}, the spectral region showing the largest changes as the specimen passed from the relaxed state to the contracted state. The activated specimen absorbed significantly more than the relaxed specimen at 3500 cm^{-1}. This increase may be indicative of decreased hydrogen bonding strength of muscle water during contraction.

Figure 3b shows the representative IR spectra from relaxed (blue) and activated (red) specimens. Deionized water (green) is shown for comparison. Consistent with findings in the single myofibril (Figure 1), the spectra of the relaxed bundle show almost complete absence of free OH (3620 cm^{-1}) compared to liquid water. This indicates stronger hydrogen bonding strength of muscle water compared with that of deionized water. The most notable feature of Figure 3b is the shoulder peak near 3500 cm^{-1} that appears upon activation, indicating "breakup" of the hydrogen bonding network. However, even with a significant dehydrogen bonding, the activated muscle still largely lacked free OH. The changes seen in the OH stretch region of IR spectra upon activation were reversible at least up to two activate−relax cycles, indicated by the appearance and disappearance of the a shoulder peak at 3500 cm^{-1} in activated and relaxed states, respectively.

For more detailed spectral analysis of the OH stretch region, second-derivative analysis was performed on the original spectra. The results are shown in Figure 3c. They show several peaks corresponding to the symmetric and asymmetric CH_2

dx.doi.org/10.1021/jz5000879 | J. Phys. Chem. Lett. 2014, 5, 947−952

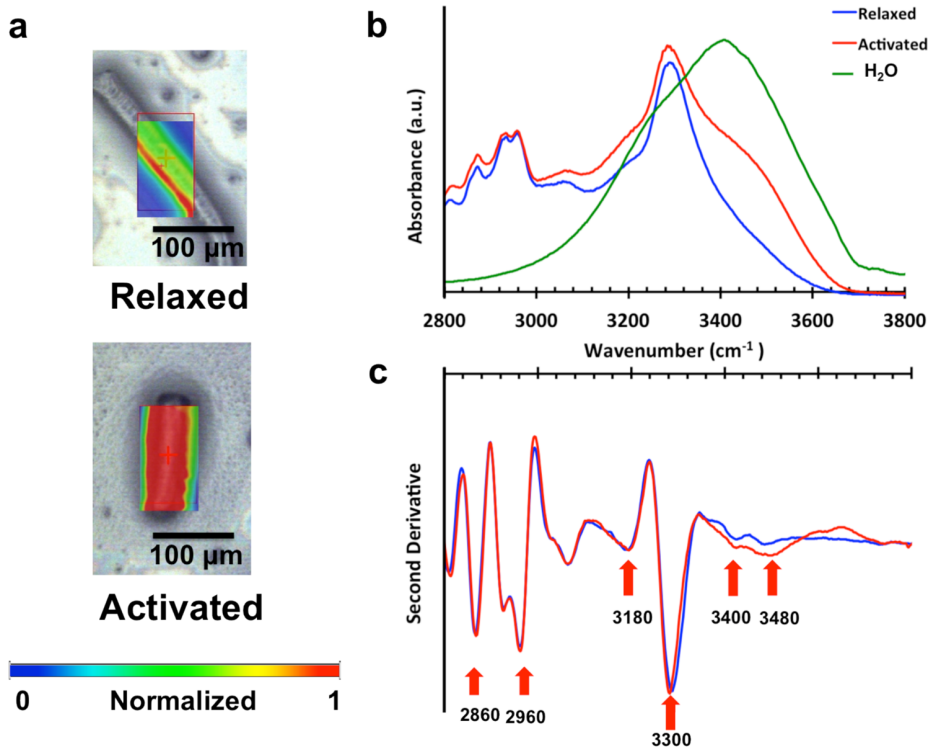

Figure 3. (a) Bright-field images of a relaxed and activated rabbit psoas myofibril bundle with overlays of IR images at 3500 cm^{-1} showing a significant increase in absorption during contraction. For the color map, the absorption of activated muscle at 3550 cm^{-1} is normalized to 1 for comparison. (b) IR spectra of relaxed (blue) and activated (red) muscle and deionized water (green). (c) Second-derivative spectra of relaxed and activated muscle.

stretches of the lipids (~2852 and 2924 cm^{-1}), the asymmetric CH_3 stretch of the lipids (2960 cm^{-1}), the symmetric NH stretch of amide A and amide B (3300 and 3057 cm^{-1}), besides the water peaks (3180, 3400, 3480 cm^{-1}). Table 1 summarizes

Table 1. Assignment of IR Bands and Their Major Contributors

wavenumber (cm^{-1})	vibrational mode assignment and major contribution
~3620	νOH of free OH[19]
~3400	νOH of partially hydrogen-bonded water19
~3300	amide A, νNH of proteins[20]
~3230	νOH of ice-like water[19]
~2960	$\nu_{as}CH_3$ of lipids, proteins and nucleic acids[20]
~2924	$\nu_{as}CH_2$ of lipids[21]
~2860	$\nu_{s}CH_2$ of lipids[21]
~1650	amide I, νC=O stretch[20]
~1550	amide II[20]

those peaks. While other peaks do not show any obvious shifts, the amide A band shows a blue shift (i.e., to higher frequency) of about 10 cm^{-1}. Such a shift has been associated with an α-helix to β-sheet transition.[16]

In Figure 3c, second-derivative water peaks are seen corresponding to 3180, 3400, and 3480 cm^{1}. Compared with liquid water (Figure 1), the component corresponding to ice-like water occurs at a lower frequency, by about 20 cm^{-1}. This shift indicates that fully coordinated modes of water in muscle contain slower vibrational modes, presumably due to dipolar coupling of water and protein oscillators. Upon activation, the ratio of the amide A peak (3300 cm^{-1}) and the 3480 cm^{-1} water peak increases, showing an increase in the number of broken hydrogen bonds per protein molecule. Thus, the second-derivative analysis confirms the results obtained from the original spectra, a significant breakup of hydrogen bonds during activation. The absence of free OH in both relaxed and activated myofibril bundles shows that the breakup of hydrogen bonding during activation still leaves water molecules hydrogen-bonded to at least one neighboring water molecule.

To confirm that the observed changes in muscle water are not artifacts arising from differences in absorption from the different physiological solutions, we collected infrared spectra of both activating and relaxing solutions (Figure S1, Supporting Information). Comparison with the spectra of deionized water confirmed that both physiological solutions had IR spectra indistinguishable from that of deionized water.

The amide bands in vibrational spectra of proteins are useful tools for determining the secondary structure of proteins and the proteins' stability.[22] Specifically, the amide I peak provides sensitive information on protein secondary structures (i.e., α-helix, β-sheets, β-sheet turns, side chains, etc.).[23] Figure 4a shows representative spectra of the corresponding spectral region in relaxed (blue) and activated (red) myofibril bundles. These spectra were taken from the same spectra as Figure3b. In the relaxed state, the myofibril bundle shows a classic amide I peak centered at ~1650 cm^{-1} and an amide II peak centered at ~1550 cm^{-1}. Upon activation, the amide I peak splits into two (Figure 4a), the new peak appearing at ~1600 cm^{-1}, over and above the original peak at ~1650 cm^{-1}. Moreover, the centroid of the 1650 cm^{-1} peak is red-shifted to lower frequency by about 15 cm^{-1}. While detailed theoretical description of amide I splitting has posed significant challenges, experimental results

dx.doi.org/10.1021/jz5000879 | J. Phys. Chem. Lett. 2014, 5, 947−952

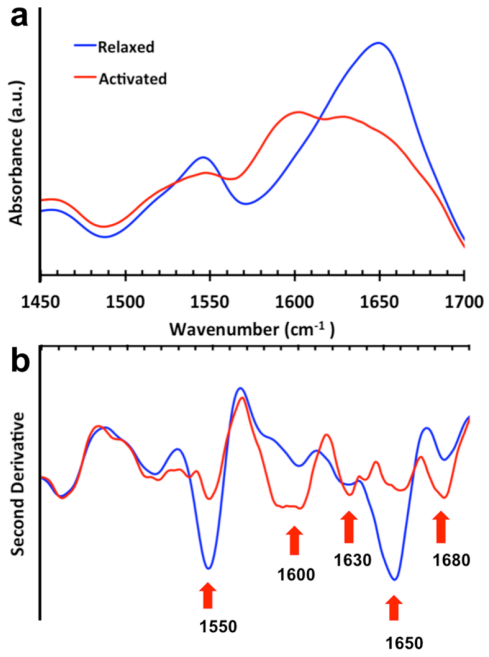

Figure 4. (a) IR spectra of a relaxed (blue) and activated (red) myofibril bundle in amide I and II spectral regions. (b) Second derivative of the IR spectra.

indicate that splitting of the amide I peak to lower frequency is associated with β-sheet-rich structures.[24] Thus, the red shifting of the 1650 cm^{-1} peak centroid indicates the formation of intermolecular β-sheets arising out of aggregation of unfolded proteins in activated muscle. The new peak appearing in the amide I region at ~1600 cm^{-1} is assigned to the amino acid side chains of proteins including both hydrogenated and hydroxylated glutamine (H-Gly and OH-Gly), whose transport plays an important role in phosphorylation of muscle and contraction.[20,25] Thus, increased absorption at ~1600 cm^{-1} seen here may be due to formation of side chains during contraction. Contrary to the amide I band, the amide II band showed less change with activation: diminished absorbance, with no change in the peak location.

To examine these spectral features in more detail, we looked at the second-derivative spectra. Figure 4b shows the second derivative of the original spectra in the amide I and II region. Several features are of interest. First, the relaxed muscle has markedly higher composition of α-helix (1652 cm^{-1}) than activated muscle. Second, the peaks centered at ~1630 and ~1680 cm^{-1} increased significantly in amplitude when muscle went from relaxed to activated. These peaks represent β-sheets and β-turns, respectively.[20] Taken together, these findings show that muscle proteins lost helical order during activation, similar to the conclusions drawn earlier from X-ray diffraction studies.[26]

The activation-associated changes of muscle water are appreciable (Figure 2b). However, the myofibril bundle contains water both inside of the myofibril and between the myofibrils. To ensure that the observed changes in hydrogen bonding are indeed due to changes within the myofibrils, that is, associated with myosin, actin, and so forth, we probed single myofibrils, where the only water present in the sample lies within the contractile apparatus. Contraction is ordinarily less pronounced in honeybee myofibrils but was confirmed by monitoring shortening of sarcomeres in bright-field images. The statistics are summarized in Figure S2 (Supporting Information).

The results obtained with the single myofibril (Figure 5) largely concur with those obtained with the myofibril bundles

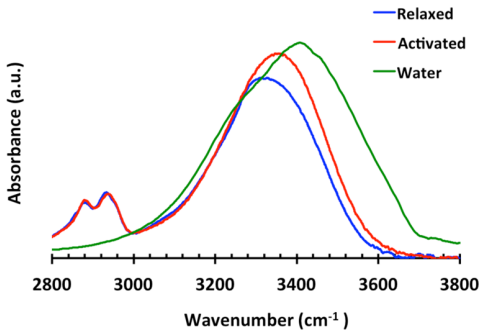

Figure 5. IR spectra of a relaxed (blue) and activated single myofibril (red). The IR spectrum of liquid water is shown for comparison (green).

(Figure 4). As seen with rabbit myofibril bundles (Figure 3b), the representative spectrum of relaxed single myofibril shows an OH stretch peak significantly red-shifted from that of deionized water. This shift indicates stronger hydrogen bonding than liquid water. Moreover, as the specimen passed from relaxed (blue) to activated (red), the hydrogen bonding strength decreased, as indicated by a ~25 cm^{-1} blue shifting of the centroid of the water OH stretch peak. The dehydrogen bonding agrees with results obtained from myofibril bundles. Hence, the major findings in muscle water hydrogen bonding are consistent in both single myofibrils and myofibril bundles, indicating that those changes occur within the actomyosin complex.

This study was carried out to understand the chemical environment of skeletal muscle water and its possible role in contraction. Our results show that water in relaxed muscle is significantly more structured than bulk water, with little or no free OH present. This was found inside of myofibril bundles as well as inside of single myofibrils. The most notable result of this study was the sensitivity of the water hydrogen bonding environment to distinct physiological states. When the myofibril was activated, the well-hydrogen-bonded muscle water lost order as the muscle proteins changed conformation. Water evidently plays some role in the contractile process.

It is widely believed that water inside of biological tissues is similar to bulk water, except for the first two or three protein hydration layers. However, more recent results have shown that hydrophilic surfaces can extensively order nearby water.[27−29] Further, recent NMR measurements show that in confined geometries such as inside of reverse micelles, protein hydration shells can extend out to several dozens of layers.[30] Considering the confined geometry inside of the myofilament lattice, it is no surprise that most of the muscle water is well-structured. Thus, muscle water differs substantially from bulk water.

While modern understanding of muscle contraction is largely dominated by the cross-bridge theory originally proposed by Sir Andrew Huxley and H. E. Huxley,[31,32] many experimental results remain at odds with that theory. The most notable are shortening of thick filaments during contraction[33] and generation of force even with no apparent overlap of thick and thin filaments,[34] where no attachment of myosin heads to actin filaments can occur. Both findings indicate the need for

dx.doi.org/10.1021/jz5000879 | J. Phys. Chem. Lett. 2014, 5, 947−952

reconsideration of that mechanism.[9,35] On the other hand, the breakup of water structure during contraction implies that the high viscosity issue mentioned above may be less of a problem for the prevailing theory than initially considered. If the water remained highly viscous, not only could cross-bridges fail to swing, but also, any kind of filamentary motion might confront substantial difficulty.

Several physical changes occur immediately following stimulation but prior to force generation. These include changes in thick filament length,[33] sudden decreases in viscoelasticity,[36] loss of axial and helical order in myosin,[37] and latency relaxation.[38] All of those changes occur within milliseconds after stimulation and well before the onset of force generation. While these changes are seemingly necessary preconditions for force generation, their mechanisms have remained unclear. Changes in water structure might potentially explain some or all of those changes and help provide better understanding of the molecular mechanism of muscle contraction.

Given the breakup of water structure during contraction, a lingering question is which of the two events comes first, changes in protein conformation or breakup of ordered hydration water. Time-resolved studies will be needed to answer this important question, which may have relevance also for other biological systems.

METHODS

Solutions. Several different solutions were used to simulate different states of contraction. Relaxing solution (pH 7.0) had a composition (in mM) of 10 MOPS, 64.4 K^+ propionate, 5.23 Mg^{2+} propionate, 9.45 Na_2SO_4, 10 EGTA, 0.188 $CaCl_2$, 7 ATP, and 10 creatine phosphate. Activating solution consisted (in mM) of 10 MOPS, 45.1 K^+ propionate, 5.21 Mg^{2+} propionate, 9.27 Na_2SO_4, 10 EGTA, 9.91 $CaCl_2$, 7.18 ATP, and 10 creatine phosphate. Glycerol solution consisted of half glycerol and half rigor solution, the latter containing (in mM) 50 Tris (pH 7.4), 100 NaCl, 2 KCl, 2 $MgCl_2$, and 10 EGTA.

Skeletal Myofibril Preparation. Two types of specimens were studied, myofibril bundles and single myofibrils. Myofibril bundles were prepared from rabbit psoas muscles. Briefly, muscles were dissected bluntly from the backs of rabbits, along the length of the fibers. They were cut into thin strips and tied at both ends to a wooden stick in order to maintain their natural length. The prepared muscle strips were placed in glycerol solution and stored in a freezer at −20 °C for long-term storage. To obtain myofibril bundles, the muscle strips stored in glycerol solution were transferred to rigor solution for 60 min and then cut into 2 mm segments across the fiber cross section. A tissue segment was diced using a blender (Sorvall Omni Mixer) in 7 mL of rigor solution using the following protocol: twice × 5 s at 1100 rpm, once × 5 s at 2500 rpm, and once × 1 s at 3100 rpm. The resulting myofibril bundles were typically about 50 μm in diameter and several hundred micrometers long. Eight myofibril bundles were probed both in relaxed and activated states to confirm the consistency of the data (n = 8).

Single honeybee myofibrils were prepared from the thorax region of honeybee flight muscles. The dissected specimen was stored at −20 °C in a 50/50 glycerol/rigor solution mixture for long-term storage. To prepare single myofibrils, the muscle tissue was washed in rigor solution and cut using a blender in 2 mL of rigor solution using the following protocol: once × 5 s at 2500 rpm and once × 10 s at 4000 rpm. The resulting myofibrils were typically 4−5 μm in diameter and tens of micrometers long. Ten single myofibril samples were probed in both activated and relaxed states for consistency (n = 10).

Synchrotron Radiation Fourier Transform Infrared (SR-FTIR) Spectromicroscopy. The SR-FTIR measurements were made using a Nicolet Magna 760 FTIR bench and a Nicolet Nic-Plan IR microscope with 15× and 32× objectives, at the Advanced Light Source, Lawrence Berkeley National Laboratory, Infrared Beamline 1.4.3. Myofibril bundle experiments were carried out with a 15× objective, while single myofibril experiments were carried out using a 32× objective. Thirty-two scans of IR spectra were collected between 800 and 4000 cm^{-1} at 4 cm^{-1} resolution and averaged. SR-FTIR spectra were initially collected to identify the chemical environment of relaxed muscle. To do this, a drop of myofibril bundle suspension was dispensed onto a CaF_2 window and then immersed in relaxing solution for 30 min on ice. To collect the SR-FTIR spectra of activated muscle, activating solution was drop dispensed onto the myofibril bundle, and measurements were made after the specimen had visibly finished contracting. For obtaining spectral maps of myofibril bundles, a total of eight myofibril bundles were probed in both relaxed and activated states for consistency. Each sample was scanned with a 5 μm step size. For single honeybee myofibrils, 13 myofibrils were probed in both relaxed and activated states. Each sample was scanned with a 1 μm step size. Second-derivative analysis was performed for enhancement of spectral resolution using the Savitsky−Golay method.[39] To minimize evaporation during data collection, the myofibril bundle was kept in a water-tight custom chamber with a Tefon fitting.

ASSOCIATED CONTENT

Supporting Information

Description of the material included along with IR spectra. This material is available free of charge via the Internet at http://pubs.acs.org.

AUTHOR INFORMATION

Corresponding Author

*E-mail: ghp@u.washington.edu

Notes

The authors declare no competing financial interest.

ACKNOWLEDGMENTS

This study was supported by a grant from the NIH (5R01 GM093842). The Advanced Light Source is supported by the Director, Office of Science, Office of Basic Energy Sciences, of the U.S. Department of Energy under Contract No. DE-AC02-05CH11231.

REFERENCES

(1) Chaplin, M. Do We Underestimate the Importance of Water in Cell Biology? *Nat Rev Mol Cell Biol* **2006**, *7*, 861−866.

(2) Cheung, M. S.; Garcia, A. E.; Onuchic, J. N. Protein Folding Mediated by Solvation: Water Expulsion and Formation of the Hydrophobic Core Occur after the Structural Collapse. *Proc. Natl. Acad. Sci. U.S.A.* **2002**, *99*, 685−690.

(3) Makarov, V.; Pettitt, B. M.; Feig, M. Solvation and Hydration of Proteins and Nucleic Acids: A Theoretical View of Simulation and Experiment. *Acc. Chem. Res.* **2002**, *35*, 376−384.

(4) Svergun, D. I.; Richard, S.; Koch, M. H. J.; Sayers, Z.; Kuprin, S.; Zaccai, G. Protein Hydration in Solution: Experimental Observation

by X-ray and Neutron Scattering. *Proc. Natl. Acad. Sci. U.S.A.* **1998**, *95*, 2267−2272.
(5) Born, B.; Kim, S. J.; Ebbinghaus, S.; Gruebele, M.; Havenith, M. The Terahertz Dance of Water with the Proteins: The Effect of Protein Flexibility on the Dynamical Hydration Shell of Ubiquitin. *Faraday Discuss.* **2009**, *141*, 161−173.
(6) Ebbinghaus, S.; Kim, S. J.; Heyden, M.; Yu, X.; Heugen, U.; Gruebele, M.; Leitner, D. M.; Havenith, M. An Extended Dynamical Hydration Shell around Proteins. *Proc. Natl. Acad. Sci. U.S.A.* **2007**, *104*, 20749−20752.
(7) Frauenfelder, H.; Chen, G.; Berendzen, J.; Fenimore, P. W.; Jansson, H.; McMahon, B. H.; Stroe, I. R.; Swenson, J.; Young, R. D. A Unified Model of Protein Dynamics. *Proc. Natl. Acad. Sci. U.S.A.* **2009**, *106*, 5129−5134.
(8) Oplatka, A. Critical Review of the Swinging Crossbridge Theory and of the Cardinal Active Role of Water in Muscle Contraction. *Crit. Rev. Biochem. Mol. Biol.* **1997**, *32*, 307−360.
(9) Pollack, G. H. *Muscles & Molecules: Uncovering the Principles of Biological Motion*; Ebner & Sons Publishers: Seattle, WA, 1990; p 300.
(10) Goertz, M. P.; Houston, J. E.; Zhu, X. Y. Hydrophilicity and the Viscosity of Interfacial Water. *Langmuir* **2007**, *23*, 5491−5497.
(11) Widdas, W. F.; Baker, G. F. The Surface Energy of Water: The Largest but Forgotten Source of Energy in Biological Systems. *Cytobios* **2001**, *106*, 7−54.
(12) Levenson, E.; Lerch, P.; Martin, M. C. Spatial Resolution Limits for Synchrotron-Based Infrared Spectromicroscopy. *Infrared Phys. Technol.* **2008**, *51*, 413−416.
(13) Holman, H.-Y. N.; Bechtel, H. A.; Hao, Z.; Martin, M. C. Synchrotron IR Spectromicroscopy: Chemistry of Living Cells. *Anal. Chem.* **2010**, *82*, 8757−8765.
(14) Holman, H.-Y. N.; Hao, Z.; Martin, M. C.; Bechtel, H. A. Infrared Spectromicroscopy: Probing Live Cellular Responses to Environmental Changes. *Synchrotron Radiat. News* **2010**, *23*, 12−19.
(15) Holman, H.-Y. N.; Miles, R.; Hao, Z.; Wozei, E.; Anderson, L. M.; Yang, H. Real-Time Chemical Imaging of Bacterial Activity in Biofilms Using Open-Channel Microfluidics and Synchrotron FTIR Spectromicroscopy. *Anal. Chem.* **2009**, *81*, 8564−8570.
(16) Falk, M.; Ford, T. A. Infrared Spectrum and Structure of Liquid Water. *Can. J. Chem.* **1966**, *44*, 1699−1707.
(17) Noble, M. I.; Pollack, G. H. Molecular Mechanisms of Contraction. *Circ. Res.* **1977**, *40*, 333−342.
(18) Yu, L. C.; Dowben, R. M.; Kornacker, K. The Molecular Mechanism of Force Generation in Striated Muscle. *Proc. Natl. Acad. Sci. U.S.A.* **1970**, *66*, 1199−1205.
(19) Falk, M.; Ford, T. A. Infrared Spectrum and Structure of Liquid Water. *Can. J. Chem.* **1966**, *44*, 1699−.
(20) Barth, A. Infrared Spectroscopy of Proteins. *Biochim. Biophys. Acta* **2007**, *1767*, 1073−1101.
(21) Birarda, G.; Grenci, G.; Businaro, L.; Marmiroli, B.; Pacor, S.; Piccirilli, F.; Vaccari, L. Infrared Microspectroscopy of Biochemical Response of Living Cells in Microfabricated Devices. *Vib. Spectrosc.* **2010**, *53*, 6−11.
(22) Byler, D. M.; Susi, H. Examination of the Secondary Structure of Proteins by Deconvolved FTIR Spectra. *Biopolymers* **1986**, *25*, 469−487.
(23) Pelton, J. T.; McLean, L. R. Spectroscopic Methods for Analysis of Protein Secondary Structure. *Anal. Biochem.* **2000**, *277*, 167−176.
(24) Litvinov, R. I.; Faizullin, D. A.; Zuev, Y. F.; Weisel, J. W. The α-Helix to β-Sheet Transition in Stretched and Compressed Hydrated Fibrin Clots. *Biophys. J.* **2012**, *103*, 1020−1027.
(25) Rennie, M. J.; Low, S. Y.; Taylor, P. M.; Khogali, S. E.; Yao, P. C.; Ahmed, A. Amino Acid Transport During Muscle Contraction and Its Relevance to Exercise. *Adv. Exptl. Med. Biol.* **1998**, *441*, 299−305.
(26) Reconditi, M.; Brunello, E.; Linari, M.; Bianco, P.; Narayanan, T.; Panine, P.; Piazzesi, G.; Lombardi, V.; Irving, M. Motion of Myosin Head Domains during Activation and Force Development in Skeletal Muscle. *Proc. Natl. Acad. Sci. U.S.A.* **2011**, *108*, 7236−7240.
(27) Yoo, H.; Paranji, R.; Pollack, G. H. Impact of Hydrophilic Surfaces on Interfacial Water Dynamics Probed with NMR Spectroscopy. *J. Phys. Chem. Lett.* **2011**, *2*, 532−536.
(28) Zheng, J.-m.; Pollack, G. H. Long-Range Forces Extending from Polymer−Gel Surfaces. *Phys. Rev. E* **2003**, *68*, 031408.
(29) Pollack, G. H. *The Fourth Phase of Water: Beyond Solid, Liquid, and Vapor*; Ebner and Sons: Seattle, WA, 2013.
(30) Nucci, N. V.; Pometun, M. S.; Wand, A. J. Site-Resolved Measurement of Water−Protein Interactions by Solution NMR. *Nat. Struct. Mol. Biol.* **2011**, *18*, 245−249.
(31) Huxley, H.; Hanson, J. Changes in the Cross-Striations of Muscle During Contraction and Stretch and Their Structural Interpretation. *Nature* **1954**, *173*, 973−976.
(32) Huxley, A. F. Muscle Structure and Theories of Contraction. *Prog. Biophys. Biophys. Chem.* **1957**, *7*, 255−318.
(33) Nagornyak, E. M.; Blyakhman, F. A.; Pollack, G. H. Stepwise Length Changes in Single Invertebrate Thick Filaments. *Biophys. J.* **2005**, *89*, 3269−3276.
(34) Carlsen, F.; Knappeis, G. G.; Buchthal, F. Ultrastructure of the Resting and Contracted Striated Muscle Fiber at Different Degrees of Stretch. *J. Biophys. Biochem. Cytol.* **1961**, *11*, 95−117.
(35) Pollack, G. H. *Cells, Gels and the Engines of Life: A New, Unifying Approach to Cell Function*; Ebner & Sons: Seattle, WA, 2001; p 305.
(36) Ford, L. E.; Huxley, A. F.; Simmons, R. M. Tension Responses to Sudden Length Change in Stimulated Frog Muscle Fibres near Slack Length. *J. Physiol.* **1977**, *269*, 441−515.
(37) Brunello, E.; Bianco, P.; Piazzesi, G.; Linari, M.; Reconditi, M.; Panine, P.; Narayanan, T.; Helsby, W. I.; Irving, M.; Lombardi, V. Structural Changes in the Myosin Filament and Cross-Bridges during Active Force Development in Single Intact Frog Muscle Fibres: Stiffness and X-ray Diffraction Measurements. *J. Physiol.* **2006**, *577*, 971−984.
(38) Länneergren, J. The Effect of Low-Level Activation on the Mechanical Properties of Isolated Frog Muscle Fibers. *J. Gen. Physiol.* **1971**, *58*, 145−162.
(39) Savitzky, A.; Golay, M. J. E. Smoothing and Differentiation of Data by Simplified Least Squares Procedures. *Anal. Chem.* **1964**, *36*, 1627−1639.